GudrunN and GudrunX

Programs for correcting raw neutron and x-ray total scattering data to differential cross section

Alan K Soper

March 5, 2012

Table of Contents

Introduction

The first data analysis workshop for liquids and disordered materials was held at The Cosener's House in May 1989. At that time there was no Windows or laptops or Java, and all the data analysis at ISIS was done on Digital Equipment Corporation (DEC, later to become Compaq, eventually bought out by Hewlett-Packard in 2002) central computers using a data analysis environment called Genie II. At that time the ISIS data analysis suite for analysis of time-of-flight diffraction data from liquid and amorphous samples (ATLAS) was set up to run within Genie II, using a series of scripts, with standalone executables to perform specific functions such as calculating attenuation and multiple scattering coefficients, or focussing the detectors into groups.

Towards the end of the 1990's it became apparent that Genie II was not compatible with other operating systems like Unix or Windows, so a new version, Open Genie was invented. Unfortunately scripts written in the old version of Genie were not easily compatible with those in the new, so translating the scripts was going to be a lot of work. This prompted two reactions, namely (a) ATLAS did not really do the data analysis correctly, i.e. it binned the raw data into groups of detectors, then proceeded to correct them for background, attenuation, etc., and (b) an environment was needed that would work on multiple platforms and was not subject to future whims of the providers of computing resources for it to work or not.

So the decision was made to move over to a standalone computing environment that would perform the analysis correctly and over which we, the providers, could have total control of what the analysis actually did. Since Fortran is universally available on many computing platforms, and since many of the earlier routines were written in Fortran, this seemed a natural computing language to write the data analysis package in. The program was called Gudrun because it is (to me) an interesting German name but the similarity with its translation by some to "good-run" was not lost on the author either!

Gudrun is a standalone program that will analyse diffraction data, detector by detector, all the way from raw neutron counts to final differential scattering cross section, combine the detectors in groups of detectors, finally merging all into a single spectrum, and will even perform the Fourier transform of these data if you ask it to. Obviously it has become increasingly complicated over the years and the demand for some sort of description of what the program actually does has been growing steadily.

The input file to Gudrun is of course rather long and difficult to understand, so some years ago I started playing around with the idea of a graphical user interface (GUI) to

help prepare this input file. This is called GudrunGUI. It is written in Java and it allows the user to both input all the necessary data they need to run Gudrun, to run both the PURGE routine and Gudrun itself, and to plot the outcomes. Probably the Java program that runs the GUI is now more complicated than Gudrun itself! But it does seem to have helped a lot of people to run Gudrun and to hopefully make it easier to get an accurate analysis of their diffraction data, something that was traditionally restricted to individual specialists.

Much more recently, an x-ray version of Gudrun was produced, GudrunX. Corresponding to this, the neutron version is now called GudrunN. GudrunX is currently aimed primarily at analysing data from a laboratory x-ray source, but can readily be applied to synchrotron radiation if the data are in the correct format. GudrunX runs entirely within Java and so if the number of detecting elements were to increase to the level found in neutron experiments a standalone Fortran (or other language) version of GudrunX might have to be prepared.

This manual attempts to describe what the various routines do, with some explanation why they do it. It is not however a detailed description of all the subroutines. That will have to be left to another time... In order to understand the steps involved in analysing diffraction data, and so make intelligent decisions when choosing which parameters to use, it is unfortunately necessary to understand something about how neutrons and x-rays interact with matter, what the diffracted signals might contain, and how diffractometers work. So included in this manual is an outline of the diffraction experiment (Chapter 1) and a summary of the theory of structure in disordered systems (Chapter 2). Feel free to ignore these sections if you are already familiar with the topics, but they can be used for reference if necessary. Chapter 3 describes the processes that Gudrun and GudrunX perform, and Chapter 4 will, when complete, show how to run the programs and what to expect.

Please note that the term "diffraction" is used widely throughout this manual, even though strictly speaking for liquids there is no elastic scattering. This is because the routines described here assume there is no energy analysis on the scattered neutron or x-ray beam and the output differential cross sections and radial distribution or pair distribution functions are calculated *as if* the scattering had been measured in the static approximation, i.e. negligible energy transfer. Hence the term "scattering" is reserved primarily for experiments where energy analysis is performed on the incident or scattered neutron or x-ray beams.

The question of authorship of a manual such as this is difficult, since without the input from a huge number of people, especially in this case the users of ISIS, none of it would have happened. However I do have to thank in particular members of the ISIS Disordered Materials Group, Silvia Imberti, Emma Barney, Alex Hannon and Daniel Bowron for their enormous efforts in studying and testing the routines and making sure they do what they claim to be doing. I am particularly indebted to Silvia and Emma for preparing a list of slides on how to run the programs - these form the basis for Chapter 4. Other people to be thanked include Sylvia McLain, for creating an earlier version of this manual, Piers Buchanan for some of the early testing of Gudrun, and Thomas Proffen for numerous

suggestions, many of which have now been incorporated in the latest version. I am indebted to Michel Koch for a comprehensive proof-reading of the present document. (Probably there are others who should be mentioned, so please let me know!) A separate account of GudrunX has recently appeared in the literature Soper and Barney [2011].

Originally ATLAS had multiple authors because the routines could be adopted and edited by anyone who cared to do so, and this did indeed happen. In principle the same is true of Gudrun, but in practice it has not happened to any significant extent, mostly because editing somebody else's program can be a nightmare: as it is even I am wary of making too many big changes in one go for fear of generating rubbish. Although I make no warranty that the routines do what they are supposed to do, I do feel it would not be fair to list as authors people who would probably not be keen to try to fix the program if something is not working correctly.

Finally I would very much like to hear any suggestions for how things could be presented differently, and ideas for additional features, either in the program itself or in this manual.

Chapter 1

X-ray and neutron diffraction

1.1 The diffraction experiment

There are at seven principle components to a diffraction experiment:-

1. A source of *radiation*;
2. An incident beam *monochromator* and *collimator*;
3. The *sample* being investigated;
4. A scattered beam collimator;
5. Radiation *detector(s)*;
6. Data acquisition *electronics* to count the events seen in the detector;
7. Data analysis software, to convert the "raw" counts to useful differential cross section data.

This manual is mostly about the last of these items, data analysis, but in order to understand the way it works it is necessary to understand the elements of the diffraction experiment and the ways they differ for different types of incident radiation. The elements of the experiment are summarised in Fig. 1.1.

A beam of monochromatic radiation, wavelength λ impinges on the sample from the left, is scattered by that sample into scattering angle 2θ and then detected by the detector. The data are measured versus the variable $Q = \dfrac{4\pi \sin\theta}{\lambda}$.[1] The wavelength is normally selected either by means of a monochromator in the incident beam, or, in the case of time-of-flight neutron scattering, by measuring the time taken to travel by the neutron from

[1] X-ray crystallographers often use the alternative unit $s = \dfrac{2\sin\theta}{\lambda}$. Equally sometimes Q is written as k. For the purposes of this manual we will use the Q notation, defined as above.

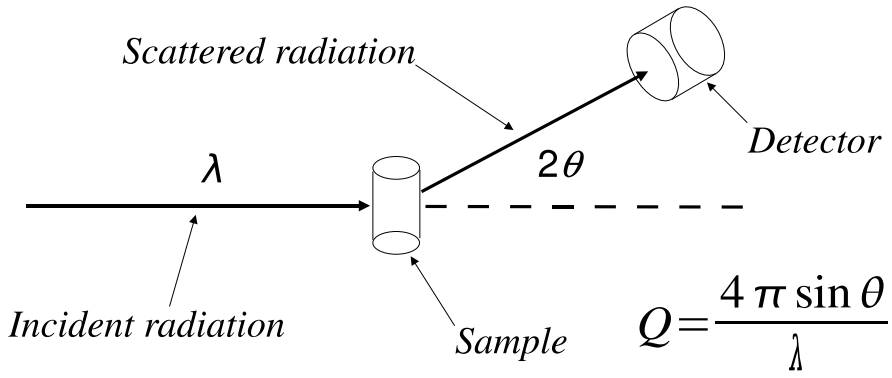

Figure 1.1: Primary layout of a neutron or x-ray diffractometer

source to detector, or, in the case of energy dispersive x-ray scattering, by detecting the energy of the scattered x-ray.

It is Q which determines the length scale that is probed by the diffraction experiment, with small Q corresponding to large distances and large Q corresponding to small distances. Any combination of θ and λ that gives the required Q values should in principle give equivalent data, although, as will be seen later, use of large scattering angles and long wavelengths with neutrons can in certain circumstances give rise to unwanted "recoil" effects that should be avoided if possible.

The simplicity of the underlying diffraction experiment belies many of the subtleties that are associated with it:-

1. Unless the sample is crystalline, the underlying diffraction signal from a liquid or amorphous material is intrinsically weak and contains only diffuse scattering features.

2. It is impossible to make a truly monchromatic beam, because if you ever did so, there would be no incident radiation flux with which to detect your already weak diffraction pattern! This means the diffraction pattern can only be measured with a finite *resolution* function. This problem is particularly serious with neutron sources, which often have intrinsically much lower fluxes than x-ray sources. There is a highly non-linear relationship between the width of the allowed wavelengths which get through the collimator and the final radiation flux on the sample. In other words, a change in resolution by a factor of 2 might affect the flux by a factor of 8, for example. See Caglioti et al. [1958].

3. Samples normally have to be contained in one or more *containers* (sample holder, thermal radiation shields, pressure cell, etc.

4. Inevitably some of the radiation reaching the detector has not come from the sample. This is called *background* scattering which has to be removed from the detected radiation counts.

5. Because the signal from the sample is intrinsically weak, you are very dependent on the detector and its electronics not introducing any spurious structure into the observed data. This structure might be caused by spurious background counts which vary with time and position, or it might be caused by residual instabilities in the electronics themselves.

6. For a sample to scatter a measurable amount of radiation it also therefore has to attenuate that scattering to some extent, so that corrections for *attenuation* have to be made to both the scattering from the sample and from any surrounding containers.

7. Equally, if the sample scatters sufficiently to give a measurable signal, then some of that signal will come from *multiple scattering* events, namely those where the radiation is scattered twice or more before it leaves the sample. Since they mix up different scattering angles (and wavelengths if the scattering is inelastic) such events do not contribute a useful signal to the scattering pattern. Roughly speaking, if a sample scatters $x\%$ of the incident beam, then, depending on the amount of radiation *capture* in the sample, the multiple scattering will be around $x\%$ of the primary scattering. Radiation capture occurs when the radiation is captured by an atom of the sample instead of being scattered by it.

8. In addition for light atoms nuclear recoil for neutrons and electron recoil for x-rays in the scattering process lead to distortions to the diffraction pattern that need to be corrected for.

9. There may be other side effects to be taken account of. For example some materials may fluoresce in the x-ray beam, giving an additional sample dependent background. For neutrons a few elements have very high neutron capture cross sections, and many have nuclear resonances (mostly heavier elements and at higher neutron energies).

10. Stability is another important requirement of the diffraction experiment from liquids and glasses. Stability in the incident beam, stability in the sample itself and in the sample positioning, and stability in the detector electronics. This is because both x-ray and neutron measurements tend to occupy several hours of beam for each sample, so that if different samples are to be compared reliably, the parameters associated with the diffractometer itself should not drift in the course of a measurement. In this the observed diffraction pattern differences do indeed arise from the two samples, and not from some systematic effect of the instrument on which they were measured.

11. Finally, in order to calculate useful quantities from the data related to the structure of the material in the sample, it is essential to put the scattered data onto to some sort of absolute scattering cross section scale. This is typically measured in the units

of scattering cross-sectional area per atom per steradian (for neutrons) or electrons^2 per atom per steradian (for x-rays).

Although neutron and x-ray diffraction are closely analogous in all these aspects, there are some fundamental differences in the way the data have to be treated, so in the next two sections we look at each technique in turn, and highlight the salient distinct features of the data analysis process.

1.2 Neutron diffraction

Neutrons are scattered by the atomic nucleus. The only exception to this rule occurs if the atom has a residual magnetic moment, in which case the magnetic moment of the neutron will interact with the atomic magnetic moment, giving extra scattering in addition to the nuclear scattering. In order to see diffraction effects related to the arrangement of the atoms it is necessary to use neutron wavelengths comparable to the typical spacing between atoms, 10^{-10}m. This wavelength is roughly 10^4 times larger than the nuclear dimensions, so, provided the neutron energy is well away from any nuclear resonances, the scattering is called "s-wave", which means there is no angular momentum transfer in the scattering process. (If the neutron energy is near a nuclear resonance of one of the atomic components in a material, then nuclear physics takes over and for the most part the information obtained by scattering neutrons is not useful. Fortunately this mostly happens only with heavier nuclei and at higher neutron energies.) To a neutron therefore an atom normally appears as an extremely small blip in space, mathematically effectively a δ-function.

For this reason neutrons give us arguably the most direct insight into the position and motion of atoms, both as individual particles, the *self* scattering, and as pairs of atoms, the *distinct* scattering: the neutron probes directly the site-site correlation functions between atomic centres. However because the atomic nucleus is so small, the neutron-nucleus interaction is weak, so neutrons are mostly very penetrating, and a lot of effort is required to make neutron sources which are bright enough to perform useful diffraction and other types of neutron scattering experiments.

1.2.1 Neutron sources

There are two primary ways in which neutrons can be produced for a diffraction experiment - either by a nuclear reactor or by the neutron spallation process. Nuclear reactors produce neutrons through neutron-induced nuclear fission. In the process a nuclei, typically uranium or plutonium, captures a neutron and subsequently splits, or fissions, into two daughter nuclei, releasing at least two high-energy ($\sim$ 2MeV) neutrons and a large amount of kinetic energy, typically 200 MeV for each fission event. These neutrons are too energetic to sustain the nuclear reaction, so the uranium fuel is typically surrounded by a *moderator* made up of some hydrogenous material (often water or heavy water) to slow

them down and so enable the chain reaction to continue. Hydrogen is used for this because its mass is almost the same as the neutron, leading to maximum neutron energy loss on collision. Neutron absorbing control rods can be readily inserted into the reactor to shut down the chain reaction when necessary.

In a spallation neutron source production of neutrons is achieved by accelerating bunches of protons in a linear accelerator (LINAC) or synchrotron (or both as at ISIS) to sufficiently high energies ($\sim$ 800MeV at ISIS, but up to 3GeV at the SNS (USA) and JPARC (Japan)) so that when they collide with a heavy metal *target* nucleus they produce highly excited nuclear states. These states decay, either immediately or after a delay, by throwing off nuclear particles such as neutrons, γ-rays and neutrinos. The maximum energy of neutrons produced in this way corresponds to the energy of the impinging proton beam, and hence the neutrons from a spallation source are much more energetic than those at a reactor neutron source. If the target is uranium, up to 30 neutrons per proton can be produced. Other non-fissioning targets such as tantalum or tungsten produce about half the number of neutrons produced by uranium. However there is a significant delayed neutron background with uranium which can be awkward to account for in the diffraction data and significantly offsets the increased neutron flux. Hence most spallation sources today use targets made of tantalum or tungsten, or, in the case of the newer high power sources, liquid mercury (SNS, J-PARC). To enhance the flux of neutrons, the target is surrounded by a *reflector* made of beryllium to reflect the fleeing neutrons back into the target area and so increase the neutron flux seen on the neutron beam lines.

The main benefit of a spallation source compared to a reactor source is that it is intrinsically safe: it can be switched off at the touch of a button and there is no nuclear fuel produced (the plutonium produced in a nuclear reactor is both highly radioactive and extremely toxic). More important scientifically, if the proton beam is pulsed into short pulses ($\sim$ 400ns wide at ISIS), then all the neutrons set out from the target at effectively the same time, so the energy can be measured from the time of flight to the detector. Hence there is no need for a monochromator stage at a pulsed neutron source, which means many more of the neutrons produced by the facility go into measuring useful data. As we go through the sections other advantages and disadvantages of reactors versus pulsed neutron sources will be highlighted.

1.2.2 Neutron moderation

As already described, neutron moderation, that is the process of slowing the neutrons down, is an essential part of a nuclear reactor since without it the chain reaction could not be sustained. It is also important from the point of view of the diffraction experiment since the de Broglie wavelength of a neutron is given by

$$\lambda = \frac{h}{m_n v} \tag{1.1}$$

where h is Planck's constant, m_n is the mass of the neutron and v is its group velocity. It is important that this wavelength corresponds reasonably closely to the typical spacing

between atoms (typically a few Å, where 1Å$= 10^{-10}$m). In fact for liquids and amorphous materials we need values of Q which extend to large values (~ 50Å^{-1}), so generally wavelengths < 1Å are utilised. On the other hand for small angle scattering which concentrates on obtaining very small Q values, much longer wavelengths up to ~ 20Å might be used.

To help gauge the values of wavelength (λ, expressed in Å), energy (E, expressed in meV), wave vector ($k = \dfrac{2\pi}{\lambda}$, expressed in Å^{-1}), time-of-flight (TOF $= 1/v$, expressed in μs/m), and temperature (T, expressed in K), it is helpful to write down the relevant conversion factors:

$$\begin{aligned}
\lambda\ [\text{Å}] &= 0.395603 \times 10^{-2}\text{TOF (TOFin } [\mu\text{s/m}]) && (1.2)\\
\text{TOF } [\mu\text{s/m}] &= 252.778\lambda\ (\lambda \text{ in } [\text{Å}]) && (1.3)\\
E\ [\text{meV}] &= \frac{81.8042}{\lambda^2}\ (\lambda \text{ in } [\text{Å}]) && (1.4)\\
&= 2.07212k^2\ (k \text{ in } [\text{Å}^{-1}] && (1.5)\\
&= 0.0861734T\ (T \text{ in } [\text{K}]) && (1.6)
\end{aligned}$$

Hence a room temperature of 300K corresponds to a kinetic energy of 25.85meV. Neutrons of such energies are therefore called *thermal* neutrons and will have a wavelength of ~ 1.78Å and TOF $\sim 450\mu$s/m, corresponding to a velocity of 2222 m/s. Because the water in a reactor is (hopefully!) close to room temperature and the neutrons are heavily moderated, the spectrum of neutrons coming from a reactor looks rather similar to a standard Maxwell thermal distribution. (Note that the term "time of flight", TOF, is used interchangeably to refer to either the actual time taken by the neutron to fly from target to detector, or, as here, the inverse velocity, normally expressed in μs/m.)

For a spallation source, there is no chain reaction to be kept going, but the neutrons emitted are much too energetic to be useful for diffraction from atoms, so they too have to be slowed down by the use of a moderator. The moderator is again made up of a material with a high hydrogen content, but the spectrum of neutrons can be tailored to a significant extent by the choice of moderator and its temperature. A water moderator produces are relatively "hot" spectrum of neutrons whereas a liquid hydrogen moderator produces a much lower energy spectrum (longer wavelengths).

The same effect can be achieved at a reactor neutron source. By inserting "hot" and "cold" sources - essentially separate moderators at correspondingly higher or lower temperatures - in the reactor moderating region, the wavelength spread in the neutron beamline can be tailored to suit particular types of experiment. Neutron cold sources have proven to be particularly effective and productive in this regard, and it would be difficult to imagine neutron scattering as a technique today without these devices.

In principle, maximum neutron production would be achieved at a pulsed source by making the moderator thick, as in the reactor case, but to do so would also make the neutron pulse unacceptably broad in time, leading to significant loss of resolution. Hence spallation source moderators are a compromise between the conflicting demands for a

Spectrum constant	Methane	Water
J [10^{10}n/sr 100cm^2 μA s]	5.7	14.7
T [eV]	0.011	0.033
Φ_0 [10^{10}n/sr eV 100cm^2 μA s]	2.7	3.5
A	0.92	0.90
W_1 [$\sqrt{\text{eV}}$]	1.7	4.0
W_2	7.0	10.6

Table 1.1: Values of the spectral constants for the ISIS Target 1 methane and ambient water moderators

narrow pulse width and maximum possible neutron flux. Because the spallation source is under-moderated, the pulsed neutron spectrum consists of two parts, a slowing down part, or *epithermal* spectrum, and a Mawellian thermal distribution:

$$\Phi(E) = \Phi_{max}(E) + \Delta(E)\Phi_{epi}(E) \tag{1.7}$$

where

$$\Phi_{max}(E) = J\frac{E}{T^2}\exp\left\{-\frac{E}{T}\right\} \tag{1.8}$$

$$\Phi_{epi}(E) = \frac{\Phi_0}{E^A}, \tag{1.9}$$

the joining function, $\Delta(E)$, is given by

$$\Delta(E) = \left[1 + \exp\left\{\frac{W_1}{\sqrt{E}} - W_2\right\}\right]^{-1} \tag{1.10}$$

and J, T, Φ_0, A, W_1 and W_2 are fitting constants to be determined by fitting to a set of data. Typical values for these constants are shown in Table 1.1 and Fig. 1.2 shows plots of these functions.

1.2.3 Neutron collimation and monochromation

For most of the experiments covered by this manual the requirement is to measure the diffraction pattern over a wide range of Q. This is achieved normally by using a range of neutron wavelengths, but in all cases, both reactor and time-of-flight, short wavelengths are required, which means, as a general rule neutron guides are of limited usefulness. Neutrons are therefore generally collimated by making small holes of the appropriate shape and size in large blocks of shielding material and lining these holes up so that a narrow beam is directed onto the sample. Shielding materials typically include concrete (including borax impregnated concrete), steel, borated wax, lead shot (to reduce γ transmission), boron carbide, B_4C, in various forms, and cadmium and gadolinium. The latter two materials have very high capture cross sections for neutrons, but are only effective below, $\sim$ 300meV -

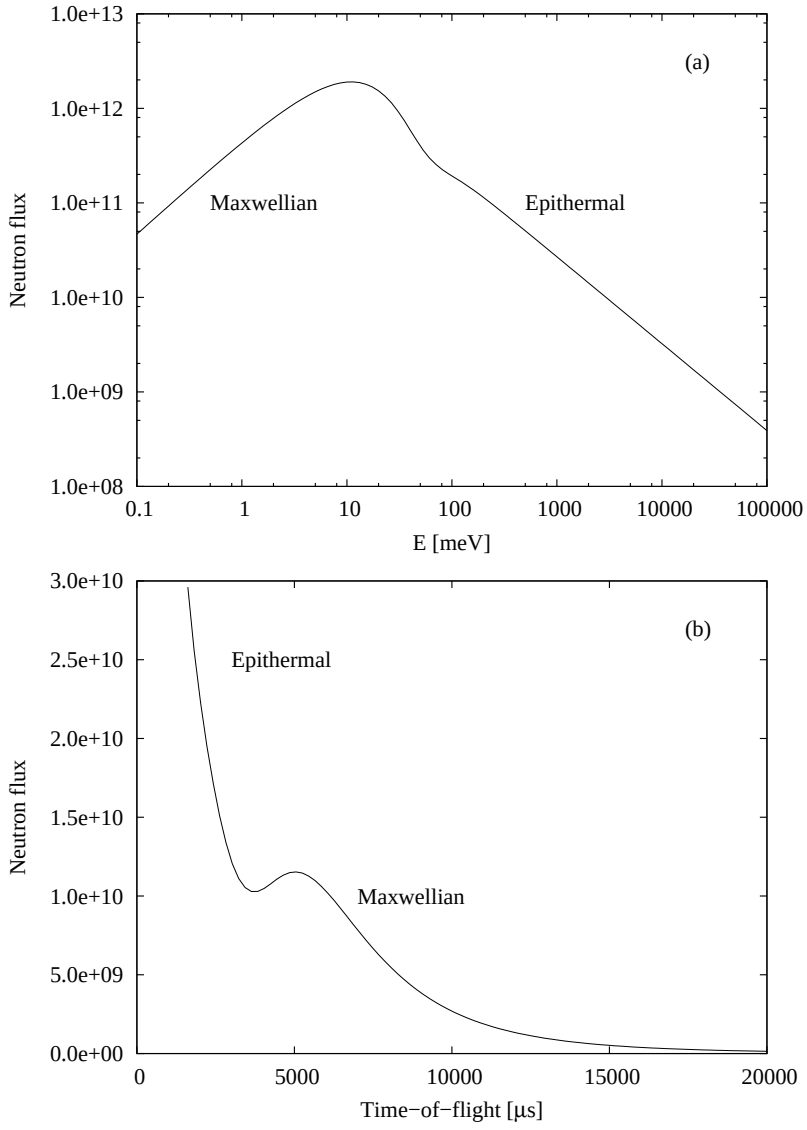

Figure 1.2: Neutron spectra from the ISIS methane moderator. The top graph (a) shows the flux as a function of energy, the bottom graph (b) shows the flux as a function of time of flight, based on 12m total flight path. To convert to time of flight the spectrum as a function of energy must be multiplied by the Jacobian $\frac{\partial E}{\partial t} = \frac{2E}{t}$

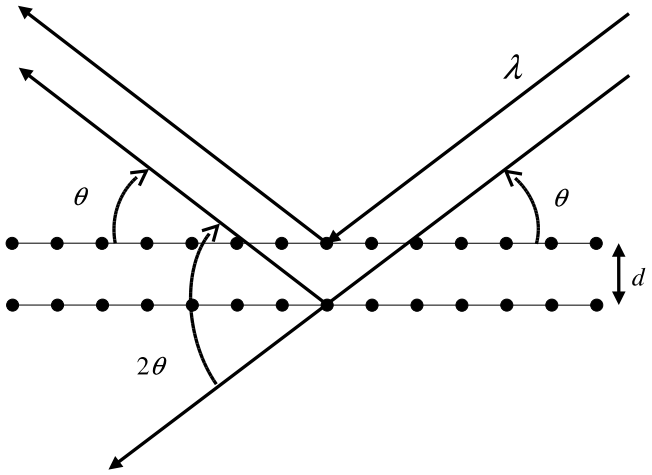

Figure 1.3: Illustration of Bragg's law for crystal diffraction. A reflection will occur if $n\lambda = 2d\sin\theta$.

Cu face	d-spacing [Å]	λ [Å]
200	1.807	0.70
220	1.278	0.50
331	0.829	0.35

Table 1.2: Planes of Cu single crystal used to monochromate the neutron beam at D4C.

above this energy they are effectively transparent to neutrons - and so are good at mopping up stray neutrons *once* they have been slowed down sufficiently. Hence Cd and Gd are more commonly found at reactor sources where the overall neutron energies are lower. Modern diffractometers allow the beam dimensions at the sample to be adjusted to suit different sample environments. Because the neutron shielding must be able to deal with a very wide range of neutron energies, the biological shields around the nuclear reactor or spallation target and associated beam lines are generally very massive and made up of composites of the above materials.

As already explained, there is no need to monochromate the beam at a pulsed source since the neutron wavelength can be obtained via time-of-flight measurements. At a reactor source the incident beam must be collimated and this is normally achieved by reflecting off a specific Bragg plane from a single crystal, Fig. 1.3. At the Institut Laue Langevin (ILL) in Grenoble, France this is typically achieved using a Cu single crystal and Table 1.2 lists the crystal planes and resulting wavelengths that can be obtained on the D4C diffractometer.

Crystalline powder experiments generally need high resolution in order to discriminate effectively between adjacent Bragg reflections and also to determine the sample contribution to the shape of individual reflections. However, because Bragg reflections are so

sharp count rate is rarely a severe constraint, unless special effects are being determined, such as the change in structure as a function of time. In contrast, with liquids and amorphous materials the structure factor consists of a few broad peaks which merge together continuously. Detailed analysis of these requires absolute measurements. In many cases, particularly those that involve measuring changes in structure as a function of pressure, temperature or isotope, count rate can be of paramount importance because of the intrinsic weakness of the signal. Increases in resolution can only be entertained if a count rate appropriate to the resolution is available.

1.2.4 Samples and containment

As already explained, in the majority of cases the sample is held in a container of some form. If the temperature is to be different from ambient then usually a *furnace* is required to go above room temperature, and to go down in temperature a *cryostat*, *closed cycle refrigerator* (CCR), or even a *dilution fridge* is required for the lowest temperatures. Helium cryostats can typically achieve temperatures of around 4.2 K or a bit lower when pumped. In addition if the pressure of the sample is to go above ambient then the thickness and material of the container become important and certainly far from ideal from the point of view of analysing the diffraction data.

For accurate structure factor measurements the mounting and containment of the sample can be crucial since the diffractometer is sensitive to small positioning offsets on the order of 1mm. This sensitivity arises from the small variations in final flight path and scattering angle which can occur from one sample to another if each sample is not placed in exactly the same position as its predecessor. One solution to this difficulty which is applicable if the sample will not be under pressure is to use a flat plate sample can with an area larger than the beam area. This largely avoids the positioning problems. However the use of a flat-plate can is not always practical and is dependent on the position of the detectors. Also, generally cylindrical cans must be used for pressure or furnace experiments and so it is essential to ensure that if cylindrical cans are used sample positioning is accurate to at least 0.1mm.

Ideally the container should be made of a purely incoherent scattering material such as vanadium or a material which has a small coherent cross-section such as titanium-zirconium alloy: this material takes advantage of the opposite phase of scattered neutrons by Ti and Zr. These materials are needed otherwise the Bragg reflections from the container can be hard to subtract completely. This problem arises because the front and back of the sample container correspond to slightly different scattering angles at the detector. Thus when the container is measured empty and then filled with sample, the neutron attenuation by the sample causes the Bragg peaks from the front of the container to be attenuated preferentially compared to those from the rear, causing an apparent shift in the position of the peaks as seen in the detector. Unfortunately the ideal of an incoherent container may be hard to meet if a particularly corrosive sample requires a special material for containment.

Another feature of the sample geometry is to be able to calculate the attenuation

corrections accurately. The current programs only do this for cylindrical and flat plate sample shapes: they should be fairly accurate so long as the sample geometry can be approximated to one of these geometries to good accuracy. However if the sample geometry cannot be approximated accurately, then the calculated corrections will be correspondingly less reliable, with the result that the output of the data analysis program will be more ambiguous. Hence the basic message must be that the sample geometry should be kept as simple as is practically possible. Of course it is to be hoped that programs appropriate to more complex geometries can be developed, particularly where the containment material is not an incoherent scatterer, but in spite of lots of talk about doing this, it has so far not been achieved to any practical extent.

1.2.5 Neutron detector

Neutron detection is typically achieved via capture by a ^{3}He nucleus. The nuclear reaction involved is denoted by ^{3}He(n,p)^{3}H, which means

$$^3\mathrm{He} + \mathrm{n} \longrightarrow \mathrm{p} +^3 \mathrm{H} \tag{1.11}$$

The proton is accelerated towards a charged wire, creating an avalanche that is detected electronically. Placing sensor electronics at each end of the wire, one can determine the position along the wire where the event occurred, expressed as the ratio of amount of charge deposited at each end of the wire. ^{3}He gas is normally stored on a tube or other suitable container at sufficient pressure to give essentially a "black" detector for thermal neutrons. This process is extremely insensitive to other types of radiation that may be present such as γ particles.

At ISIS much use is made of the alternative reaction ^{6}Li(n,^{3}H)^{4}He. In this case the charged particles are detected by embedding ^{6}Li in a plastic scintillator containing ZnS. Photomultipliers are used to detect the scintillation events. In principle ^{6}Li is much more readily available, but the associated electronics are generally more complex than for ^{3}He, so the associated detector cost is still quite high. In addition ^{6}Li is more γ sensitive than ^{3}He, so for some applications requiring very low backgrounds it is not so suitable. A very marked advantage of the ^{6}Li-scintillator combination is that it is very versatile for producing a range of detector shapes and sizes, and so is therefore very useful in large area detectors. It can also be made roughly twice as efficient as ^{3}He for high energy neutrons, which is helpful when epithermal neutrons need to be detected effectively.

1.3 X-ray diffraction

Unlike neutrons, x-rays are scattered by the atomic electrons, which are necessarily quite diffuse and extend well beyond the nucleus, sometimes out as far as neighbouring atoms. Indeed when a covalent bond is formed the associated valence electrons are shared between the two atoms that are bonded. It follows that the x-ray diffraction pattern probes the electron distribution around each atom and betweeen atoms, but if it is assumed that the

electrons are placed symmetrically with respect to the nucleus of each atom, the so-called "independent atom approximation", then x-ray scattering probes the positions and motions of the atoms as does neutron scattering, but the correlations are convoluted with the (broad) electron density distribution. This has the unfortunate side effect that the intensity of scattering of materials by x-rays falls rapidly with increasing Q, making determination of the high-Q part of the diffraction pattern much more difficult with x-rays than with neutrons. If, moreover the electrons are not centred on the atomic nucleus, then the simple convolution described above no longer works, although in the majority of cases since x-rays are scattered mostly by the core electrons, this lack of centro-symmetry is not a major source of error.

However it does mean that an x-ray is a strongly interacting radiation which is readily absorbed and scattered by atoms. Hence x-ray sample sizes are generally $\sim$ 10 times smaller than those for neutrons and the types of materials needed to contain samples for x-ray diffraction are quite different to the ones used for neutron diffaction.

Note that because the interactions of x-rays with matter is generally more complex than those of thermal neutrons and depend significantly on the manner in which the x-rays are produced and detected, the account given here is representative of what might happen in an x-ray scattering experiment rather than an accurate account of what actually happens in particular cases.

1.3.1 X-ray sources

X-ray sources fall into two categories, namely the laboratory "x-ray tube", in which a beam of electrons impinges on a metal target at high energy producing a beam of x-rays, and the synchrotron source, in which a circulating beam of relativistic electrons radiates x-rays in a cone close to the plane of the electron orbit as synchrotron radiation. Either source requires a degree of monochromation of the incident beam as does the fixed wavelength neutron diffractometer, unless an energy sensitive detector is available.

For the x-ray tube some degree of monochromation is achieved quite naturally. This is because the incident electrons can knock an electron out from one of the lower energy levels of the constituent atoms of the target. The atom responds by allowing a higher energy electron drop into the vacated energy level, causing the release of an x-ray photon: because the electron is transferred between two well defined energy levels, the energy of the emitted photon is known quite precisely, giving rise to a partly monochromatic beam. Of course several transitions are possible, so there are in fact several spikes in the emitted x-ray intensity pattern corresponding to these different energy levels. The lowest energy levels are designated "K-α, K-β, L-α, L-β, and so on, corresponding to electron transitions between the corresponding orbitals in the atom.

In addition to the sharp spikes in intensity at specific energies, there is a general "bremsstrahlung" radiation coming from electrons being decelerated in the material over a range of energies. This creates a "white" beam of x-rays and if a monochromator is not being used the effect of this white beam scattering by the sample has to be corrected for.

For synchrotron radiation, the range of energies and wavelengths is extremely broad

and the intensities are very high, so that use of a monochromator is mandatory in order not to instantly vapourise the sample material and to be able to make sense of the scattered data. The x-ray beam from a synchrotron is also horizontally polarised, meaning that the electric field vector is in the plane of the electron orbit.

The useful relationships between x-ray energy, wavelength and wavevector are based on $E = \dfrac{hc}{\lambda} = \hbar ck$ where c is the velocity of light:

$$E \text{ [keV]} = \frac{12.3984}{\lambda} (\lambda \text{ in [Å]}) \quad (1.12)$$

$$= 1.97327k \ (k \text{ in [Å}^{-1}\text{]}) \quad (1.13)$$

$$\lambda \text{ [Å]} = \frac{12.3984}{E} (E \text{ in [keV]}) \quad (1.14)$$

Hence an x-ray tube operating at say 30keV will produce x-rays with wavelengths down to 0.413Å. Molybdenum is a common material for the x-ray tube anode. This has K-α lines at 17.479372 and 17.37429keV which corresponds to wavelengths 0.7093 and 0.7136 Å respectively. At a synchrotron a broad range of x-ray energies is generated up to of order $\sim$ 100keV or more, depending on the operating energy of the synchrotron. Hence for both laboratory and synchrotron x-ray sources the energy is already appropriate for doing diffraction from atomic structures, so there is no need for the equivalent of the neutron moderator, although devices like wigglers and undulators can enhance the intensity dramatically in particular energy regions.

1.3.2 X-ray collimation and monochromatisation

In the simplest cases x-ray collimation is achieved by the use of absorbing slits as with neutrons, though these tend be of size $\sim$ 1mm or less, compared to the 10-30mm wide slits used in neutron scattering. However more sophisticated x-ray optical devices are possible in some circumstances.

X-ray monochromatisation and focussing is achieved using single crystals or diffraction gratings and mirrors (only for soft x-rays), but once again the size required for such devices is mostly far smaller than would be used in a typical neutron experiment because the ultimate beam size required is much lower.

1.3.3 Samples and containment

As with neutrons most materials to be investigated with x-rays require containment of some form or the other. Unless very high x-ray energies are involved, it is essential that the thickness of this containment is kept to an minimum. The normal rule of thumb is that the sample thickness, t, should be equal to the inverse of the attenuation coefficient: $t = \frac{1}{\mu}$, although this can be difficult to realise when heavy elements are present. Thin silica capilliaries, with wall thicknesses of order 10μm are good for the purpose of containing

samples as they are also generally inert to most corrosive materials. Generally speaking the scattering from a silica capilliary is small compared to that from the sample it contains. If a thin film window for a sample container is required then mica, silicon nitrite or polycarbonate film is useful as they contains only low atomic weight elements and can be stretched to make a smooth, thin, and flat surface.

1.3.4 X-ray detectors

Compared to neutrons, the methods for detecting x-rays are far more numerous, so only a very cursory overview will be given here. Sodium iodide crystals, which produce light scintillations detectable by a photomultiplier tube when struck by an x-ray, are a common form of x-ray detector. Semiconductor detectors work by collecting the electron-hole pairs that form when an x-ray interacts. Yet others work with a sheet of scintillator, behind which is placed a charge coupled device (CCD) or other photon detector. Such devices allow a large solid angle detector to be built. Image plate detectors use a phosphor screen which is read out (offline or online) using a laser and photomultiplier. Gas mixture (Ar/Xe) detectors with charge division or delay line electronics are still in use on some synchrotron beamlines and on laboratory x-ray sources. Pixel area detectors (PAD) are also becoming increasingly popular.

Two important qualities of the x-ray detector to be used for liquid and amorphous materials diffraction are its linearity and its uniformity. Linearity means that if the intensity of scattered photons in one part of the spectrum is double that in another, the response of the detector mirrors that intensity change accurately. Hence detectors which count photons are generally more suitable for this purpose than current measuring devices, whose linearity can be difficult to assess. Uniformity means that if a detector is a multidetector and so has many detecting elements, each of those elements gives the same response when subject to the same irradiation. Once again this can be difficult to ensure for large area detectors, so such devices require very careful calibration before they can be used on a real material. Alternatively, only that part of the diffraction pattern that has been sampled by all elements of the detector is used in the subsequent data analysis.

1.4 Diffractometer resolution

The resolution of a pulsed neutron diffractometer is quite different in form to that from a fixed incident wavelength diffractometer with a monochromating crystal. The latter case was dealt comprehensively by Caglioti et al. [1958].

Theoretically, the Bragg diffraction peak from a crystalline material placed in the radiation beam would be infinitely narrow. This ideal situation can never be realised in practice because invariably neither the scattering angle, nor the incident wavelength are precisely defined, leading to a spread in values of both. Indeed for neutrons the crystal mosaic spread of a monochromating crystal is often made larger if possible to enhance

the flux of radiation scattered by the crystal. [2] This causes the beam on the sample to have an intrinsic divergence (spread in angles) and spread in wavelengths. However for the monochromating crystal this spread in angles and spread in wavelengths are correlated, since all radiation particles reflected by the crystal must satisfy Bragg's law, Fig. 1.3.

For the pulsed neutron diffractometer on the other hand, the neutrons emerge more or less at random from the moderator face with a range of energies that mostly do not correlate with the position in the moderator. Hence the divergence of the incident beam in a pulsed neutron diffractometer is to a good approximation independent of the wavelength spread. (This rule might not apply quite so rigorously if a neutron guide is present.) In that case the change in Q with change in scattering angle and wavelength is given by

$$\begin{aligned} \Delta Q &= \left(\frac{\partial Q}{\partial \theta}\right)\Delta\theta + \left(\frac{\partial Q}{\partial \lambda}\right)\Delta\lambda \\ &= Q\left(\cot\theta\Delta\theta - \frac{\Delta\lambda}{\lambda}\right) \end{aligned} \tag{1.15}$$

so that because the two types of varation are uncorrelated:

$$\left\langle(\Delta Q)^2\right\rangle = Q^2\left(\cot^2\theta\left\langle(\Delta\theta)^2\right\rangle + \frac{\left\langle(\Delta\lambda)^2\right\rangle}{\lambda^2}\right). \tag{1.16}$$

Equation 1.16 shows that the resolution of the diffractometer has two components, one that arises from the angular spread of the neutron beam, and one that arises from the intrinsic wavelength spread of the neutron pulse. The angular spread arises from the finite size of the neutron moderator (or the allowed angular divergence of the incident beam collimator or guide, whichever is the smaller), the finite size of the sample, and the finite size of the detector (again modified by any collimation that may be in the scattered beam. Clearly this "geometrical" contribution to the resolution will diverge at low scattering angles ($2\theta \to 0$). To avoid this low angle divergence one should ideally place the sample far from the moderator and the detector far from the sample, conditions that will also cause the detected count rate to fall dramatically. Hence the placing of the low angle detectors in a diffractometer has to be a compromise between acceptable count rate and acceptable resolution. The choice in a particular circumstance can really only be gauged by ray-tracing to find the best combination.

On the other hand at large scattering angles the geometrical contribution to the resolution becomes very small ($\cot\theta \to 0$) so the resolution is dominated by the wavelength spread in the incident beam. So this wavelength spread represents the limiting resolution of the diffractometer. Generally it can be reduced by making the moderator narrower (but this also results in loss of flux) or by increasing the time-flight. (Note that $\dfrac{\Delta\lambda}{\lambda} = \dfrac{\Delta t}{t}$, where Δt represents the time spent in the moderator and t represents the time taken to

[2] This does not happen at synchrotron sources because the flux of x-rays is usually so large, that the monochromating crystal can have negligible mosaic, giving rise to superb resolution at these facilities.

travel from the moderator to the detector, and since Δt is fixed by the size of the moderator, the ratio $\dfrac{\Delta t}{t}$ can be made smaller by increasing the flight path to the detector.) However increasing the time-of-flight will also result in a loss of intensity unless a neutron guide is employed.

Note that for any given scattering angle the ratio $\dfrac{\langle(\Delta Q)^2\rangle}{Q^2}$ is (approximately) a constant for the time-of-flight diffractometer. It is not exactly constant because the time width of the pulses varies somewhat with the energy of the neutron.

For the case of a diffractometer with a monochromator, the simple argument given above no longer applies. In general there will be three collimators in a fixed wavelength diffractometer. One to focus the white radiation beam onto the monochromating crystal, one to focus the beam from the crystal onto the sample, and one to collimate the beam towards the detector. Each of these collimation stages limits the angular spread of the beam. The resulting general expression for the full width at half maximum of the resolution function, $\langle\Delta Q\rangle_{1/2}$, Caglioti et al. [1958], is given in terms of the angular spreads of each collimation stage, α_1, α_2, and α_3, the mosaic spread of the monochromating crystal, β, and the parameter $a = \dfrac{\tan\theta}{\tan\theta_B}$, where $2\theta_B$ is the Bragg scattering angle of the monochromator:

$$\langle\Delta Q\rangle_{1/2} = \left[\frac{U - Va + Wa^2}{X}\right]^{\frac{1}{2}}, \tag{1.17}$$

where

$$\begin{aligned} U &= \alpha_1^2\alpha_2^2 + \alpha_1^2\alpha_3^2 + \alpha_2^2\alpha_3^2 + 4\beta^2(\alpha_2^2 + \alpha_3^2), \\ V &= 4\alpha_2^2(\alpha_1^2 + 2\beta^2), \\ W &= 4(\alpha_1^2\alpha_2^2 + \alpha_1^2\beta^2 + \alpha_2^2\beta^2), \end{aligned} \tag{1.18}$$

and

$$X = \alpha_1^2 + \alpha_2^2 + 4\beta^2. \tag{1.19}$$

Fig. 1.4 gives an example of this resolution function, expressed as the ratio $\langle\Delta Q\rangle_{1/2}/Q$, for a diffractometer where $\alpha_1 = \alpha_2 = \alpha_3 = \beta = 0.5°$, $\lambda = 0.7$Å, and $2\theta_B = 22.3366°$ (see Table 1.2). It will be seen that the resolution width is large at small angles as expected, goes through a minimum at a scattering angle of about 40°, then rises gradually with increasing scattering angle. Hence the best resolution on a fixed wavelength diffractometer is not at the largest scattering angles, unlike the case of the time-of-flight neutron diffractometer. Instead the precise scattering angle of the best resolution will depend on the individual angular spreads of each collimation section and the monochromating crystal divergence. Note however that this expression includes only horizontal angular spread and does not include the effect of vertical divergence. Nor does it include the effect of a double crystal monochromator which have become very common on many neutron and x-ray diffractometers.

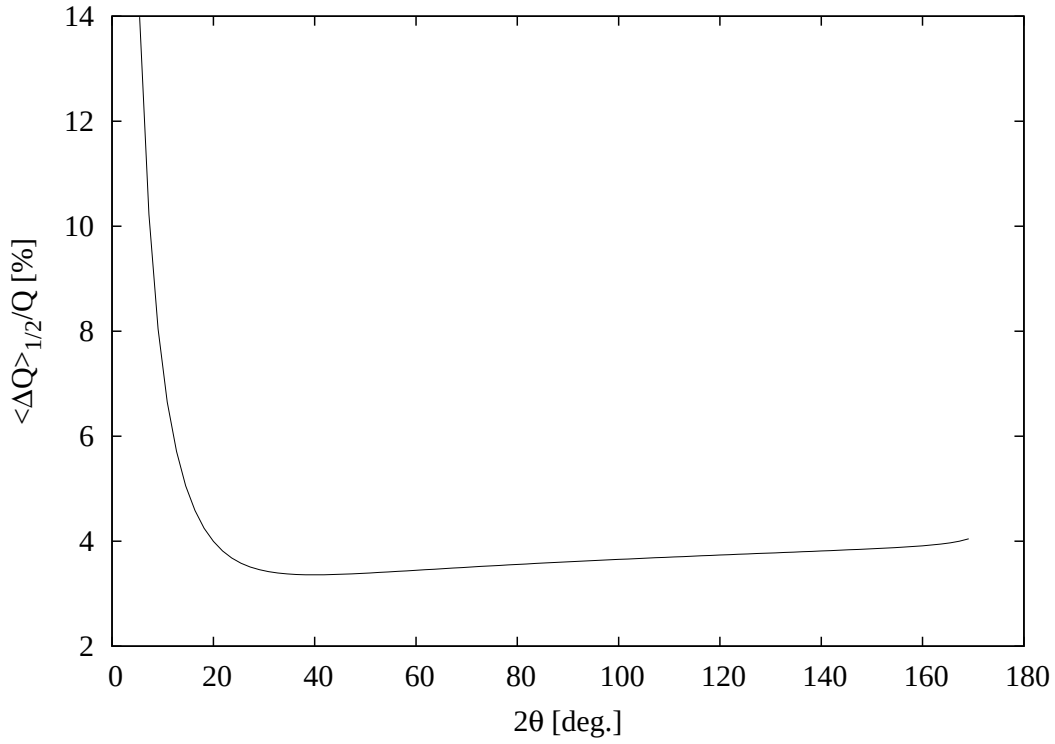

Figure 1.4: FWHM of resolution function ($\langle \Delta Q \rangle_{1/2} / Q$) as a function of scattering angle for $\alpha_1 = \alpha_2 = \alpha_3 = \beta = 0.5°$, $\lambda = 0.7$Å, and $2\theta_B = 22.3366°$. Note that this plot does not refer to any actual diffractometer, but is plotted simply to show how the resolution of a fixed wavelength diffractometer varies with scattering angle, 2θ. The resolution of any particular diffractometer will depend on the appropriate values of the above parameters.

Chapter 2

Overview of diffraction theory

2.1 Distribution functions

2.1.1 Radial distribution function, pair correlation function, and higher correlation functions

To characterise the structure of a disordered material, the simplest function that can be conceived is the radial distribution function (RDF), also sometimes called the pair distribution function (PDF) or pair correlation function (PCF). Formally there is a distinction between the radial distribution function, $g(r)$, and the pair correlation function, $g(\mathbf{r})$, in that

$$g(r) = \langle g(\mathbf{r}) \rangle_\Omega \tag{2.1}$$

where the average is over the directions of $\mathbf{r}$.

So what exactly is $g(r)$ or $g(\mathbf{r})$? Sometimes $g(\mathbf{r})$ is described as the probability of two atoms being separated by the displacement $\mathbf{r}$, but strictly $g(\mathbf{r})$ is not a probability. We suppose the number density at some position in the material is $\mathbf{r}$ is $n(\mathbf{r})$. The position of atom j is given by $\mathbf{R}_j$ in which case the local number density can be expressed as

$$n(\mathbf{r}) = \sum_i \delta(\mathbf{r} - \mathbf{R}_i) \tag{2.2}$$

If we roam around the material at the atomic level and it is crystalline we will see a regular fluctuation in the density caused by the repeated structure of the unit cell. However if it is a liquid or a glass there is no such regular order and all we will see is the random distribution of the atoms, except that there can be no atomic overlaps (unless the pressure is enormously high). This means that the centre of each atom is surrounded by a void caused by the repulsive interaction that takes over when atoms get too close to one another. Beyond that we would struggle to see very much because the arrangement of atoms would vary so much from place to place.

In order to learn more about how the atoms are arranged in the material we have to perform an *autocorrelation* on this density distribution:

$$G(\mathbf{r}) = \frac{1}{N}\int d\mathbf{r} n(\mathbf{r}')n(\mathbf{r}'+\mathbf{r}) = \frac{1}{N}\sum_{ij}\delta(\mathbf{r}+\mathbf{R}_j-\mathbf{R}_i) \tag{2.3}$$

where the last equality arises from substituting (2.2) into the middle term. It will be apparent that the terms with $j = i$ can be separated from those where $j \neq i$. Hence we write

$$\begin{aligned} G(\mathbf{r}) &= \delta(\mathbf{r}) + \frac{1}{N}\sum_{i\neq j}\delta(\mathbf{r}+\mathbf{R}_j-\mathbf{R}_i) \\ &= \delta(\mathbf{r}) + \rho g(\mathbf{r}) \end{aligned} \tag{2.4}$$

where ρ is the average atomic number density (typically expressed in units of atoms per Å^3). It can be seen therefore that $G(\mathbf{R})$ divides into two parts, a "self" part involving correlations of an atom with itself, and a "distinct" part involving correlations between distinct atoms.

(2.4) acts as the formal definition for $g(\mathbf{r})$. In effect you are sitting on an atom and counting all the atoms that you find at a given displacement, $\mathbf{r}$, from that atom, converting that number to a local density. This local density is then averaged over all the atoms in the system and compared with the density of atoms in the system as a whole. Therefore $g(\mathbf{r})$ is a convenient way of keeping track of how the local number density varies with respect to an atom on average and with respect to the average number density.

The properties of the Dirac δ-function are such that

$$\int \delta(\mathbf{r})d\mathbf{r} = 1.0 \tag{2.5}$$

which means that $\delta(\mathbf{r})$ is a density. This term arises from the fact that every atom must correlate with itself at $\mathbf{r} = 0$. It doesn't tell us anything about how the atoms are distributed in the material, but it does have an important bearing on the radiation scattering properties of the material.

Sometimes $g(\mathbf{r})$ is written as $g_2(\mathbf{r}_1, \mathbf{r}_2)$ to emphasize that it is the correlation between two atoms at positions $\mathbf{r}_1$ and $\mathbf{r}_2$ respectively, with $\mathbf{r} = \mathbf{r}_2 - \mathbf{r}_1$. It is possible to define a hierarchy of such correlation functions, which are related to one another, Hansen and MacDonald [1986], Cusack [1987]. Thus $g_3(\mathbf{r}_1, \mathbf{r}_2, \mathbf{r}_3)$ is the correlation between three atoms at the positions $\mathbf{r}_1$, $\mathbf{r}_2$ and $\mathbf{r}_3$, with

$$g_2(\mathbf{r}_1, \mathbf{r}_2) = \frac{1}{N-2}\rho\int g_3(\mathbf{r}_1, \mathbf{r}_2, \mathbf{r}_3)d\mathbf{r}_3 \tag{2.6}$$

and N is the number of atoms in the system.

As pointed out by Cusack [1987], equation 2.6 alerts us to the possible dangers in what we are about to do. In particular several or a range of $g_3(\mathbf{r}_1, \mathbf{r}_2, \mathbf{r}_3)$ functions might give

rise to the same $g_2(\mathbf{r}_1, \mathbf{r}_2)$ function. If the only information we have to go on is based on $g_2(\mathbf{r}_1, \mathbf{r}_2)$ we might come away with an incorrect picture of the local order in the system being investigated. More will be said about this important point in later chapters as much of the controversy about structure in liquids and glasses arises from the attempt to interpret $g_2(\mathbf{r}_1, \mathbf{r}_2)$ in terms of many body correlations.

For isotropic atomic liquids far away from any boundaries, the directional dependence of $\mathbf{r}$ can be ignored since on average the correlation function will look the same whichever direction we look, so that $g(\mathbf{r}) \equiv g(r)$, that is the pair correlation function and the radial distribution function become the same thing. For molecular systems this is not true in general, since the pair correlation function around a molecule may well look different depending on which direction away from the molecule at the origin we look, irrespective of whether the molecule is near a surface or in the bulk material.

What does $G(\mathbf{r})$ look like? Figure 2.1 gives 1- and 2- dimensional representations of this function for liquid nickel (Schenk et al. [2002]). We note that at the core, for $r < \sim 2$Å, the distribution function goes to zero, due to the impossibility of two different nickel atoms occupying the same space. Beyond this a series of ripples emanate out, rather like ripples on a pond when a stone is dropped in it. These ripples arise as a result of the sharp "repulsive" interaction at short distances caused by the atom at the origin, which prevents other atoms overlapping it. This repulsive interaction sets up a reaction in the local distribution of atoms, which also cannot overlap each other. Bear in mind however that unlike the ripples on a pond, the density fluctuations here occur in a sphere in 3-dimensions. The graphs in Fig 2.1 are essentially 1- and 2-dimensional sections through that sphere.

The $\delta(\mathbf{r})$ in $G(\mathbf{r})$ is shown in Fig 2.1 (bottom) as the small white dot at the centre of the plot. Also, at large enough $\mathbf{r}$, there are no correlations between atoms so $G(\mathbf{r}) = \rho$, that is it becomes a uniform distribution. Hence we can rewrite the pair correlation function as:

$$G(\mathbf{r}) = \delta(\mathbf{r}) + \rho(1 + h(\mathbf{r})) \tag{2.7}$$

where $h(\mathbf{r}) \equiv g(\mathbf{r}) - 1$ is sometimes called the *total* correlation function. Therefore $h(\mathbf{r})$ is well behaved at both $\mathbf{r} = 0$ and $\mathbf{r} = \infty$, going to -1 and 0 at these limits respectively. It is $h(\mathbf{r})$ that contains the structural information about a liquid or glass that we seek and it specifically does not include the correlation of the atoms with themselves.

2.1.2 Multicomponent systems.

One generalisation of the functions of the previous sections is needed. As defined $g(\mathbf{r})$ is the pair correlation function for all the atoms of the system. If there is more than one atom type (oxygen, silicon, carbon, germanium, etc.) present then it is useful to split the pair correlation function into several terms, one for each pair of atom types. This was first suggested by Faber and Ziman [1965] and we shall use definitions analogous to theirs throughout. Hence $g_{\alpha\beta}(\mathbf{r})$ would be the pair correlation function between atoms of type α

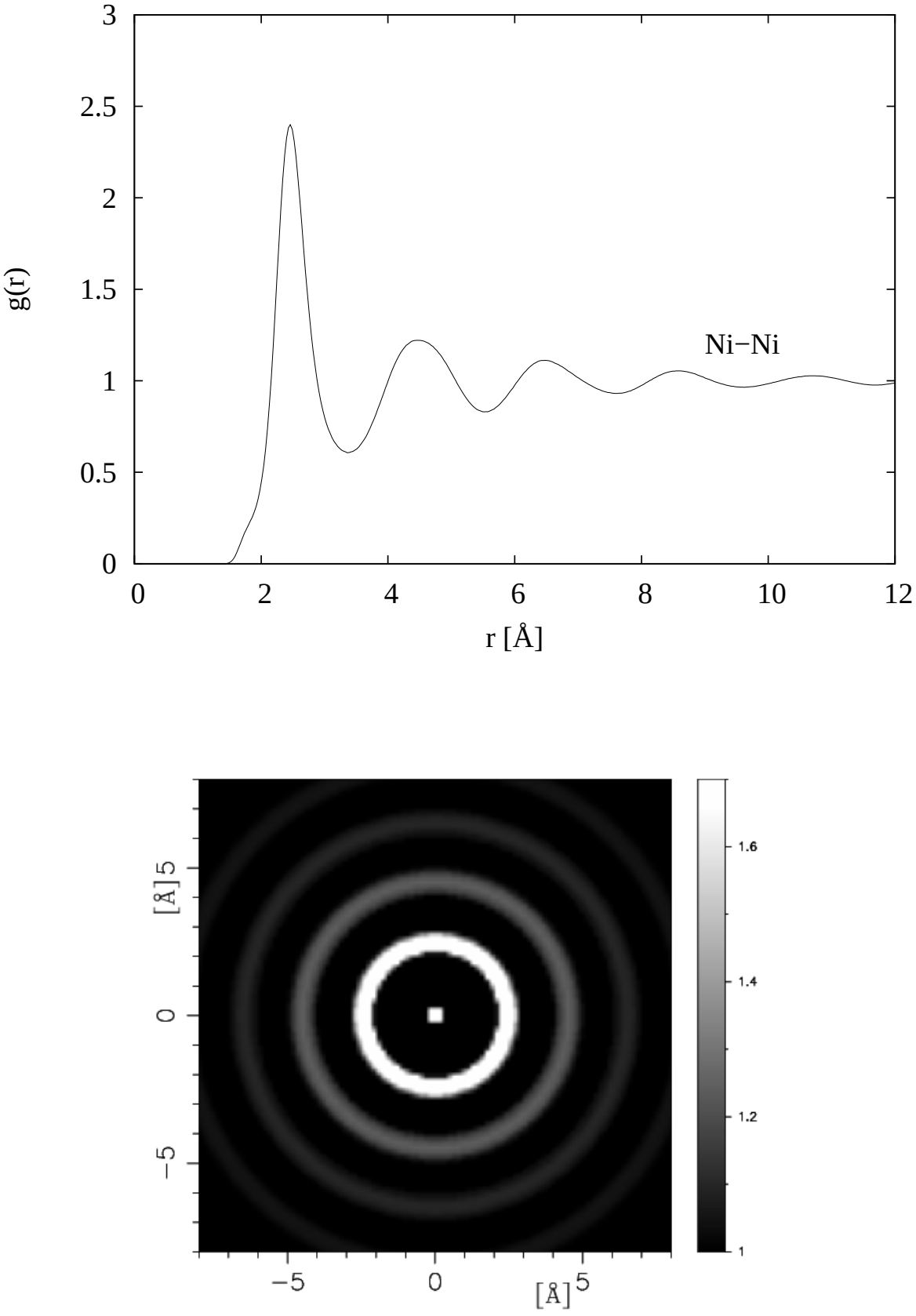

Figure 2.1: Radial distribution function, $g(r)$, for supercooled liquid nickel shown in 1-dimensional (top) and 2-dimensional (bottom) representations. Derived from data shown in Schenk et al. [2002], Lee et al. [2004]

and β. If there are J distinct atom types in the system, then the number of distinct pair correlation functions is $J(J+1)/2$.

It doesn't matter which order α and β are specified since by definition

$$g_{\alpha\beta}(\mathbf{r}) \equiv g_{\beta\alpha}(-\mathbf{r}) \tag{2.8}$$

from which follows

$$g_{\alpha\beta}(r) \equiv g_{\beta\alpha}(r) \tag{2.9}$$

In terms of these site-site correlation functions the full autocorrelation function of the system would be defined as:

$$G(\mathbf{r}) = \sum_{\alpha} c_\alpha \delta(\mathbf{r}) + \rho \sum_{\alpha,\beta \geq \alpha} (2 - \delta_{\alpha\beta}) c_\alpha c_\beta g_{\alpha\beta}(\mathbf{r}) \tag{2.10}$$

where $c_\alpha = \rho_\alpha/\rho$ and ρ_α is the number density of atoms of type α. The Kronecker $\delta_{\alpha\beta}$ is needed in (2.10) to avoid double counting pairs of atoms of the same type. The atomic fractions are needed to take account of the different percentages of the different types of atom present.

Once again it is standard to write

$$g_{\alpha\beta}(\mathbf{r}) = 1 + h_{\alpha\beta}(\mathbf{r}) \tag{2.11}$$

with $h_{\alpha\beta}(\mathbf{r})$ the site-site total pair correlation function between atoms of type α and β.

2.1.3 Coordination numbers

Based on the pair correlation function or radial distribution function, it is possible to calculate the number of atoms that coordinate a given atom at the origin. This is called the coordination number, $N(r_{min}, r_{max})$, and is defined relative to some specified distance range, r_{min} to r_{max}, after integrating over all the directions of $\mathbf{r}$:

$$N(r_{min}, r_{max}) = \rho \int_{r_{min}}^{r_{max}} g(\mathbf{r}) d\mathbf{r} = 4\pi\rho \int_{r_{min}}^{r_{max}} r^2 g(r) dr \tag{2.12}$$

In Fig. 2.1 the number density of the supercooled liquid Ni was 0.0843 atoms/Å^3, so that integrating over the first peak in $g(r)$ gives a coordination number $N(1.0, 3.7) \approx 13.2$ atoms.

Coordination numbers in a multicomponent system are defined in an exactly analogous manner to Eq. 2.12. The number of β-type atoms around an α-type atom at the origin would be given by:

$$\begin{aligned} N_{\alpha\beta}(r_{min}, r_{max}) &= 4\pi\rho_\beta \int_{r_{min}}^{r_{max}} r^2 g_{\alpha\beta}(r) dr \\ &= 4\pi c_\beta \rho \int_{r_{min}}^{r_{max}} r^2 g_{\alpha\beta}(r) dr \end{aligned} \tag{2.13}$$

Note however that unlike $g_{\alpha\beta}(r)$, in general $N_{\alpha\beta}(r_1, r_2) \neq N_{\beta\alpha}(r_1, r_2)$ because of the different prefactors outside the integral in each of these functions. In fact based on Eq. 2.13 and the equality Eq. 2.8 it is clear that $c_\alpha N_{\alpha\beta}(r_1, r_2) = c_\beta N_{\beta\alpha}(r_1, r_2)$, so that if one of these numbers is known, the other can be derived directly from the ratio of atomic fractions:

$$N_{\beta\alpha}(r_1, r_2) = \frac{c_\beta}{c_\alpha} N_{\alpha\beta}(r_1, r_2) \tag{2.14}$$

2.1.4 Fluctuations

An intrinsic quality of a disordered material is that its density is not everywhere constant, but varies from place. Measured over the size of a typical sample of the material, e.g. 10^{-2}m, these fluctuations in density are very small, but measured over dimensions comparable to with the dimensions of atoms, i.e. 10^{-9}m, the fluctuations can become extremely large, varying by factors of 2 or 3 or even more. In addition for a liquid, these fluctuations have a temporal quality, caused by both the intrinsic disorder in the material and the fact that the atoms and molecules in the liquid are diffusing from place to place in a series of random - Brownian - motions.

It is easy to forget just how fast this diffusion really is. Looking out over a calm lake at sunset, we might say the water is "still". Yet in reality, the individual water molecules are far from still. The self diffusion constant for water is $\approx 2 \times 10^{-5}\text{cm}^2\text{s}^{-1}$. This means after one second a water molecule has diffused $\approx 45\mu$m. If we assume a water molecule has a diameter of 0.3nm, this implies on average a water molecule will diffuse $\approx$ 150,000 molecular diameters in one second! By any macroscopic scale this is a huge distance. Of course one might argue that the timescale for a water molecule is much shorter than our own, which is correct. But the point is that on a macroscopic timescale of seconds, the water molecules are moving around over huge distances relative to their size.

The magnitude of these density fluctuations is captured precisely in the theory of liquids. If $N(V)$ is the number of atoms found in a particular volume V, then it can be shown for a monatomic system that

$$\begin{aligned} \lim_{V\to\infty} \frac{\langle (N(V) - \langle N(V)\rangle)^2\rangle}{\langle N(V)\rangle} &= \rho k_B T \chi_T \\ &= 1 + 4\pi\rho \int_0^\infty r^2 \left(g(r) - 1\right) \mathrm{d}r \end{aligned} \tag{2.15}$$

where k_B is Boltzmann's constant, χ_T is the isothermal compressibility and the angle brackets represent ensemble averages. This equation shows that there is an integral link between the structure and the thermodynamics. This value is also called the "zero limit", $S(0)$, since it represents the value of the structure factor at $Q = 0$ - see equation (2.19 in the next section.

For multicomponent systems the situation is more complicated since not only are there density fluctuations but also there will now be concentration fluctuations. These concentration fluctuations are represented in the thermodynamics via the so-called Kirkwood-Buff

integrals:

$$\begin{aligned} G_{\alpha\beta} &= 4\pi \int r^2 \left(g_{\alpha\beta}(r) - 1\right) \mathrm{d}r \\ &= V \left(\frac{\langle N_\alpha N_\beta \rangle - \langle N_\alpha \rangle \langle N_\beta \rangle}{\langle N_\alpha \rangle \langle N_\beta \rangle} - \frac{\delta_{\alpha\beta}}{\langle N_\alpha \rangle} \right) \end{aligned} \tag{2.16}$$

A useful reference in this regard is Ben-Naim [2006], where more details of the application of these integrals can be found. An alternative representation of concentration fluctuations for two-component systems in terms of number-number, concentration-concentration, and number-concentration structure factors is given by the Bhatia-Thornton representation, see Cusack [1987]. The concentration-concentration structure factors have been further generalised to multi-component systems, Gazzillo [1994].

2.2 Radiation diffraction theory

2.2.1 The differential scattering cross section and structure factor.

Figure 1.1 showed the schematic layout of a diffraction experiment. After corrections for attenuation, multiple scattering, recoil scattering, detector efficiency, polarization, and so on, the quantity measured in a radiation diffraction experiment is called the differential scattering cross-section, $\left(\frac{d\sigma}{d\Omega}\right)(\lambda, 2\theta)$. The primary purpose of the present account is to learn how we extract this quantity from the raw diffraction data.

Fig. 2.2 shows a typical structure factor (after all corrections) for crystalline and liquid nickel. It is from data such as this that the radial distribution functions shown in Fig. 2.1 must be derived.

The scattered radiation amplitude from an array of N point atoms at positions $\mathbf{R}_1 \cdots \mathbf{R}_N$ is given by $A(\mathbf{Q}) = \sum_j b_j \exp(i\mathbf{Q} \cdot \mathbf{R}_j)$, where b_j is the scattering length or form factor for atom j. For neutron scattering b is simply a number which however depends on the spin and isotope state of the nucleus. For x-rays or electrons, or when scattering from magnetic materials with neutrons, the scattering length is called "the atomic form factor", which is Q dependent, and which is usually given the symbol $f(Q)$. [1] Hence the scattered intensity per unit atom, otherwise called the structure factor, is:

$$\begin{aligned} F(\mathbf{Q}) &= \frac{1}{N} \left| A(\mathbf{Q}) \right|^2 \\ &= \frac{1}{N} \sum_{jk} b_j b_k \exp[i\mathbf{Q} \cdot (\mathbf{R}_j - \mathbf{R}_k)] \end{aligned} \tag{2.17}$$

[1] Strictly speaking the atomic form factor is the scattering length of the atom divided by the scattering length of a single electron, and so is a dimensionless number. X-ray differential cross sections are therefore normally quoted in the units of electrons^2 per atom per steradian, since the value of $f_0(Q) = Z$, i.e. the atomic number of the atom.

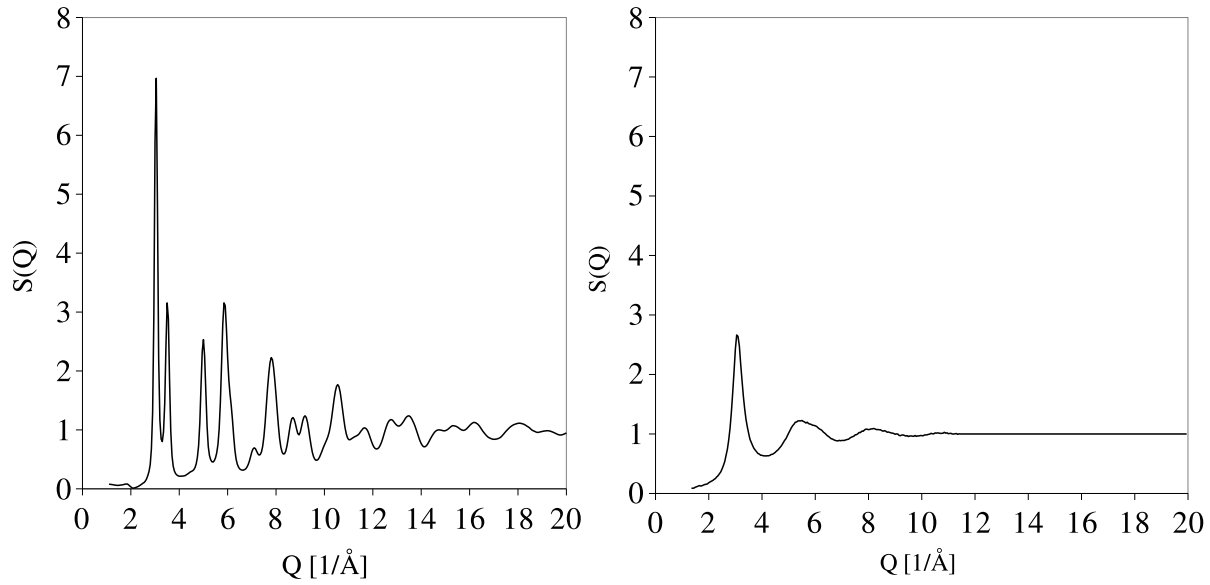

Figure 2.2: Comparison of diffraction pattern from crystalline nickel (left) with that from supercooled liquid nickel (right), Schenk et al. [2002]. Both datasets are on the same scale. Note the much weaker amplitude of the peaks in the liquid compared to the crystal.

Here $\mathbf{Q}$ represents the change in wave vector between incident ($\mathbf{k}_i$) and scattered ($\mathbf{k}_f$) radiation beams. Thus $\mathbf{Q} = \mathbf{k}_i - \mathbf{k}_f$ and the modulus $|\mathbf{Q}| = Q = 4\pi\dfrac{\sin\theta}{\lambda}$, where 2θ is the scattering angle and λ is the radiation wavelength. Note that, as in the definition of the autocorrelation function (2.4), the sum in (2.17) can be divided into two parts, namely terms for which $j = k$, the so-called 'self' terms, and terms for which $j \neq k$, the distinct or interference terms. Hence the scattering experiment is in effect counting the atoms as a function of displacement from an atom at the origin. The main distinction between (2.17) and (2.4) is that now each term is weighted by the product of the scattering lengths of the two atoms at the end of the vector $(\mathbf{R}_j - \mathbf{R}_k)$.

Using (2.10) the discrete sum in (2.17) can be replaced by integrals, with the each term being weighted by the corresponding product of scattering lengths and collecting together terms which involve the same pair of atom types:

$$F(\mathbf{Q}) = \sum_{\alpha} c_\alpha b_\alpha^2 + \sum_{\alpha\beta \geq \alpha} (2 - \delta_{\alpha\beta}) c_\alpha c_\beta b_\alpha b_\beta S_{\alpha\beta}(\mathbf{Q}) \tag{2.18}$$

with the partial structure factors defined by

$$S_{\alpha\beta}(\mathbf{Q}) = \rho \int g_{\alpha\beta}(\mathbf{r}) \exp(i\mathbf{Q}\cdot\mathbf{r}) d\mathbf{r} \tag{2.19}$$

which becomes

$$\begin{aligned} S_{\alpha\beta}(Q) &= \langle S_{\alpha\beta}(\mathbf{Q})\rangle_{\Omega} \\ &= 4\pi\rho \int r^2 g_{\alpha\beta}(r) \frac{\sin Qr}{Qr} dr \end{aligned} \tag{2.20}$$

for an isotropic system.

The average in (2.20) is over the orientations of $\mathbf{r}$ with respect to $\mathbf{Q}$, and the second equality is allowed on the understanding that $g(\mathbf{r})$ is isotropic with respect to these orientations. In short, the diffraction pattern is a 3-dimensional Fourier transform of the pair correlation function, weighted by the scattering lengths or form factors for each pair of atoms. If, as in molecular liquids, the pair correlation function is a function of the orientation of $\mathbf{r}$ then this orientational information is obscured in the scattering process, Gray and Gubbins [1984]. This is not however to say there is no orientational information in the diffraction data from molecular liquids, as will be shown later.

The Fourier transform of a constant in r-space is a δ-function in Q

$$\int \exp(i\mathbf{Q}\cdot\mathbf{r}) d\mathbf{r} = \delta(\mathbf{Q}). \tag{2.21}$$

Hence, using (2.11), the partial structure factors become

$$S_{\alpha\beta}(\mathbf{Q}) = \rho\delta(\mathbf{Q}) + H_{\alpha\beta}(\mathbf{Q}) \tag{2.22}$$

where

$$H_{\alpha\beta}(\mathbf{Q}) = \rho \int h_{\alpha\beta}(\mathbf{r}) \exp(i\mathbf{Q}\cdot\mathbf{r}) d\mathbf{r} \tag{2.23}$$

or

$$H_{\alpha\beta}(Q) = 4\pi\rho \int_0^{\infty} r^2 h_{\alpha\beta}(r) \frac{\sin Qr}{Qr} dr \tag{2.24}$$

Including these definitions in (2.20 leads to the final expression:

$$\begin{aligned} F(Q) &= \langle F(\mathbf{Q})\rangle_{\Omega} \\ &= \sum_{\alpha} c_\alpha b_\alpha^2 + \sum_{\alpha\beta\geq\alpha} (2-\delta_{\alpha\beta})\, c_\alpha c_\beta b_\alpha b_\beta \left[\delta(\mathbf{Q}) + H_{\alpha\beta}(Q)\right] \end{aligned} \tag{2.25}$$

It will be seen that the $\delta(\mathbf{r})$ in (2.4) or (2.10) has become a constant independent of Q in $F(Q)$ while the constant level of 1.0 in $g(\mathbf{r})$ or $g_{\alpha\beta}(\mathbf{r})$ has become a $\delta(\mathbf{Q})$ function in reciprocal (Q) space. Hence the self correlation of atoms gives rise to a scattering level determined only by the product of scattering lengths or form factors for each atom type, while the distinct correlations (correlations between different atoms), as represented by the total correlation function, $h_{\alpha\beta}(r)$, give rise to oscillations about this constant level.

Traditional practice is that the $\delta(\mathbf{Q})$ function in (2.25) is not shown, since it can never be observed. Nonetheless its presence should not be ignored because it plays a fundamental role in the theory of small angle scattering Glatter and Kratky [1982].

With neutron scattering there is a subtlety to the expression for the differential cross section (2.25) in that the neutron scattering length is dependent on the spin and isotope state of the atomic nuclei. This means the expression for $F(Q)$ has to be averaged over the spin and isotope states of the atomic nuclei. Assuming the spin and isotope states are uncorrelated with the positions of the atoms, then the general expression for the structure factor becomes:

$$\begin{aligned} F_n(Q) &= \sum_{\alpha} c_\alpha \left\langle b_\alpha^2 \right\rangle \\ &\quad + \sum_{\alpha\beta \geq \alpha} (2 - \delta_{\alpha\beta})\, c_\alpha c_\beta \left\langle b_\alpha \right\rangle \left\langle b_\beta \right\rangle [\delta(\mathbf{Q}) + H_{\alpha\beta}(Q)] \end{aligned} \tag{2.26}$$

where the angle brackets represent the spin and isotope averages. Since this averaging is done inside the product of scattering lengths for the self terms, but outside the product for the distinct terms, in general the weighting term on the self terms will be different from the that on the corresponding distinct terms. The difference $\langle b^2 \rangle - \langle b \rangle^2$ is sometimes referred to as the "incoherent" scattering, although this terminology is not generally useful. More importantly there are some instances where the nuclear spins *do* correlate with nuclear position - molecular hydrogen at low temperature is a case in point, in which case the simple expression (2.26) becomes more complex Sears [1966].

The form (2.25) contains a hidden approximation, sometimes called the "static" approximation. The point is that in real experiments, the radiation will either lose energy to the scattering system or gain energy from the scattering system. This is called "inelastic" scattering. The approximation we make is that the *change* in energy of the incident radiation in scattering from the sample is *small* compared to its incident energy. This approximation has been discussed extensively for both x-rays and neutrons by numerous authors, see for example Compton [1923], Placzek [1952], Powles [1979], Egelstaff [1987], Egelstaff and Soper [1980], Howe et al. [1989]. It will be discussed a little more in section 2.3, where we describe briefly what can be done to alleviate the problems caused by inelasticity in the scattering process. For the time being we assume the "static" approximation holds, i.e. we will ignore inelasticity effects, though we should always be aware that these may be present in our data.

For x-rays, there is no spin or isotope dependence of the atomic form factors, so the x-ray structure factor is written as:-

$$\begin{aligned} F_x(Q) &= \sum_{\alpha} c_\alpha f_\alpha^2(Q) \\ &\quad + \sum_{\alpha\beta \geq \alpha} (2 - \delta_{\alpha\beta})\, c_\alpha c_\beta f_\alpha(Q) f_\beta(Q) [\delta(\mathbf{Q}) + H_{\alpha\beta}(Q)] \end{aligned} \tag{2.27}$$

2.2.2 Sum rules and the role of the self scattering in data normalisation

Although it is usually treated as a background which has to be subtracted from the diffraction data, the self scattering actually provides an important constraint on the distinct scattering. The point is that from (2.17) the structure factor must always be ≥ 0, whatever values the scattering lengths or atomic form factors adopt, and irrespective of whether or not there is incoherent scattering. From (2.25) this means that

$$\sum_{\alpha} c_\alpha b_\alpha^2 + \sum_{\alpha,\beta\geq\alpha} (2-\delta_{\alpha\beta}) c_\alpha c_\beta b_\alpha b_\beta H_{\alpha\beta}(\mathbf{Q}) \geq 0,\ \mathbf{Q}>0 \tag{2.28}$$

or

$$\sum_{\alpha,\beta\geq\alpha} (2-\delta_{\alpha\beta}) c_\alpha c_\beta b_\alpha b_\beta H_{\alpha\beta}(\mathbf{Q}) \geq -\sum_{\alpha} c_\alpha b_\alpha^2,\ \mathbf{Q}>0 \tag{2.29}$$

There is a further sum rule that can be derived, namely following 2.17 we write

$$F_{\alpha\alpha}(\mathbf{Q}) = \frac{1}{N_\alpha}\left|\sum_{j_\alpha} \exp[i\mathbf{Q}\cdot\mathbf{R}_{j_\alpha}]\right|^2 \geq 0 \tag{2.30}$$

where the sum is *only* over α-type atoms, of which there are N_α. Comparing this with 2.18 and using (2.22) it follows that

$$H_{\alpha\alpha}(\mathbf{Q}) \geq -\frac{1}{c_\alpha},\ \mathbf{Q}>0 \tag{2.31}$$

There appears to be no equivalent sum rule on the individual cross terms, $H_{\alpha\beta}(\mathbf{Q})$, but combining 2.31 with 2.29 it is seen that

$$\sum_{\alpha,\beta>\alpha} 2c_\alpha c_\beta b_\alpha b_\beta H_{\alpha\beta}(\mathbf{Q}) \geq -\sum_{\alpha} c_\alpha b_\alpha^2 - \sum_{\alpha} c_\alpha^2 b_\alpha^2 H_{\alpha\alpha}(\mathbf{Q}),\ \mathbf{Q}>0 \tag{2.32}$$

For the neutron differential cross section Eq. 2.26 it should be noted that the positivity of the differential cross section must apply irrespective of whether there is incoherent neutron scattering or not. Hence we write

$$\sum_{\alpha,\beta\geq\alpha} (2-\delta_{\alpha\beta}) c_\alpha c_\beta \langle b_\alpha\rangle \langle b_\beta\rangle H_{\alpha\beta}(\mathbf{Q}) \geq -\sum_{\alpha} c_\alpha \langle b_\alpha\rangle^2 \quad ,\ \mathbf{Q}>0 \tag{2.33}$$

while for x-rays the rule is

$$\sum_{\alpha,\beta\geq\alpha} (2-\delta_{\alpha\beta}) c_\alpha c_\beta f_\alpha(Q) f_\beta(Q) H_{\alpha\beta}(\mathbf{Q}) \geq -\sum_{\alpha} c_\alpha f_\alpha^2(Q) \quad ,\ \mathbf{Q}>0 \tag{2.34}$$

In other words the distinct or interference scattering will oscillate about a baseline set by the coherent self scattering for both neutrons and x-rays. Therefore it makes sense to generate a normalised distinct structure factor relative to this baseline, namely

$$F_{norm}^{(n)}(\mathbf{Q}) = \left(\left(\frac{d\sigma}{d\Omega} \right)^{(n)} (\lambda, 2\theta) - \left(\frac{d\sigma}{d\Omega} \right)_{self}^{(n)} (\lambda, 2\theta) \right) / \sum_{\alpha} c_\alpha \langle b_\alpha \rangle^2 \tag{2.35}$$

for neutrons, and

$$F_{norm}^{(x)}(\mathbf{Q}) = \left(\left(\frac{d\sigma}{d\Omega} \right)^{(x)} (\lambda, 2\theta) - \left(\frac{d\sigma}{d\Omega} \right)_{self}^{(x)} (\lambda, 2\theta) \right) / \sum_{\alpha} c_\alpha f_\alpha^2(Q) \tag{2.36}$$

for x-rays, where $\left(\frac{d\sigma}{d\Omega} \right)_{self}^{(n)} (\lambda, 2\theta) = \sum_\alpha c_\alpha \langle b_\alpha^2 \rangle$ and $\left(\frac{d\sigma}{d\Omega} \right)_{self}^{(x)} (\lambda, 2\theta) = \sum_\alpha c_\alpha f_\alpha^2(Q)$. Note that the inequalities (2.33) and (2.34) must hold, whatever values of the scattering lengths or form factors are used. With these definitions, it is seen that $F_{norm}(\mathbf{Q}) \geq -1$ and the distinct scattering oscillates around zero for all $\mathbf{Q}$, as expected for a distinct structure factor, 2.22, for both neutrons and x-rays. This is not particularly important for neutrons in the static approximation, since the neutron differential cross section will in any case oscillate about a constant. For x-rays however it is important due to the pronounced Q dependence of the form factors.

Traditionally, X-ray diffraction data are not normalised as per 2.36 but as

$$F_{norm}^{(x)}(\mathbf{Q}) = \frac{\left(\left(\frac{d\sigma}{d\Omega} \right)^{(x)} (\lambda, 2\theta) - \left(\frac{d\sigma}{d\Omega} \right)_{self}^{(x)} (\lambda, 2\theta) \right)}{\left(\sum_\alpha c_\alpha f_\alpha(Q) \right)^2} \tag{2.37}$$

With this latter definition however it is not possible to ensure that $F_{norm}^{(x)}(\mathbf{Q}) \geq -1$, nor that the distinct scattering oscillates about $F_{norm}^{(x)}(\mathbf{Q}) = 0$ for all $\mathbf{Q}$. Hence (2.36) is the preferred normalisation for x-ray diffraction data. Figure 2.3 shows the consequence on the baseline of the distinct structure factor of using this traditional x-ray normalisation compared to that proposed in (2.36) for SiO_2.

2.2.3 Isotope substitution and other methods

It has been seen in section 2.2.1 that for neutron scattering, the differential scattering cross section depends on the isotope state of the scattering nucleus. This fact has been widely exploited in studies of multicomponent systems, particularly binary systems, to attempt to extract the individual partial structure factors, Enderby et al. [1966], Edwards et al. [1975], Biggin and Enderby [1981]. In essence the idea is to measure the diffraction pattern from several otherwise identical samples which contain different amounts of isotopes for one or more of the components. Each diffraction pattern will emphasise different partial structure

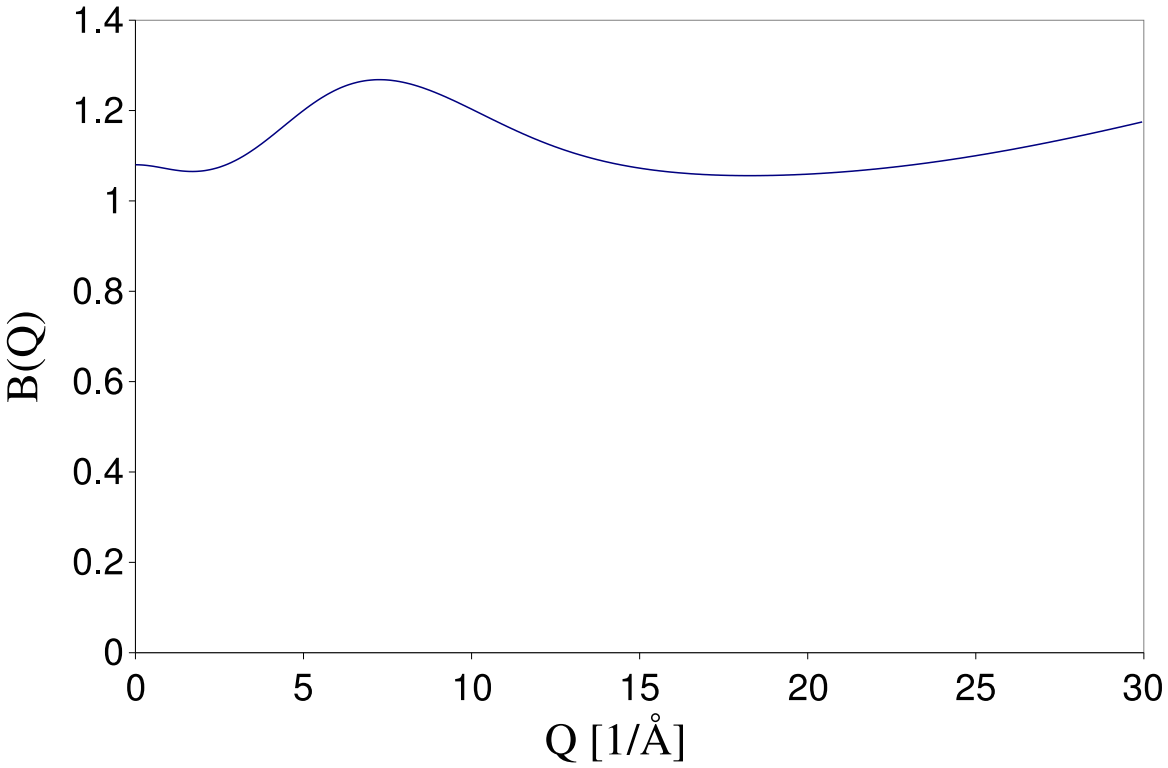

Figure 2.3: Baseline, $B(Q) = \frac{\sum_\alpha c_\alpha f_\alpha^2(Q)}{\left(\sum_\alpha c_\alpha f_\alpha(Q)\right)^2}$ as a function of Q about which the normalised x-ray distinct structure factor for SiO_2 oscillates if the x-ray diffraction data are normalised according to (2.37) instead of (2.36). In this case $\alpha =$ Si and O, and $c_{Si} = \frac{1}{3}$ and $c_O = \frac{2}{3}$

factors, depending on the precise values of the neutron scattering lengths for each isotope. Then, by inverting the matrix of neutron scattering weights, one can in principle obtain the partial structure factors by summing the diffraction cross sections after multiplying them by the appropriate set of inversion factors. However, due the weak weighting of some of the partial structure factors this has to be done with some care, otherwise small systematic errors in the data can become blown up into large errors in the extracted partial structure factors. This effect has been studied in detail and various remedial approaches adopted, Edwards et al. [1975], Soper [2005, 2007]

Other ways to get information on partial structure factors out of the data include combined use of x-ray and neutron diffraction, about which more will be said in later chapters, or even in one case the joint use of neutron, x-ray and electron diffraction data, Palinkas et al. [1977]. Extended x-ray absorption fine structure (EXAFS) is of course a very widely used technique to extract information about correlations around a particular atomic site, but this topic is so well developed that it requires a separate treatment in its own right, Rehr and Albers [2000], Filipponi et al. [1995], Filipponi and DiCicco [1995]. Anomalous x-ray diffraction can be used in some cases, Price and Saboungi [2002], Ramos et al. [2005], where an absorption edge occurs at a sufficiently high x-ray energy.

2.3 Inelasticity effects

2.3.1 Neutron diffraction

As mentioned above the theory given in the preceding sections contains a fundamental assumption, namely that the neutron being scattered by the sample is so energetic that the gain or loss of energy that occurs as a result of the scattering event is immaterial compared to its starting energy. This is an ideal which unfortunately can never be realised in practice, particularly for light atoms like hydrogen where the exchange of energy is potentially large due to the comparable masses of the scattering nucleus and of the neutron. Further details of this interaction have been discussed fairly extensively in a recent review, Soper [2009]. The original analysis was due to Placzek [1952] which involved a Taylor expansion of the dynamic structure factor about its elastic value. This expansion however did not work for light atoms, and to this day there has been no fully successful method of removing these inelasticity effects.

The double differential scattering cross section for scattering into unit solid angle and per unit energy transfer was shown by Van Hove [1954] to be equal to $b^2\frac{k_f}{k_i}S(Q,\epsilon)$, where $S(Q,\epsilon)$ is the dynamic scattering law, ϵ is change in neutron energy after the scattering process, and b is the scattering length of the atom. Generalised to a multicomponent system, each of the static structure factors of equation (2.26) has its dynamic counterpart, dependent on (Q,ϵ), and with separate self and interference terms, $S_\alpha(Q,\epsilon), H_{\alpha\beta}(Q,\epsilon)$

respectively, with the sum rules

$$\int_{-\infty,\ \text{const.}Q}^{\infty} S_\alpha(Q,\epsilon)d\epsilon = 1.0 \tag{2.38}$$

$$\int_{-\infty,\ \text{const.}Q}^{\infty} H_{\alpha\beta}(Q,\epsilon)d\epsilon = H_{\alpha\beta}(Q) \tag{2.39}$$

Hence the full double differential scattering cross section for a multicomponent system is written as $\frac{d^2\sigma}{d\Omega d\epsilon} = \frac{k_f}{k_i}F_n(Q,\epsilon)$ where

$$\begin{aligned} F_n(Q,\epsilon) &= \sum_\alpha c_\alpha \left\langle b_\alpha^2 \right\rangle S_\alpha(Q,\epsilon) \\ &\quad + \sum_{\alpha\beta\geq\alpha} (2-\delta_{\alpha\beta})\, c_\alpha c_\beta \left\langle b_\alpha \right\rangle \left\langle b_\beta \right\rangle H_{\alpha\beta}(Q,\epsilon). \end{aligned} \tag{2.40}$$

The essence of Placzek's work was to show that inelasticity affects primarily the *self* scattering, leaving the distinct scattering only weakly affected. He came to this conclusion by deriving the first moment of each of these dynamic structure factors:

$$\int_{-\infty,\ \text{const.}Q}^{\infty} \epsilon S_\alpha(Q,\epsilon)d\epsilon = \frac{\hbar^2Q^2}{2M_\alpha} = E_{R,\alpha} \tag{2.41}$$

$$\int_{-\infty,\ \text{const.}Q}^{\infty} \epsilon H_{\alpha\beta}(Q,\epsilon)d\epsilon = 0.0, \tag{2.42}$$

where M_α is the mass of the scattering atom and $E_{R,\alpha}$ is referred to as the "recoil energy" of atom α. These equations show that whereas for the self scattering the energy transfer is finite and indeed increases parabolically with Q, the distinct scattering energy transfer always averages to zero, whatever the value of Q. This does not mean that distinct scattering is zero for finite energy transfer, but does mean there will be positive and negative contributions to the distinct scattering with increasing energy transfer, giving a net energy transfer of zero.

The conclusion that inelasticity affects primarily the self scattering seems to be borne out by the analysis of Soper [2009], even when light hydrogen is present in the scattering sample. This means that inelasticity contributes a Q-dependent self-scattering background to the differential scattering cross section, but it does not have a major impact on the distinct scattering which is being investigated. For cases where the Placzek expansion method does not work, experimenters typically use some sort of *ad hoc* polynomial method to remove this inelastic scattering, Fischer et al. [2006] or other method, Soper [2009]. Such a background subtraction procedure runs the risk of introducing systematic effects which have nothing to do with the structure of the material, and so the process of subtracting the self background has to be done with due caution.

2.3.2 Theory of time-of-flight diffraction

If k_i is the incident neutron wavevector and k_f is the scattered neutron wavevector, then conservation of momentum and energy in the nuclear collision require that the momentum transfer, $\hbar Q$, and energy transfer, ϵ, are given by

$$Q^2 = k_i^2 + k_f^2 - 2k_i k_f \cos 2\theta \tag{2.43}$$

$$\epsilon = \frac{\hbar^2}{2m}\left(k_i^2 - k_f^2\right) \tag{2.44}$$

where m is the mass of the neutron. For a fixed wavelength diffraction experiment k_i is defined by the incident beam monochromator, but for a time-of-flight (TOF) experiment the incident and final wavevectors are determined from the requirement that all neutrons that arrive at the detector in a given time channel have the same time-of-flight from the source. This constraint is satisfied by the condition

$$\frac{1+R}{k_e} = \frac{1}{k_i} + \frac{R}{k_f} \tag{2.45}$$

where R is the ratio of scattered to incident flight paths and k_e is the wavevector at zero energy transfer, i.e. $k_i = k_f$. Therefore k_e is determined from the total time-of-flight for a particular channel, and we define the elastic momentum transfer as

$$Q_e = 2k_e \sin\left(\frac{\theta}{2}\right) \tag{2.46}$$

Diffraction data from glasses and liquids are normally reported as a function of this elastic Q value, but it should be remembered they actually contain contributions from a range of Q values and energy transfers. It also should be noted that the fixed wavelength condition is recovered when R=0, i.e. zero scattered flight path, since then it takes no time for the neutrons to travel to the detector, so the time-of-flight fixes the incident wavevector, $k_i = k_e$.

Fig. 2.4 shows the trajectory in (Q, ϵ) space sampled by a time-of-flight neutron diffraction experiment on the SANDALS diffractometer at Isis at a scattering angle of 30.71° over a range of Q_e values. Also shown is the recoil energy of a proton, equation (2.41). The latter represents approximately the centroid of the scattering kernal for the self scattering of a proton, irrespective of whether it is bound to a molecule or not. It can be seen that a very wide range of Q and ϵ is sampled under all time-of-flight conditions. In particular the experiment explores energy transfers which go into 10s of eV which is well above any likely molecular vibration energies and enters the region of electronic excitations and molecular dissociation. At high Q_e the trajectories approach the ideal constant Q trajectory in the region of the recoil energy, but at low Q_e the trajectories become highly curved near $Q = Q_e$. Hence one might expect that inelasticity corrections are larger at low Q_e in the TOF experiment, as indeed is observed.

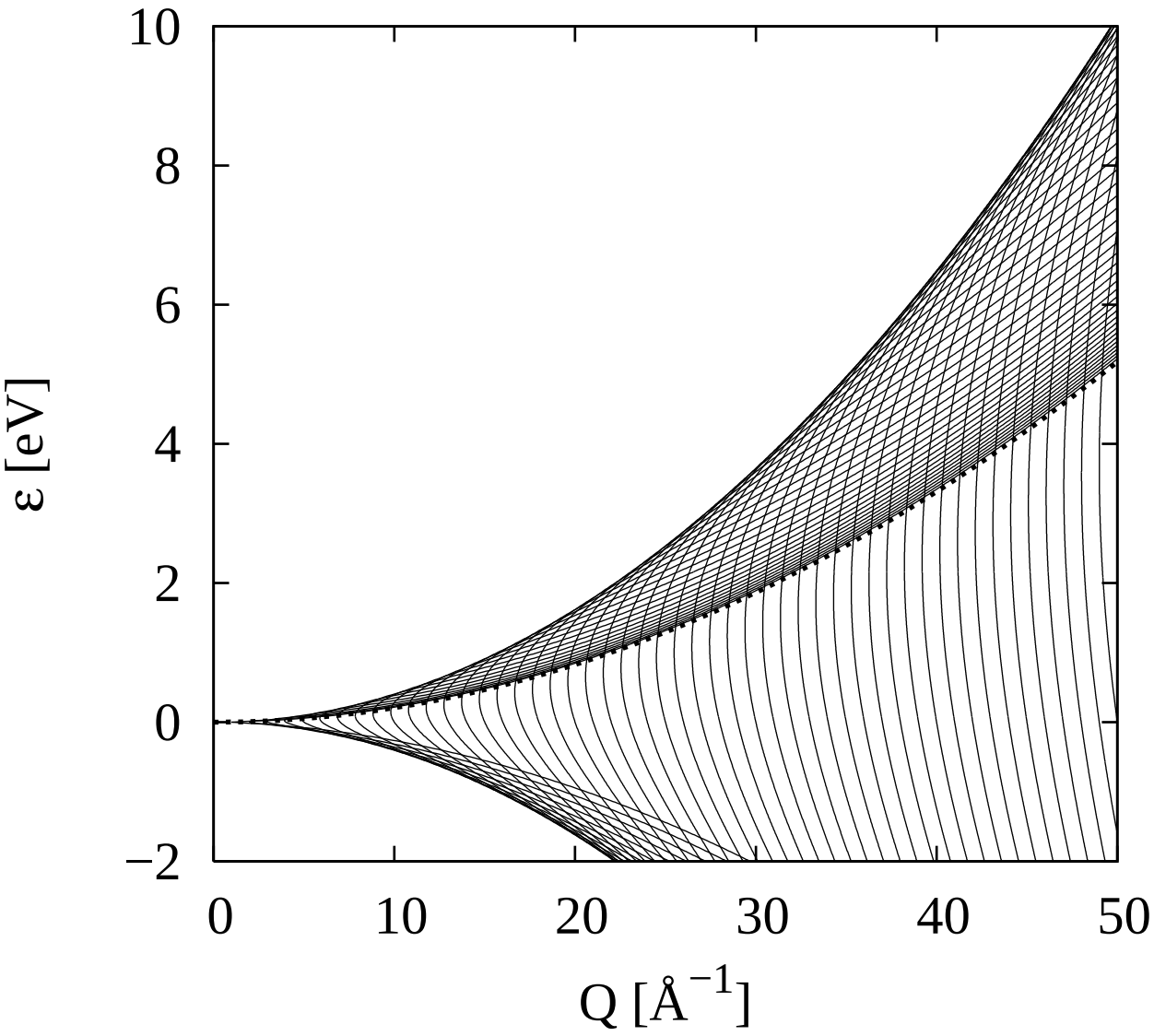

Figure 2.4: Constant time-of-flight trajectories sampled in a time-of-flight neutron diffraction experiment on the SANDALS diffractometer at ISIS at a scattering angle of 30.71°. The flight path ratio R is 0.134 in this case. Trajectories are shown for 50 values of Q_e in the range 0 - 50 Å^{-1} in steps of 1Å^{-1}. The dashed line shows the recoil energy of a proton: this is the centroid of the self scattering kernel for a hydrogen atom. The upper and lower limits on the energy transfer for any given Q value are set by the kinematic equations, 2.43 and 2.44, and the scattering angle of the detector: as the scattering angle is made smaller, these lines become further apart, and the (Q, ϵ) trajectories become more parallel to the ϵ-axis, implying that the ideal experiment would measure the diffraction pattern at low scattering angles and high incident neutron energy, conditions that are difficult to realise in practice. Negative energy transfers are mostly not sampled due to the detailed balance factor in the dynamic scattering law.

The diffraction scattering cross section obtained in a TOF experiment is therefore an integral of the double differential scatering cross section along paths of constant TOF, such as are shown in Fig. 2.4. Because both the incident and final wavevectors vary along this path, and because the incident flux of neutrons depends on the incident wavevector, while the detection efficiency depends on the final wavevector, the integral to be evaluated is non-trivial (see for example Powles 1993 or Egelstaff 1987):

$$\frac{d\sigma}{d\Omega} = \int_{const.TOF} \frac{\Phi(k_i)}{\Phi(k_e)} \left(\frac{\partial k_i}{\partial k_e}\right)_\epsilon \frac{E_d(k_f)}{E_d(k_e)} \frac{k_f}{k_i} F_n(Q,\epsilon) d\epsilon \tag{2.47}$$

It is assumed here that the raw data have been divided by the incident neutron flux, $\Phi(k_i)$, and detector efficiency, $E_d(k_f)$, at the elastic wavevector, k_e. The Jacobian $\left(\frac{\partial k_i}{\partial k_e}\right)_\epsilon$ is required to allow for the uneven sampling of the incident spectrum for different values of ϵ along a path of constant TOF. It is straightforward to show, using equations 2.44 and 2.45, that

$$\left(\frac{\partial k_i}{\partial k_e}\right)_\epsilon = \frac{k_i^2}{k_e^2} \frac{1+R}{\left[1+R\left(\frac{k_i}{k_f}\right)^3\right]} \tag{2.48}$$

It will be noted that the expression (2.48) has the role of a "sampling factor" since it is close to unity for $k_f \approx k_i$, but drops to zero for $k_f \ll k_i$. The hardness of this cut-off depends on the value of R: when $R = 0$ the sampling factor becomes a step function at $k_f = 0$.

Although the integral (2.47) can be awkward to integrate, depending on the nature of the dynamic scattering law, there is no difficulty in principle with doing this since all the other terms in the kernel are either well known or can be estimated sufficiently accurately to give confidence in the final diffraction cross section. The only quantity that is not well defined is the dynamic scattering law itself, $F_n(Q,\epsilon)$, since this is generally an unknown at the outset.

A number of approximate methods exist, based on a Taylor expansion about $Q = Q_e$ (see for example Placzek 1952, Powles 1973), to estimate the effect of inelasticity on the diffraction pattern without detailed knowledge of the dynamic scattering law. These are generally useful when the mass of the scattering atom is much larger than the mass of the neutron, but they do not work for light atoms like hydrogen and deuterium. Hence for light atoms there is no choice but to perform the integral (2.47) numerically using a model scattering law, combined with estimates of the incident neutron spectrum and detector efficiency function. Fig. 2.5 shows the estimated time-of-flight differential scattering cross section for H_2O as a function of Q_e for a range of scattering angles, using the harmonic oscillator model of the dynamic scattering law described in Soper [2009]. Also shown is the actual scattering data measured on SANDALS at the same scattering angles.

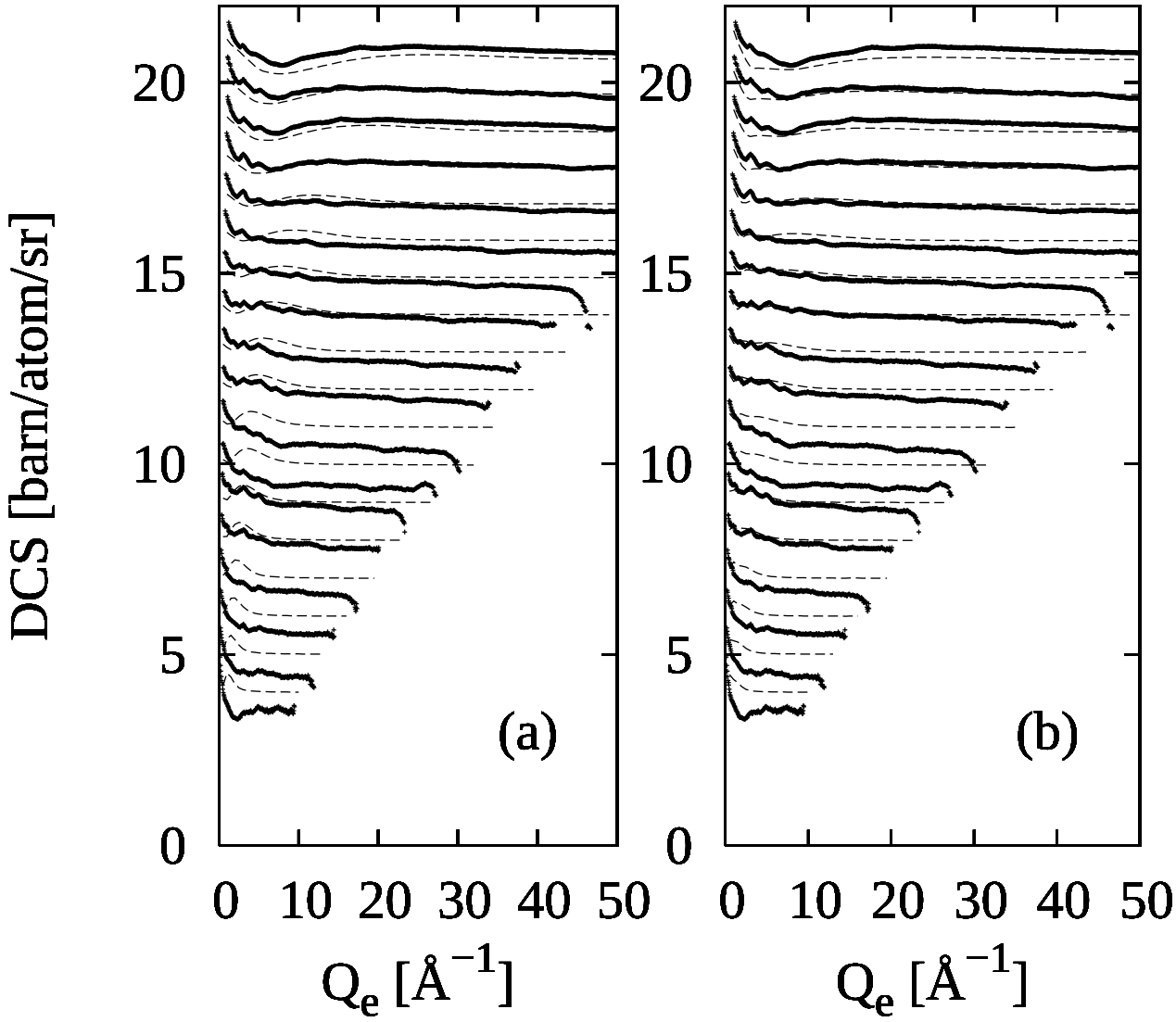

Figure 2.5: Estimated time-of-flight differential scattering cross sections for H_2O using the two models, (a) and (b), described in Soper [2009] (dashed lines). Also shown is the actual data as measured on SANDALS (pluses).

2.3.3 Inelasticity corrections at a reactor (fixed wavelength) neutron source

When the incident wavelength is fixed by a monochromator, as in a reactor neutron source experiment, then the elastic and incident wavevectors become the same, $k_e = k_i$, and the final wavevector ranges over all values, $k_f \geq 0$. Theoretically these conditions can be obtained by setting the flight path ratio $R = 0$ in the TOF equation (2.45) and the Jacobian (2.48). Hence the revised integral (2.47) becomes:

$$\frac{d\sigma}{d\Omega} = \int_{const.\theta} \frac{E_d(k_f)}{E_d(k_i)} \frac{k_f}{k_i} F_n(Q,\epsilon) d\epsilon \tag{2.49}$$

Fig. 2.6 shows the (Q,ϵ) trajectories which are sampled in the fixed incident wavelength experiment. Note that at small Q_e the trajectories sample the full width of $F_n(Q,\epsilon)$, while at high Q_e, only part of the scattering is sampled. Hence at large Q_e (large scattering angles) the scattering falls markedly for light atoms. Figure (2.7) shows the consequence of running the same harmonic oscillator model calculation as for Fig. 2.5(a) under the conditions of fixed incident wavelength, together with the scattering data for H_2O measured on D4C (pluses). Not only does this set of parameters appear to produce an excellent fit to the data, it is seen that the fit can be controlled quite sensitively by the choice of vibrational energies.

2.3.4 Choice of model for the dynamic scattering law

There are very few analytic forms for the dynamic scattering law that can be inserted into equations (2.47) and (2.49) to give a rapid solution of the respective integrals. Fortunately for heavier atoms, a simple form of the dynamic scattering law, or the use of the Placzek expansion in terms of the moments of the scattering law, will give adequate results. The simplest possible form for the scattering law is that of a free atom of kinetic energy k_BT - this is called the"ideal gas" scattering law:

$$S_\alpha^{(ideal)}(Q,\epsilon) = \sqrt{\frac{M_\alpha}{2\pi k_B T \hbar^2 Q^2}} \exp\left[-\frac{\left(\frac{\hbar^2 Q^2}{2M_\alpha} - \epsilon\right)^2}{4\frac{\hbar^2 Q^2}{2M_\alpha} k_B T} \right]. \tag{2.50}$$

This formula satisfies all the known constraints on the dynamic scattering law, namely the zeroth, first and second moments, and detailed balance. (Detailed balance is the quantum mechanical requirement that

$$S_\alpha(Q,-\epsilon) = \exp\left(-\frac{\epsilon}{k_B T}\right) S_\alpha(Q,\epsilon).) \tag{2.51}$$

It should be emphasized that for any formula for the dynamic scattering law to be useful it must satisfy at least these four constraints, which is the reason why there are so few analytic

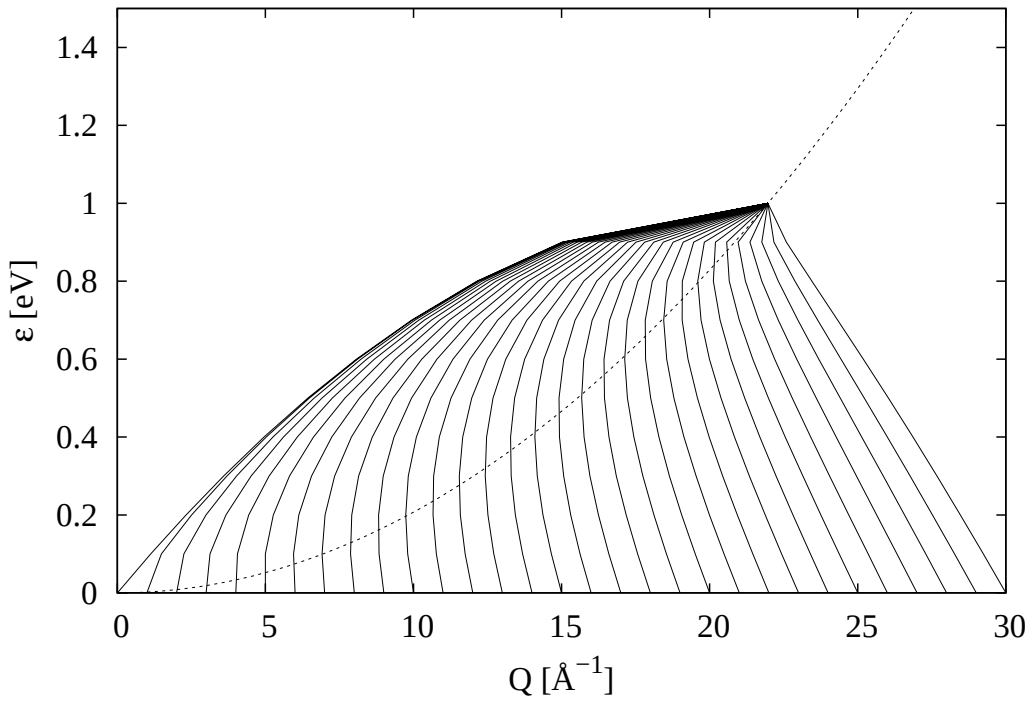

Figure 2.6: Constant scattering angle trajectories sampled in a fixed incident wavelength neutron diffraction experiment, assuming the incident neutron energy is 1eV. Trajectories are shown for 29 values of Q_e in the range 0 - 30 Å^{-1} in steps of 1Å^{-1}. The dashed line shows the recoil energy of a proton: this is the centroid of the self scattering kernal for a hydrogen atom. It will be noted that at low Q_e (low scattering angle) the trajectories fully cover all energy transfers around the proton recoil energy line, but at high Q_e only part of the proton scattering is sampled. Obviously the effect of inelasticity becomes much less pronounced as $M_\alpha \gg m$. The region for $\epsilon < 0$ is not shown since the scattering law only makes weak contributions in this region due to detailed balance. In other words, except at very low energy transfers ($\epsilon \leq k_B T$), most of the inelasticity arises from the neutron losing energy rather than gaining energy.

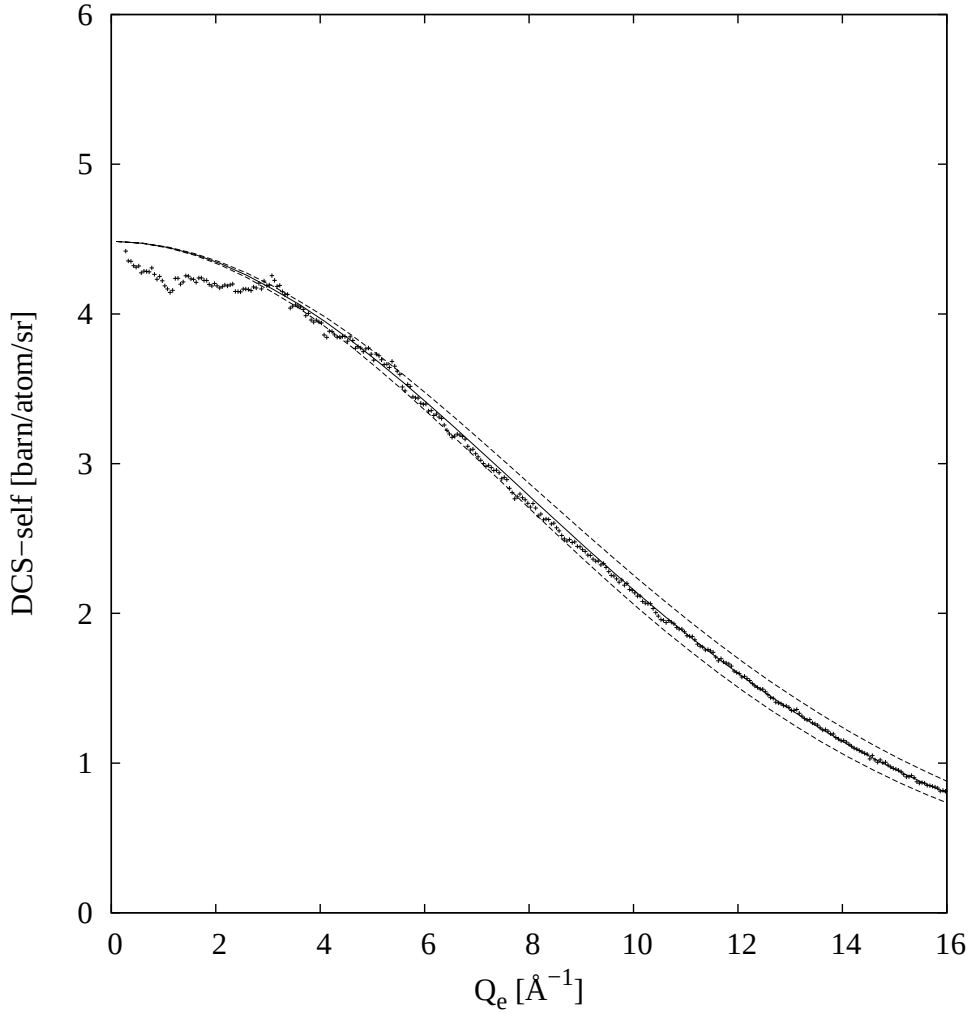

Figure 2.7: Predicted self differential scattering cross section for H_2O (solid line) using masses and vibrational energies described in Soper [2009]. Also shown are the cases where the rotational excitation energies are varied ±20meV (dashed lines). The pluses show the data for heavy water as measured on D4C

forms which are useful. The only other form that is amenable to analytic solution is that of the harmonic oscillator, Soper [2009], but this already is much slower for evaluating integrals such as (2.47) and (2.49) because of the need to sum over many vibrational levels.

2.3.5 X-ray diffraction

For x-rays, inelastic scattering also affects primarily the self scattering. In this case, since x-rays are scattered by the electrons, the problem arises from electrons recoiling under the impact of the incident x-ray. This is a much better understood problem, having been originally studied by Compton [1923], and then subsequently revisited, Breit [1926], Dirac [1926], Klein and Nishina [1929]. The Compton scattering can be calculated for each atom within the independent atom approximation (Hubbell et al. [1975]). However the actual impact on the diffraction data is not quite so clear cut, since both the Compton scattering level and accompanying Breit-Dirac correction factor are affected by the energy response of the detector, and this is not always known precisely.

Equivalent to equations (2.43) and (2.44) one has equivalent equations for the photon:

$$Q^2 = k_i^2 + k_f^2 - 2k_i k_f \cos 2\theta \tag{2.52}$$

$$\epsilon = \hbar c\,(k_i - k_f) \tag{2.53}$$

As Compton originally showed (Compton [1923]), the recoiling electron is likely to be relativistic, so the recoil energy of the electron, $E_{R,e}$ is given by

$$E_{R,e} = m_e c^2 \left(\sqrt{1 + \frac{\hbar^2 Q^2}{m_e^2 c^2}} - 1 \right) \tag{2.54}$$

$$\approx \frac{\hbar^2 Q^2}{2m_e} \text{ for } \hbar Q \ll m_e c \tag{2.55}$$

The (Q, ϵ) trajectories corresponding to these equations are shown in Fig. 2.8. Note the more than 3 orders of magnitude difference in energy scale compared to the corresponding neutron case, Fig. 2.6. Also notice how, even on this greatly expanded energy scale, the trajectories are nearly at constant Q, so the problems with loss of intensity caused by inadequate sampling of (Q, ϵ) space which bedevil neutron experiments on light atoms, as shown in Figs. 2.6 and 2.7 will never happen with x-ray diffraction. Accordingly the static approximations, equations (2.38) and (2.39), which apply to the atomic motion will be obtained very accurately with x-rays.

In x-ray terminology such atomic scattering is called "coherent" because it involves all the electrons scattering the x-ray photon as a whole: the electron cloud remains in its ground state throughout the scattering process. The relatively small ($\lesssim$ 1eV) changes in energy associated with the atomic motions are unmeasurable unless extraordinary efforts are made to analyse the energy of the scattered beam. However inelasticity does occur with x-ray scattering in the form of exciting electrons from their ground state orbitals. This is called "incoherent" scattering because it involves individual electrons but is more

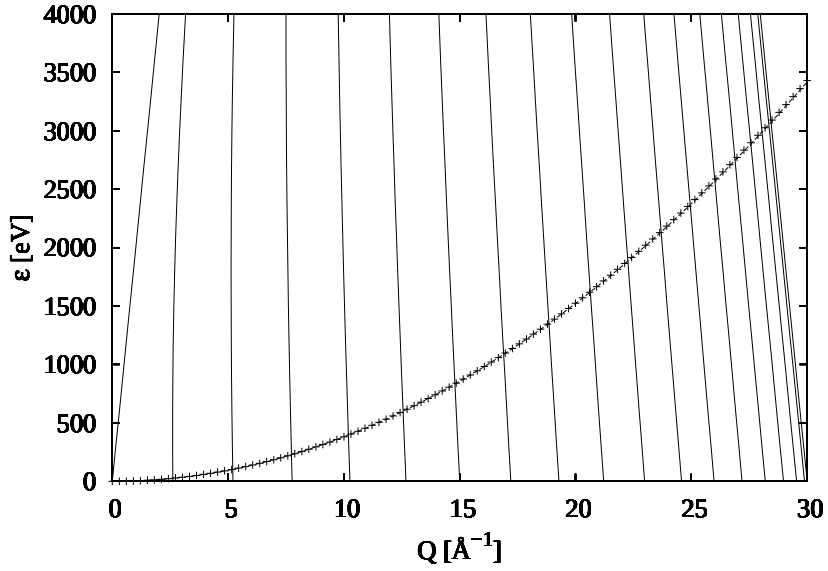

Figure 2.8: Trajectories in Q, ϵ space over which the fixed incident wavelength x-ray diffraction experiment integrates the dynamic structure factor (solid lines). For this plot the incident x-ray energy was set to 29.5989 keV, corresponding to an x-ray wavelength of 0.4189Å. The trajectories are shown for increasing scattering angles in steps of 10°, starting from 0° (left) and finishing on 180° (right). The dashed line shows the electron recoil energy, (2.54) and compares it with the classical recoil energy, (2.55), (crosses). Note that in spite of the incident energy, the recoiling electron is only just relativistic, even at the highest Q values, where the relativistic correction amounts to about 10eV in a total energy transfer of $\sim$ 3000eV.

analogous to the self scattering of neutrons by individual nuclei. It was famously studied by Compton, (Compton [1923]), who formulated the scattering from a free stationary electron and demonstrated the fundamentally quantum (and relativistic) nature of the x-ray scattering process at high incident energies. It was studied by many others, for example, Breit [1926], Dirac [1926], Klein and Nishina [1929] and it is generally accepted that the Klein-Nishina formulation for the incoherent differential cross section of a stationary free electron for an unpolarised incident x-ray beam is the correct one, Read and Lauritsen [1934]:

$$\left(\frac{d\sigma}{d\Omega}\right)_{\mathrm{KN}} = \frac{1}{2}r_e^2 P(\alpha,\theta)^2\left[P(\alpha,\theta) + P(\alpha,\theta)^{-1} - 1 + \cos^2 2\theta\right] \tag{2.56}$$

where r_e is the classical electron radius, $0.281794\times10^{-14}m$, $\alpha = \dfrac{E_i}{m_e c^2}$, which is the incident photon energy in units of the electron rest mass energy, and

$$P(\alpha,\theta) = \frac{1}{\left(1 + 2\alpha\sin^2\theta\right)}. \tag{2.57}$$

Note that the scattering angle in these equations is 2θ as before.

At the relatively low ($<$ 100keV incident x-ray energies that are used in x-ray diffraction the electrons are of course bound to the atoms, so cannot be regarded as free, particularly at small Q. As a result the inelastic (incoherent) scattering is actually zero at $Q = 0$ and grows with increasing Q eventually reaching a plateau where all Z electrons on the atom are scattering incoherently. As a result the Klein-Nishina formula needs to be corrected for the initial states of the electrons so it is normal to write:

$$\left(\frac{d\sigma}{d\Omega}\right)_{incoh} = \left(\frac{d\sigma}{d\Omega}\right)_{\mathrm{KN}} S(x,Z) \tag{2.58}$$

where $x = Q/4\pi$ and $S(x,Z)$ is an incoherent form factor which needs to be estimated.

The calculation of this form factor, of which there is one for each element, can be achieved in at least two ways. The standard method, Hubbell et al. [1975], involves a summation over the ground state electron wave functions, typically using the self-consistent Hartree-Fock method. Alternatively it is possible to use the impulse approximation and use the Compton profile (electron momentum distribution), Ribberfors [1983] to achieve the same result to good accuracy. We will not delve into these methods further here, but simply note that $S(x,Z)$ can be expressed as a series, Balyuzi [1975]:

$$S(x,Z) = Z - \sum_{i=1}^{5} a_i \exp\left(-b_i x^2\right), \tag{2.59}$$

which is useful when it is needed to calculate the Compton scattering at arbitrary values of Q. Note that at large Q (=large x) $S(x,Z) \longrightarrow Z$, but the actual scattering will fall below this limit due to the electron recoil term in the Klein-Nishina formula. It should

also be borne in mind, that although these expressions may seem comparatively complete compared to the neutron case, in fact they do not include the effect of variable detector efficiency with x-ray energy in the calculation. Hence for anything other than a "black" x-ray detector (meaning that it counts all photons with equal efficiency irrespective of their energy) the results will not be accurate. In practice it is quite hard to build such a detector.

It is worth noting here that corresponding to equations (2.58) and (2.59), the coherent scattering from a single atom is expressed, Hubbell et al. [1975] as

$$\left(\frac{d\sigma}{d\Omega}\right)_{coh} = \left(\frac{d\sigma}{d\Omega}\right)_{\mathrm{Th}} F(x,Z)^2 \tag{2.60}$$

where $F(x,Z)$ is the "atomic form factor", $f(Q)$, referred to in section 2.2.1, and for an unpolarised beam the differential Thomson scattering cross section is given by

$$\left(\frac{d\sigma}{d\Omega}\right)_{\mathrm{Th}} = \frac{1}{2}r_e^2\left[1+\cos^2 2\theta\right]. \tag{2.61}$$

The atomic form factors can also be expanded as a series, Waasmaier and Kirfel [1995]:

$$F(x,Z) = c + \sum_{i=1}^{5} a_i \exp\left(-b_i x^2\right). \tag{2.62}$$

Fig. 2.9 shows the coherent, incoherent, and total $\left(\frac{d\sigma}{d\Omega}\right)_{tot} = \left(\frac{d\sigma}{d\Omega}\right)_{coh} + \left(\frac{d\sigma}{d\Omega}\right)_{incoh}$ x-ray differential scattering cross sections for a free oxygen atom under the same conditions as shown in Fig.2.8.

Compton scattering is zero at $Q = 0$, and grows with increasing Q. Meanwhile the x-ray form factors which control the amplitude of the distinct scattering rapidly diminish with increasing Q. This means at high Q the x-ray diffraction data are dominated by the Compton scattering which forms a background that has to be subtracted in order to get to the structurally important distinct scattering. This introduces a systematic uncertainty to extracted coherent x-ray data that gets progressively worse the higher the value of Q. Once again, as with the neutron inelastic scattering, unless the data can be measured incredibly accurately, the distinct scattering can only be extracted with significant uncertainties. As will be seen later, the normalisation of x-ray data onto absolute cross section scale relies on knowing the high Q data to good accuracy.

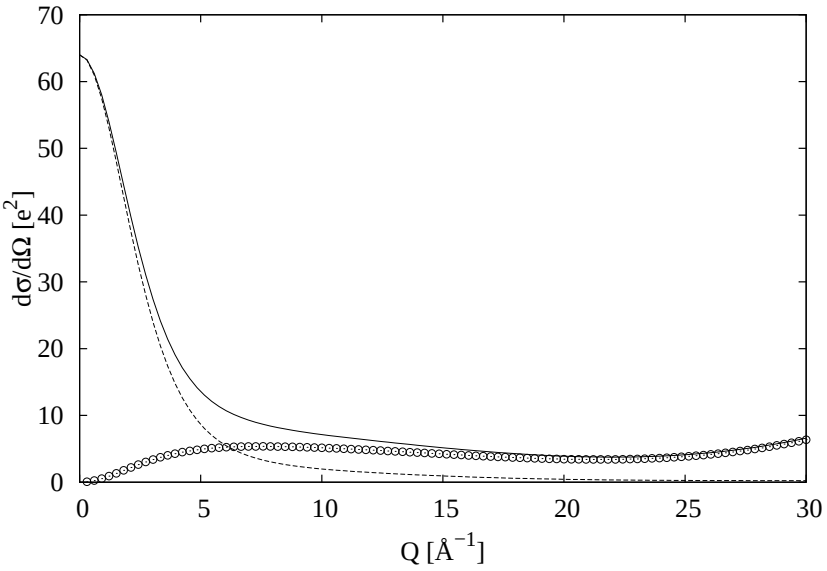

Figure 2.9: X-ray coherent (dashed) and incoherent (circles) differential scattering cross section for a single oxygen atom, as calculated from equations (2.60) and (2.58). Also shown is the sum of these two terms, $\left(\frac{d\sigma}{d\Omega}\right)_{tot}$ (solid line). Note that the total scattering goes to $Z^2 = 64$ at $Q = 0$ Å^{-1} but is below the limit $Z = 8$ at $Q = 30$Å^{-1} due to the electron recoil.

Chapter 3

Steps in Diffraction Data Analysis

3.1 Factors which affect the measured radiation counts

The previous section has shown how the diffraction cross section splits into self and distinct terms, corresponding to radiation scattering by the same atoms and by different atoms respectively, the latter giving rise to the interference pattern which contains the structural information which we seek. Moreover the single atom scattering is subject to inelastic effects which arise from nuclear (neutrons) or electron (x-rays) recoil. The question arises how do we get this differential cross section from the number of radiation counts that are actually measured in a detector?

To help understand the data analysis process, and to assist in diagnosing problems, GudrunN will, on request, output the results of each stage of the analysis, from beginning to end, into a series of files with specific file extensions. GudrunX does this automatically as there is typically only one detector to output. To help identify the various filenames the function names used in this account are the same as these extension names, with the warning that here they are shown CAPITALISED whereas in practice the file extensions are lowercase. (Note: the raw intensities such as $\mathrm{CNT}_b(\lambda, 2\theta)$, $\mathrm{CNT}_{s+c}(\lambda, 2\theta)$, etc., are output in the GudrunN program as files with extension **.cnt**. With GudrunX they appear in the same folder where the raw data are stored with extensions **.XRDtxt**.) The following presentation is an attempt to demonstrate where the various stages of the data analysis derive from. The basic method follows that originally described by Paalman and Pings [1962] and subsequently elaborated in the *ATLAS* manual. The following two graphics illustrate the basic steps in data analysis that GudrunN and GudrunX undertake.

If $\langle \Phi(\lambda, t) \rangle_t = \dfrac{\int_0^{\Delta t} \Phi(\lambda, t) dt}{\Delta t}$ is the average number of particles of radiation per unit area per unit time per unit wavelength which impinge on an assembly of N atoms, and $\mathrm{CNT}(\lambda, 2\theta)$ is the number of particles scattered by that assembly in the same time interval Δt in the wavelength range $\lambda, \lambda + \Delta\lambda$ into a solid angle $\Delta\Omega(2\theta)$ in the direction 2θ relative to the incident beam direction, then the differential scattering cross section per atom is

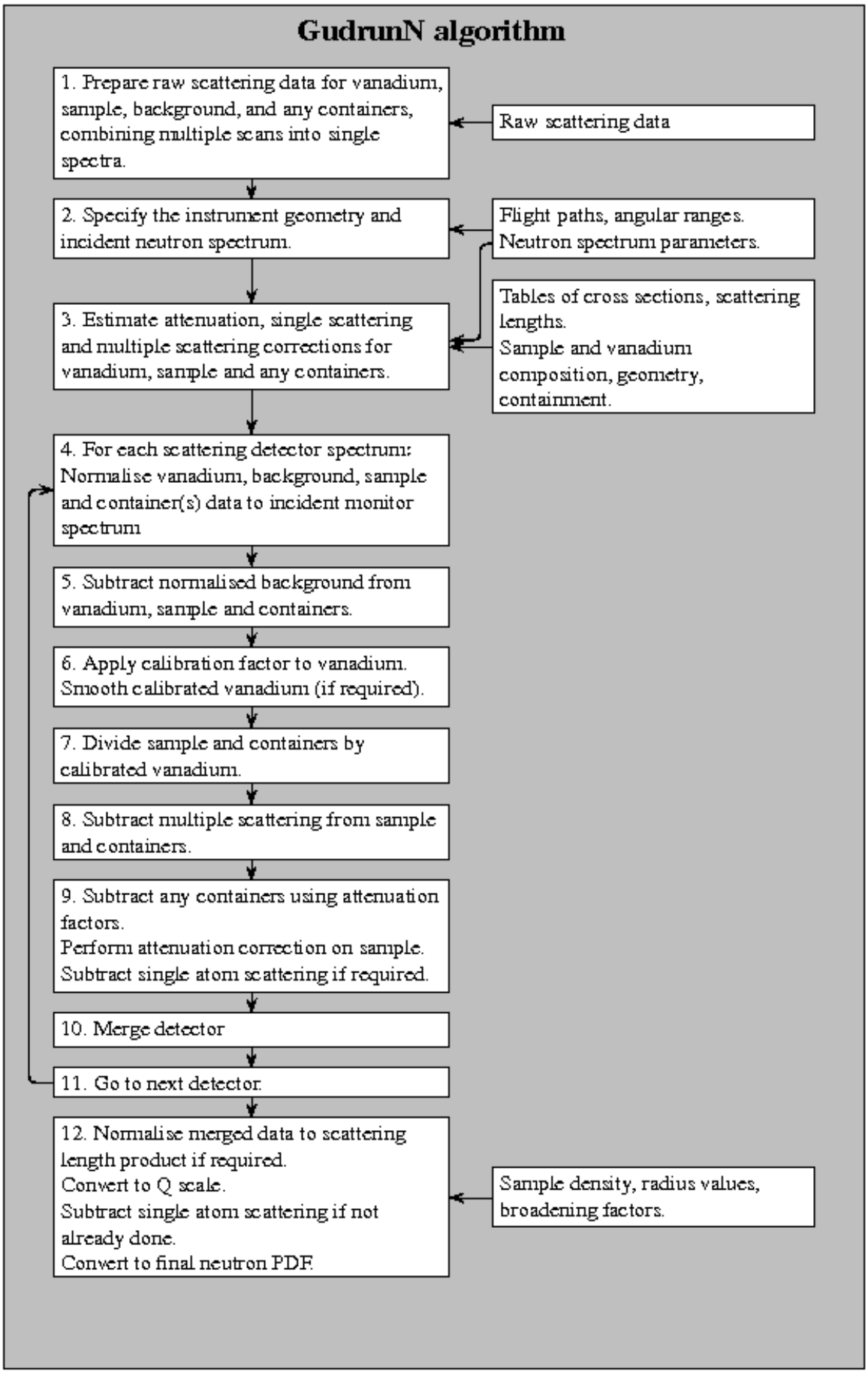

Figure 3.1: Basic flow chart of the GudrunN program.

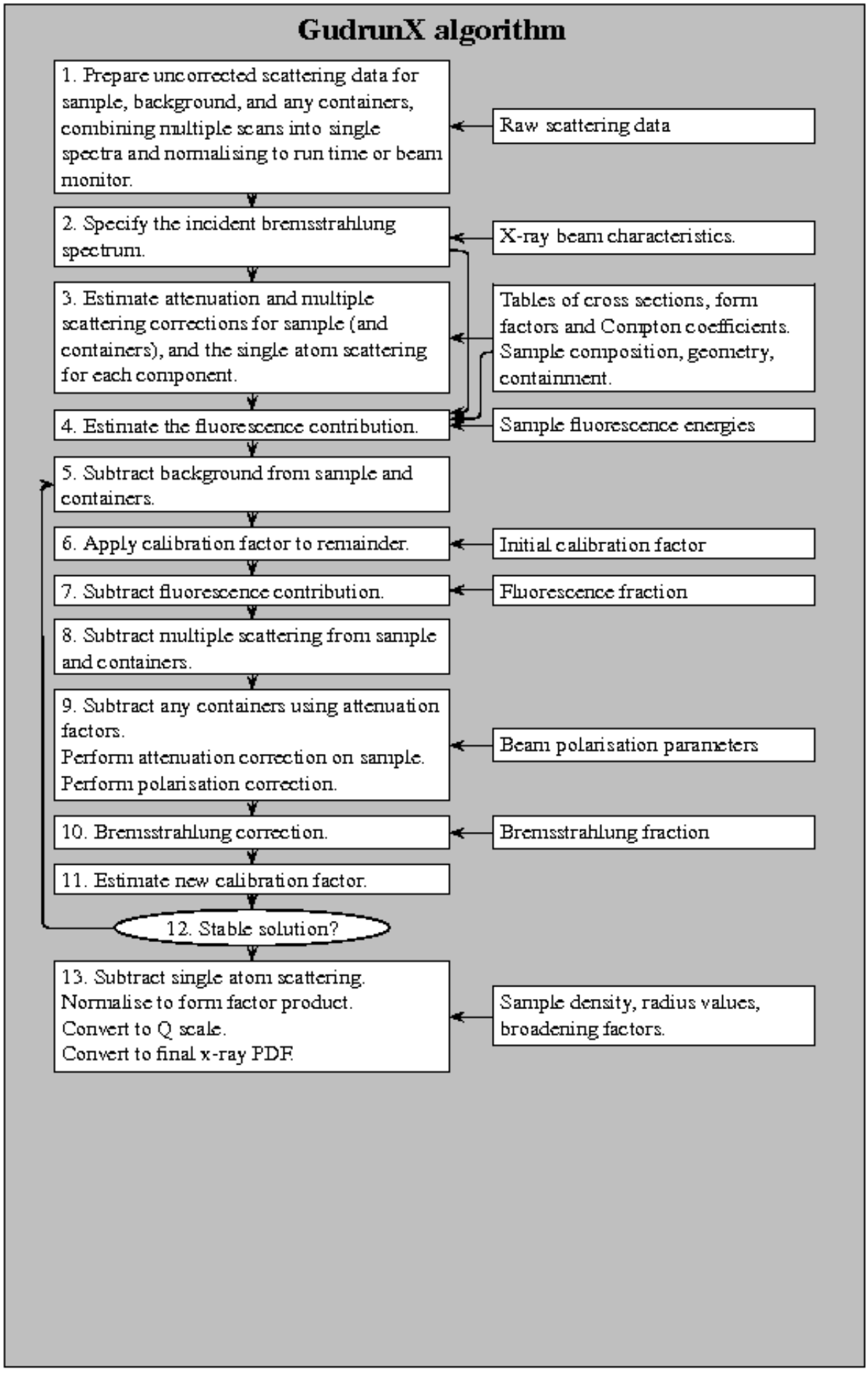

Figure 3.2: Basic flow chart of the GudrunX program.

simply

$$\frac{d\sigma}{d\Omega}(\lambda, 2\theta) = \frac{\mathrm{CNT}(\lambda, 2\theta)}{N\langle\Phi(\lambda, t)\rangle_t \Delta\lambda\Delta\Omega(2\theta)\Delta t}, \tag{3.1}$$

assuming the assembly of atoms is small enough that the effects of self attenuation and multiple scattering can be ignored. In principle we measure $\mathrm{CNT}(\lambda, 2\theta)$, so if we know N, $\langle\Phi(\lambda, t)\rangle_t$, $\Delta\lambda$, $\Delta\Omega(2\theta)$, and Δt we can get the differential cross section from the data.

Unfortunately the task is non-trivial because neutron and x-ray beams are not precisely defined quantities, neutron sources in particular are not overly stable, and neutron and x-ray detectors do not count every particle that enters them, especially at higher particle energies, so there is in practice significant uncertainty in deriving the differential cross section in this direct manner.

Writing for a particular sample, s, $\Sigma_s(\lambda, 2\theta) = \dfrac{d\sigma_s}{d\Omega}(\lambda, 2\theta)$, the number of counts in the detector can be expressed as

$$\mathrm{CNT}_s(\lambda, 2\theta) = N_s\Sigma_s(\lambda, 2\theta)\langle\Phi(\lambda, t)\rangle_t E_d(\lambda)\Delta\lambda\Delta\Omega(2\theta)\Delta t. \tag{3.2}$$

As previously $E_d(\lambda)$ is the detector efficiency at wavelength λ.

In general it is necessary to relax the requirement that the sample is small since in the majority of cases the count rate from a small sample will be too low to give useful information in a realistic time scale. When this happens then self attenuation becomes an issue, as does multiple scattering. The self attenuation appears as a factor, $A_{s,s} < 1.0$, outside the once scattered intensity, while the multiple scattering, M_s adds to the once scattered intensity:

$$\mathrm{CNT}_s(\lambda, 2\theta) = \left(A_{s,s}N_s\Sigma_s(\lambda, 2\theta) + M_s\right)\langle\Phi(\lambda, t)\rangle_t E_d(\lambda)\Delta\lambda\Delta\Omega(2\theta)\Delta t \tag{3.3}$$

where s, s means "scattering in the sample, attenuation in the sample". Both $A_{s,s}$ and M_s will dependent on λ and 2θ in general, but this dependency is not shown here. Of course the multiple scattering will be affected by attenuation in the sample, just like the once-scattered intensity, but because multiple scattering is an unwanted term which needs to be subtracted it is calculated to include the attenuation by the sample. On the other hand since we need to access the once scattered intensity, the attenuation factor for this single scattering has to be calculated as a separate quantity.

Please note that in this manual and in the GudrunN software, the term "attenuation" is used rather than the term "absorption". This is because "absorption" is sometimes used to refer specifically to the process where an atom or nucleus captures a quantum of radiation rather than scatters it. "Attenuation" here refers to all processes, both scattering and capture, by which a beam of radiation loses intensity as it passes through a material. "Capture" will refer specifically to processes where the radiation is captured by an atom or nucleus. The distinction is important for calculating multiple scattering and attenuation corrections. For example if a material has a large capture cross section, it will probably have attenuation factors $\ll 1.0$ but negligible multiple scattering. On the other hand if a

material has a large attenuation cross section, and small capture cross section, both the attenuation factor will be $\ll 1.0$ *and* the multiple scattering contribution could be large.

No detection system is perfect and the measured count rate will be subject to some intrinsic *background* counts which, like the sample, we will represent as a cross section, $B(\lambda, 2\theta)$. These background counts will appear irrespective of whether there is a sample in place or not. Such stray counts may be intrinsic detector quiet counts, or they might be radiation counts that reach the detector without being scattered by the sample. Hence the measured counts when there is no sample in position are given by:

$$\mathrm{CNT}_b(\lambda, 2\theta) = B(\lambda, 2\theta)\langle\Phi(\lambda, t)\rangle_t E_d(\lambda)\Delta\lambda\Delta\Omega(2\theta)\Delta t_b. \tag{3.4}$$

and the sample counts, with background included, will now be:

$$\mathrm{CNT}_s(\lambda, 2\theta) = (A_{s,s}N_s\Sigma_s(\lambda, 2\theta) + M_s + B(\lambda, 2\theta))\langle\Phi(\lambda, t)\rangle_t E_d(\lambda)\Delta\lambda\Delta\Omega(2\theta)\Delta t_s. \tag{3.5}$$

Commonly of course many samples will need to be contained in something - call this the *container* - which will have its own scattering pattern. In that case the attenuation factor for the sample, $A_{s,s}$ becomes $A_{s,sc}$, where s, sc means "scattering in the sample, attenuation in the sample and container", and that for the container will be $A_{c,sc}$, with a similar meaning. The multiple scattering will include both sample and container multiple scattering, M_{sc}. Now the measured number of counts becomes:

$$\begin{aligned}\mathrm{CNT}_{s+c}(\lambda, 2\theta) = \; & (A_{s,sc}N_s\Sigma_s(\lambda, \theta) + A_{c,sc}N_c\Sigma_c(\lambda, \theta) + M_{sc} + B(\lambda, 2\theta)) \\ & \langle\Phi(\lambda, t)\rangle_t E_d(\lambda)\Delta\lambda\Delta\Omega(2\theta)\Delta t_{sc}\end{aligned} \tag{3.6}$$

Note that in general different times are taken for the different measurements, Δt_{scb}, etc.

Continuing this sequence, occasionally a sample will have more than one container, such as a radiation shield or secondary containment for example. Hopefully it should now be obvious what that means for the detected count rate in terms of the scattering cross sections of the individual components:

$$\begin{aligned}\mathrm{CNT}_{s+c+f}(\lambda, 2\theta) = \; & (A_{s,scf}N_s\Sigma_s(\lambda, \theta) + A_{c,scf}N_c\Sigma_c(\lambda, 2\theta) + A_{f,scf}N_f\Sigma_f(\lambda, \theta) \\ & + M_{scf} + B(\lambda, 2\theta))\langle\Phi(\lambda, t)\rangle_t E_d(\lambda)\Delta\lambda\Delta\Omega(2\theta)\Delta t_{scf}\end{aligned} \tag{3.7}$$

where f refers to this secondary containment (such as a furnace or cryostat for example).

The effect of adding containers on the measured count rate can be continued indefinitely in principle depending on how many "containers" a particular sample has. As alluded to above, the word "container" does not necessarily refer to an actual container of the sample, but might refer to any material that surrounds the sample that either the transmitted or scattered beams have to proceed through. Currently GudrunN and GudrunX permit up to three containers plus the sample.

3.2 What measurements do you need?

The primary goal of the data analysis is to extract the sample cross section, $\Sigma_s(\lambda, 2\theta)$. The following section lists the measurements that are needed to realise that goal.

3.2.1 Sample background

of the x-ray scattering data This is an essential measurement that must be made in every case, and it is not possible to run GudrunN or GudrunX without these data. The background is normally measured with the radiation beam on but with nothing in the scattering position. This may of course not capture all the background - there could for example be a background which arises from the sample itself scattering into the surroundings and that scattered radiation being reflected into the detector. This kind of sample dependent background is very difficult to remove from the data and should be avoided if at all possible by instrument design - you typically need lots of shielding around the detector, but this must not be placed near to the detector if it can also receive scattered radiation from the sample. At low scattering angles it is possible to have background from the incident beam collimator which is transmitted through the sample, and hence is affected by the transmittance of the sample.

3.2.2 Sample with no containers

Where a sample has no container we only need two measurements, namely the counts of the background, $\mathrm{CNT}_b(\lambda, 2\theta)(\lambda, 2\theta)$, and the counts of the sample, $\mathrm{CNT}_s(\lambda, 2\theta)(\lambda, 2\theta)$.

3.2.3 Sample with one container

This will require three measurements, namely the sample background, $\mathrm{CNT}_b(\lambda, 2\theta)(\lambda, 2\theta)$, the container plus background, $\mathrm{CNT}_c(\lambda, 2\theta)(\lambda, 2\theta)$, and finally the sample plus container, $\mathrm{CNT}_{s+c}(\lambda, 2\theta)(\lambda, 2\theta)$.

3.2.4 Sample with two containers

The second container will here be called the furnace, labelled f, but of course it does not necessarily mean a furnace: it could be any sample environment equipment such as radiation shields, secondary containment, and so on. A sample with two containers will require four measurements, namely the background as before, $\mathrm{CNT}_b(\lambda, 2\theta)$, the furnace, $\mathrm{CNT}_f(\lambda, 2\theta)$, the container plus furnace, $\mathrm{CNT}_{c+f}(\lambda, 2\theta)$, and the sample plus container plus furnace, $\mathrm{CNT}_{s+c+f}(\lambda, 2\theta)$.

3.3 Purge bad detectors - time-of-flight diffraction

Most TOF diffractometers come with large arrays of detectors and it is highly unlikely that every single one will be working perfectly. Hence it is necessary to have some relatively automated way of removing detectors from the data analysis. This is called PURGE and it must be performed prior to any data processing. It produces a list of bad detectors, called **spec.bad**, which GudrunN reads: it does not use these bad detectors to prepare the final differential cross sections. Currently this option is only available for TOF diffraction.

PURGE works in the following way:-

1. A list is produced of the all the data files that will be required for a particular analysis.

2. Using the first file in the list for comparison, for each spectrum in each subsequent file in turn the ratio of counts in each time channel to counts in the corresponding spectrum and time channel in the first file is calculated. This ratio is averaged over all time channels in the spectrum. Also calculated is the standard deviation on this ratio, based on the values from the different time channels. The results are output in files with extension **.rat**. There should be an entry in this file for every spectrum in the input files. Any non-counting spectra, i.e. not a single count in any time channel, are given a ratio of 0.

3. The ratios are normalised to the ratio in the incident beam monitor, so that variations due to different run times are eliminated. Hence the ratio in the incident beam should always be 1.0 after this normalisation.

4. There now begins an iterative loop. Initially some rather large tolerances (lower and upper limits) on the allowed ratios are set. Currently these are 0.00001 and 100 respectively.

5. Working in detector groups (see Section 3.10.1 for a description of detector grouping) each spectrum ratio is assessed against the lower and upper ratio limits for that group. If below the lower limit, the spectrum is given a rating of -1, if above the upper limit it is given a rating of +1. Either case would eliminate it from the subsequent processing.

6. From the second pass onwards, i.e. not on the first pass, the standard deviations on the ratio are also assessed. A large standard deviation means a strongly counting detector, while a very small standard deviation means a weakly counting detector. Either case is suspicious and so if the standard deviation is below a specified lower limit (see stages 8 and 9 below) this is signalled by a rating of -2 while if it is above a specified upper limit this is signalled by a rating of +2. Either case will eliminate it from the further analysis. The reason for this extra test is that a very weakly counting or very noisy detector might have a perfectly good ratio, so the fact that it is noisy or excessively quiet would not be picked up by the ratio alone.

7. For those detectors which survive the previous two steps, the average ratio for the group is calculated, as is the minimum and maximum standard deviation for the group, called ERRMIN and ERRMAX respectively.

8. If the ratio ERRMAX/ERRMIN is less than a specified input value (STDFAC) then the upper and lower limits on the standard deviations are set to ERRMAX and ERRMIN respectively. Otherwise the upper limit is set to 80% of ERRMAX and the lower limit is set to 102% if ERRMIN.

9. New upper and lower limits on the spectrum ratios are also set at this stage based on the current average ratio for the group, and the spread of values about this average. The aim is reduce this spread to a range given by the specified input value RMSFAC. Obviously the smaller the value of RMSFAC the fewer spectra will survive the selection criterion. Note that in the event that the ratio for the whole group is low (below 0.2) then the limits for this group are left unchanged, since it means the scattering is weak - probably a background run of some kind - so the routine will only eliminate non-counting or very noisy detectors.

10. The sequence 5 to 9 is now repeated until no further detectors are eliminated, up to a maximum of 10 times. The sequence is then repeated for each file, assuming the results of the previous file at the outset, so that a bad detector found only in one file will be assumed bad for all the files in the list.

11. At the end the list of bad detectors is written to the file **spec.bad** and new groups file is written containing only those detectors which are deemed to have passed the selection criteria.

3.4 Calculation of the attenuation and multiple scattering factors

In order to calculate attenuation and multiple scattering factors, it is necessary to have a available the total cross section for the materials of the sample and its containers.

3.4.1 Neutron and x-ray total cross sections

For the majority of elements the total cross section of a material has two terms, that due to scattering $\sigma^{(s)}(\lambda)$ and that due to absorption (capture), $\sigma^{(a)}(\lambda)$:

$$\sigma^{(t)}(\lambda) = \sigma^{(s)}(\lambda) + \sigma^{(a)}(\lambda) \tag{3.8}$$

Strictly speaking the scattering cross section is the integral of the differential scattering cross section over all scattering angles:

$$\sigma^{(s)}(\lambda) = \int_{\Omega} \left(\frac{d\sigma}{d\Omega}\right)(\lambda, 2\theta) d\Omega. \tag{3.9}$$

and since it is the differential scattering cross section which is being sought to get the structure, it would appear one needs the answer before one can correct the data! In practice, integrating $\left(\frac{d\sigma}{d\Omega}\right)(\lambda, 2\theta)$ over all Ω is difficult to do reliably since the measurements never cover all 4πsr of Ω. Fortunately, provided the attenuation and multiple scattering cross sections are not too large, it is generally sufficiently accurate (with some notable exceptions

listed below) to use tabulated single atom values for the scattering cross section in place of their exact values.

For x-rays the scattering and absorption (capture) cross sections of the elements are listed in tables, (see **http://www.esrf.fr/computing/scientific/dabax**), from which the values for particular elements and x-ray energies can be extracted by interpolation.

For neutrons the most recent tabulation was compiled by Sears [1992], but see also: **http://www.ncnr.nist.gov/resources/n-lengths**. Occasionally revisions to some of the values in this table have been made since it was published, but so far there does not seem to be a more recent compilation.

To a reasonable approximation the neutron scattering cross section (at the energies used to measure the structure) is independent of λ. Exceptions to this rule occur when near a nuclear resonance and when a sample has strong Bragg scattering or significant inelasticity effects, such as with H and D containing materials.

Generally speaking, going through a nuclear resonance involves a change in the neutron scattering length, and is often combined with a strong emission of γ radiation from the sample. Such radiation can be picked up by some neutron detecting systems, so rendering the data useless. In addition the capture cross section in a resonance can be truly enormous, which will also render the data non-analysable. Hence a good rule of thumb is to avoid nuclear resonances if at all possible! Alternatively if is necessary to look at a material with a strong resonance it may be more appropriate to perform the experiment at a fixed wavelength source, so that the neutron wavelength can be tuned to be away from the resonance. This is possible since they mostly occur at neutron energies $>$ 1eV and so at a fixed wavelength source a reasonable Q range should still be accessible.

When a sample has a strong Bragg reflections the issue here is that the direction of these reflections depends on the wavelength. As the wavelength increases the Bragg peaks move to larger scattering angles, until eventually they may not be observable at all. At this point the scattering cross section of the material can drop dramatically due to the absence of Bragg scattering. This happens most notably in the case of beryllium metal, which has a very small capture cross section for neutrons, but strong coherent scattering length. Below about 5meV neutron energy the beryllium becomes almost transparent to incident neutrons, but above this energy it is a strong (scattering) attenuator. Hence its use as a neutron filter and reflector.

Where nuclear recoil is significant - mostly light atoms like H and D - the scattering cross section can be strongly energy dependent, so for these materials it is necessary to either seek another table giving the correct energy dependence of the cross section, or else, if the diffractometer has a monitor detector in the transmitted beam, measure the transmission cross section directly. This is described in more detail in the next section.

Away from a resonance the neutron absorption (capture) cross section is a linear function of wavelength. The constant of proportionality, the tabulated neutron absorption cross section, $\sigma^{(a)}$ is normally quoted for a neutron velocity of 2200m/s (corresponding to the energy of a neutron at ambient temperature). This corresponds to a neutron wavelength

of 1.7982Å, so at other wavelengths the capture cross section can be calculated from:

$$\sigma^{(a)}(\lambda) = \sigma^{(a)}(1.7982)\left(\frac{\lambda}{1.7982}\right) \tag{3.10}$$

3.4.2 Measuring the neutron transmission cross section

Generally it is best to measure the neutron transmission cross section of a sample at the same time that the scattering is being measured. This is because it can be difficult to reproduce the exact conditions at a later time. If tof the x-ray scattering data he sample is a flat plate of thickness L which is normal to the incident beam, the transmission of the sample is given by

$$\mathrm{TRANS}(\lambda) = \exp\left(-\mathrm{MUT}(\lambda)L\right) \tag{3.11}$$

where $\mathrm{MUT}(\lambda) = \rho\sigma^{(t)}(\lambda)$. Therefore if we can measure $\mathrm{TRANS}(\lambda)$ and we know ρ, then we can obtain $\sigma^{(t)}(\lambda)$ for the sample.

For non-flat plate samples such as cylinders the exercise is not quite so simple, since now the transmission depends on which part of the sample the beam traverses. Referring to Fig. 3.3, it is assumed $N(x)$ is the number of neutrons incident on this sample per unit width at position x. ($N(x)$ is called the *beam profile* and can be measured by placing a thin wire of vanadium in the beam and measuring the scattered counts as a function of position across the beam.) In that case the transmission of this sample is given by

$$\mathrm{TRANS}(\lambda) = \frac{\int_0^W N(x)\exp\left(-\mathrm{MUT}(\lambda)L(x)\right)dx}{\int_0^W N(x)dx} \tag{3.12}$$

assuming x is measured from one edge of the beam, and W is the width of the beam. There is no simple inversion to $\mathrm{MUT}(\lambda)$ as there was for (3.11), so it has to be solved iteratively, but some efficiency can be gained by expanding the exponential:

$$\mathrm{TRANS}_s(\lambda) = 1 - \mathrm{MUT}(\lambda)M_1 + \mathrm{MUT}^2(\lambda)M_2 - \mathrm{MUT}^3(\lambda)M_3 + \cdots \tag{3.13}$$

where

$$M_n = \frac{1}{n!}\frac{\int_0^W N(x)L^n(x)dx}{\int_0^W N(x)dx}. \tag{3.14}$$

The latter integrals depend only on the sample geometry and so need only be evaluated once.

If the sample is held in a container, then the transmission of the sample will given by a modification to (3.12):

$$\mathrm{TRANS}_s(\lambda) = \frac{\int_0^W N(x)\exp\left(-(\mathrm{MUT}_s(\lambda)L_s(x) + \mathrm{MUT}_c(\lambda)L_c(x)\right)dx}{\int_0^W N(x)\exp\left(-\mathrm{MUT}_c(\lambda)L_c(x)\right)dx} \tag{3.15}$$

so in order to solve this for $\mathrm{MUT}_s(\lambda)$ it will first be necessary to first measure (or assume some form for) $\mathrm{MUT}_c(\lambda)$. This can be achieved for example by measuring the transmission of the container on its own. There is a, by now hopefully obvious generalisation of these equations for the cases where the sample has more than one container. However the procedure is the same in each case, namely determine the cross section of the outermost container, then the next one in, and so on, until the sample cross section is obtained.

All that remains is to determine the respective values of $\mathrm{TRANS}(\lambda)$. If $E_t(\lambda)$ is the transmission monitor efficiency, and assuming the transmission monitor samples the same beam as that sampled by the incident monitor, then the ratio of monitor counts, transmission monitor over incident monitor is given by

$$\frac{\mathrm{RAWTRANS}_s(\lambda)}{\mathrm{RAWMON}_s(\lambda)} = \mathrm{TRANS}_s(\lambda)\frac{E_t(\lambda)}{E_m(\lambda)} \tag{3.16}$$

This determines the transmission, but is multiplied by the ratio of monitor efficiencies. In addition, depending on the monitor type, there may be an intrinsic "quiet" count in the monitor which should be subtracted prior to taking the ratio. Hence the input to GudrunN allows the specification of this constant, represented as some fraction of the overall number of counts in the monitor. To determine the monitor efficiency ratio it is necessary to measure the transmission when there is no sample in the beam, namely

$$\frac{E_t(\lambda)}{E_m(\lambda)} = \frac{\mathrm{RAWTRANS}_b(\lambda)}{\mathrm{RAWMON}_b(\lambda)} \tag{3.17}$$

Hence the sample transmission is obtained from:

$$\mathrm{TRANS}_s(\lambda) = \left(\frac{\mathrm{RAWTRANS}_s(\lambda)}{\mathrm{RAWMON}_s(\lambda)}\right) \Big/ \left(\frac{\mathrm{RAWTRANS}_b(\lambda)}{\mathrm{RAWMON}_b(\lambda)}\right). \tag{3.18}$$

Analogous expressions will apply when the sample has one or more containers.

GudrunN therefore allows the user either to use the Sears tables to specify the total cross section (TABLES option), or the transmission monitor (TRANSMISSION option), or else the total cross section per atom can be entered via a specified filename. However it is derived, the total cross section that is used in the program is output in the files with extension **.mut**. Despite the name of this file, be aware that it is a **cross section** file with the units of barns ($=10^{-24}\mathrm{cm}^2$ per atom. Note that for the multiple scattering correction it is necessary to have both the scattering cross section and the total cross section. In GudrunN the latter is calculated from the measured or input total cross section by subtracting the capture cross section according to (3.10)

3.4.3 Attenuation and multiple scattering corrections

The attenuation and multiple scattering corrections are calculated in GudrunN and GudrunX according to Soper and Egelstaff [1980] for cylindrical samples and according to Soper [1983], both of which papers are extensions of earlier work by Paalman and Pings

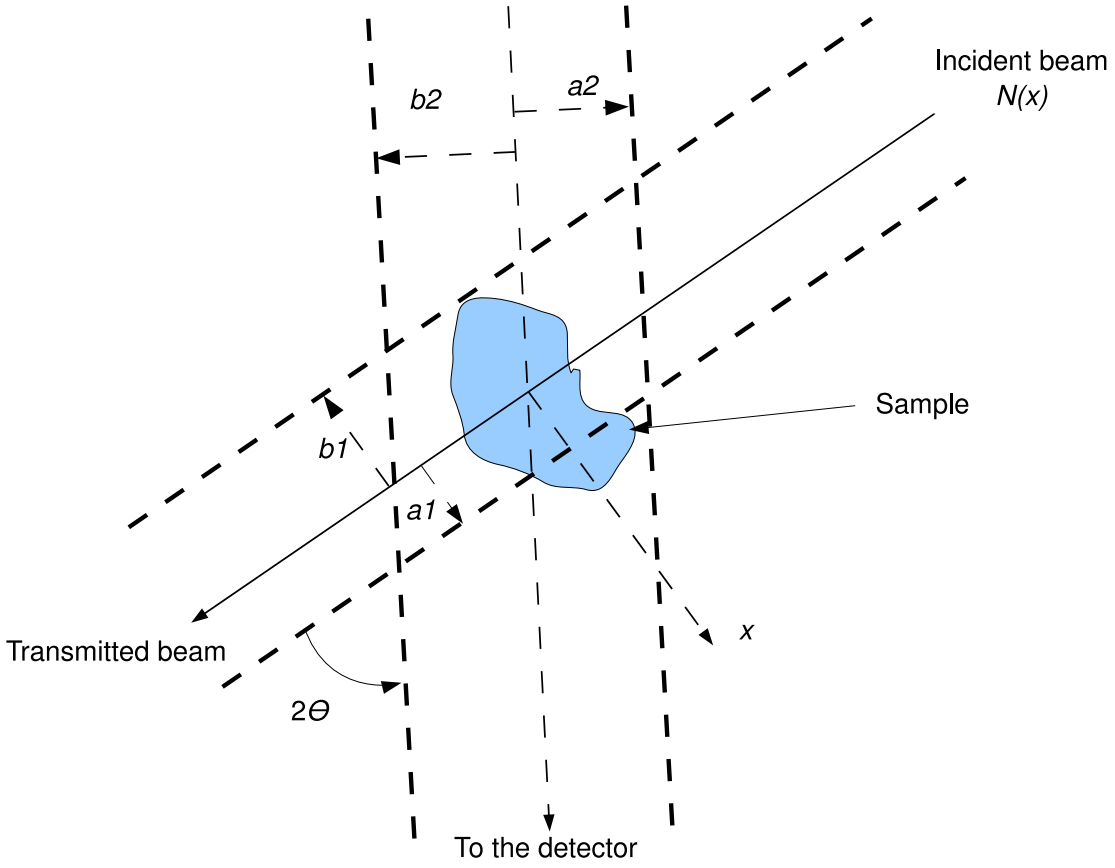

Figure 3.3: Geometry of the transmission and scattering problem for an arbitrary shaped sample. The neutron beam is incident from the top right and exits from the bottom left. The x axis is at right angles to the beam direction and the coordinates of the beam edges $a1$ and $b1$ are measured along this axis from the centre of the sample. The scattered beam goes towards the detector at scattering angle 2θ, and the coordinates of the scattered beam edges, $a2$ and $b2$, are also measured from the sample centre at right angles to the scattered beam direction. In general the beam intensity, $N(x)$ will be a function of x.

[1962], Kendig and Pings [1965] and Blech and Averbach [1965] for cylinders, and Vineyard [1954] for flat plate samples. For these calculations it is necessary to specify the beam size and position (only for cylinders) and the sample geometry and composition. Note that for both cylinders and flat plate geometries the multiple scattering is calculated using the average scattering cross section of each component (sample, container, vanadium, etc.) for a particular wavelength, and assuming the atoms in that component scatter isotropically - the same in all directions. This is NOT the same as assuming the multiple scattering is isotropic, which it certainly is not. More sophisticated corrections which involve both the true differential scattering cross section and any inelasticity effects can be contemplated, but so far have not been implemented in GudrunN or GudrunX.

3.5 Deadtime corrections

Most counting detectors have an intrinsic deadtime, τ, which is the minimum time between events needed for the detector to be able to resolve the two events as separate events: events coming closer together than this will only get counted as a single event.[1] If the data rate observed in the detector is R events per sec, the detector will be dead for a fraction of the time given by $\sim R\tau$, so the incident data rate, that is the data rate that would be observed if the detector had zero deadtime will given by $R/(1 - R\tau)$. This formula however really only works if $R \lesssim \frac{1}{2\tau}$, otherwise it can give rise to a dramatic increase in the corrected count rate, which would almost certainly indicate a fault in the electronics, rather than anything to do with actual deadtime. In GudrunN the various deadtime corrections, one for each detector module, are listed in the files with extension **.module**. In GudrunX there is currently no deadtime correction performed.

For time-of-flight neutron diffraction there is a subtlety about data rates that can get a bit confusing. This is because the counts are themselves measured as a function of time-of-flight, and the width of the time-of-flight bins is often a variable, increasing with longer times of flight. As a result the data counts in each time bin are normally divided by the time width of that bin, giving an intensity in the units (typically) of counts per μs. This however is NOT the data rate in the detector since it will increment with each pulse of neutrons! To get the data rate in the detector the number of counts per μs measured must be divided by the number of pulses of neutrons received, so the data rate is actually the number of counts per μs per neutron pulse.

The details of the deadtime correction depend a bit on the way the detectors are hooked up to the data acquisition electronics (DAE). At ISIS several detectors are often ganged into a single input of the DAE so that if that input introduces its own deadtime, due to a high count rate for example, that deadtime will affect all the detectors going to the input. In practice the deadtime of most DAE inputs is much faster than the deadtime of individual detector elements, so it is the latter which normally produces a significant deadtime correction, if any.

[1] Equivalently integrating detectors can have saturation problems.

3.6 Normalise to the incident beam monitor

Before anything can be done with the different measured datasets they need to be corrected for the different number of incident units of radiation they have each received, so that they can be compared. This number is given by the integrated monitor count, $\langle\Phi(\lambda,t)\rangle_t\Delta t)$, typically monitored by a special monitor detector placed in the incident beam which counts for exactly the same length of time that each sample is counted for. Deliberately this monitor detector has low efficiency so as not to remove too much of the incident beam, which also means it does not give $\langle\Phi(\lambda,t)\rangle_t\Delta t)$ directly, but an efficiency corrected version of this. For the sample, for example:

$$\mathrm{RAWMON}_s(\lambda) = \langle\Phi(\lambda,t)\rangle_t E_m(\lambda)\Delta\lambda\Delta t_s \tag{3.19}$$

with similar expressions for the other datasets. Here $E_m(\lambda)$ is the monitor detector efficiency.

Within Gudrun, for time-of-flight neutron diffraction, there is the further option, if the source is stable enough, to average this monitor count over a specified wavelength range to give

$$\begin{aligned}\mathrm{RAWMON}_s(\lambda) &= \frac{\int_{\lambda_1}^{\lambda_2}\langle\Phi(\lambda,t)\rangle_t E_m(\lambda)d\lambda}{(\lambda_2-\lambda_1)}\Delta\lambda\Delta t_s \\ &= \langle\langle\Phi(\lambda,t)\rangle_t E_m(\lambda)\rangle_\lambda\Delta\lambda\Delta t_s \end{aligned}\tag{3.20}$$

so that the monitor count for each wavelength value is set to this average value. This has the advantage of improving the statistics on the monitor, but of course relies on the fact that the spectrum shape does not vary with time.

Typically for a standard laboratory x-ray source there is no incident beam monitor, but because modern sources are normally very stable it is sufficient to set

$$\mathrm{RAWMON}_s(\lambda) = C\Delta\lambda\Delta t_s \tag{3.21}$$

independent of the incident x-ray flux, with C an undetermined constant which is taken to be a characteristic of the source and the same for all samples and backgrounds. For synchrotron x-ray sources there is typically a photodiode, with or without scintillator, in the incident or transmitted beam to measure the radiation flux on the sample for each measuring period.

The measured intensities for each sample and background must be normalised to the corresponding value of $\mathrm{RAWMON}(\lambda)$ so that they can be compared. For the sample and

assuming (3.19) is used for the monitor count the result is

$$\begin{aligned}
\mathrm{NORMMON}_b(\lambda,2\theta) &= \frac{\mathrm{CNT}_b(\lambda,2\theta)}{\mathrm{RAWMON}_b(\lambda)} = B(\lambda,2\theta)\frac{E_d(\lambda)}{E_m(\lambda)}\Delta\Omega(2\theta)\\
\mathrm{NORMMON}_s(\lambda,2\theta) &= \frac{\mathrm{CNT}_s(\lambda,2\theta)}{\mathrm{RAWMON}_s(\lambda)}\\
&= (A_{s,s}N_s\Sigma_s(\lambda,2\theta) + M_s + B(\lambda,2\theta))\frac{E_d(\lambda)}{E_m(\lambda)}\Delta\Omega(2\theta)\\
\mathrm{NORMMON}_{s+c}(\lambda,2\theta) &= \frac{\mathrm{CNT}_{s+c}(\lambda,2\theta)}{\mathrm{RAWMON}_{s+c}(\lambda)}\\
&= (A_{s,sc}N_s\Sigma_s(\lambda,2\theta) + A_{c,sc}N_c\Sigma_c(\lambda,2\theta) + M_{sc}\\
&\quad + B(\lambda,2\theta))\frac{E_d(\lambda)}{E_m(\lambda)}\Delta\Omega(2\theta)\\
\mathrm{NORMMON}_{s+c+f}(\lambda,2\theta) &= \frac{\mathrm{CNT}_{s+c+f}(\lambda,2\theta)}{\mathrm{RAWMON}_{s+c+f}(\lambda)}\\
&= (A_{s,scf}N_s\Sigma_s(\lambda,2\theta) + A_{c,scf}N_c\Sigma_c(\lambda,2\theta) + A_{f,scf}N_f\Sigma_f(\lambda,2\theta)\\
&\quad + M_{scf} + B(\lambda,2\theta))\frac{E_d(\lambda)}{E_m(\lambda)}\Delta\Omega(2\theta)
\end{aligned} \tag{3.22}$$

and so on. These ratios get closer to the cross-sections we are seeking, but multiplied by the value $\frac{E_d(\lambda)}{E_m(\lambda)}\Delta\Omega$, which is however not well known. Corresponding expressions will apply to the other possible monitor normalisations, (3.20) and (3.21).

3.7 Subtract the background

Irrespective of how the monitor normalisation is accomplished and provided the same method is used for all datasets, the background can now be subtracted directly:

$$\begin{aligned}
\text{SUBBAK}_s(\lambda,2\theta) &= \text{NORMMON}_s(\lambda,2\theta) - \text{NORMMON}_b(\lambda,2\theta) \\
&= (A_{s,s}N_s\Sigma_s(\lambda,2\theta) + M_s)\frac{E_d(\lambda)}{E_m(\lambda)}\Delta\Omega(2\theta) \\
\text{SUBBAK}_{s+c}(\lambda,2\theta) &= \text{NORMMON}_{s+c}(\lambda,2\theta) - \text{NORMMON}_b(\lambda,2\theta) \\
&= (A_{s,sc}N_s\Sigma_s(\lambda,2\theta) + A_{c,sc}N_c\Sigma_c(\lambda,2\theta) + M_{sc})\frac{E_d(\lambda)}{E_m(\lambda)}\Delta\Omega(2\theta) \\
\text{SUBBAK}_{s+c+f}(\lambda,2\theta) &= \text{NORMMON}_{s+c+f}(\lambda,2\theta) - \text{NORMMON}_b(\lambda,2\theta) \\
&= (A_{s,scf}N_s\Sigma_s(\lambda,2\theta) + A_{c,scf}N_c\Sigma_c(\lambda,2\theta) + A_{f,scf}N_f\Sigma_f(\lambda,2\theta) \\
&\quad + M_{scf})\frac{E_d(\lambda)}{E_m(\lambda)}\Delta\Omega(2\theta)
\end{aligned} \tag{3.23}$$

3.8 Put the data on an absolute scale

Whichever method, (3.19) - (3.21), is used to normalise the data, we are left with unknown calibration constants, $C_n(\lambda,2\theta)$ which are respectively:

$$\begin{aligned}
C_1(\lambda,2\theta) &= \frac{E_d(\lambda)}{E_m(\lambda)}\Delta\Omega(2\theta) \text{ for normalisation (3.19)} \\
C_2(\lambda,2\theta) &= \frac{\langle\Phi(\lambda,t)\rangle_t E_m(\lambda)}{\langle\langle\Phi(\lambda,t)\rangle_t E_m(\lambda)\rangle_\lambda}\Delta\Omega(2\theta) \text{ for normalisation (3.20)} \\
C_3(\lambda,2\theta) &= \frac{\langle\Phi(\lambda,t)\rangle_t E_m(\lambda)}{C}\Delta\Omega(2\theta) \text{ for normalisation (3.21)}
\end{aligned} \tag{3.24}$$

In order to be able to put the data on an absolute scale, the appropriate calibration constant needs to be determined. The method employed for neutrons is quite different to that for x-rays.

3.8.1 Data calibration for neutrons

For neutrons there is an almost ideal material for putting the diffraction data on an absolute scale. This is vanadium, which for neutrons has a small coherent scattering length. This means any distinct scattering from Bragg reflections is intrinsically very weak compared to the single atom scattering. Vanadium is a solid metal with precisely known density that is stable on its own so does not require a container and which can be formed into cylinders or flate plates as required. Also the mass of the vanadium atom means that inelasticity effects with this material will be small and so can be estimated using an approximate model (e.g. Placzek-type) model for the inelasticity.

The basic idea behind calibration with vanadium is to run a parallel experiment to that of the sample, using the same beamline conditions (apertures, detector positions,

etc.). Because the differential cross section for vanadium is dominated by single atom scattering it is mostly flat with Q_e or 2θ but with a few weak Bragg peaks whose positions are known. It also has well known attenuation and capture properties which means the attenuation and multiple scattering factors are readily calculable. Finally vanadium does not require a container, so that it is possible to estimate $C_n(\lambda, 2\theta)$ directly from the vanadium measurement.

To do this requires an extra measurement, namely one for the vanadium sample:

$$\mathrm{CNT}_v(\lambda, 2\theta) = (A_{v,v}N_v\Sigma_v(\lambda, 2\theta) + M_v + B(\lambda, 2\theta))\langle\Phi(\lambda, t)\rangle_t E_d(\lambda)\Delta\lambda\Delta\Omega(2\theta)\Delta t_v. \quad (3.25)$$

These data are put through the same sequence of steps as the sample data, in particular to be useful they must be subject to the same monitor normalisation (ensuring this is done automatically by the program):

$$\begin{aligned} \mathrm{NORMMON}_v(\lambda, 2\theta) &= \frac{\mathrm{CNT}_v(\lambda, 2\theta)}{\mathrm{RAWMON}_v(\lambda)} \\ &= (A_{v,v}N_v\Sigma_v(\lambda, 2\theta) + M_v + B(\lambda, 2\theta))C_n(\lambda, 2\theta) \quad (3.26) \\ \mathrm{SUBBAK}_v(\lambda, 2\theta) &= \mathrm{NORMMON}_v(\lambda, 2\theta) - \mathrm{NORMMON}_b(\lambda, 2\theta) \\ &= (A_{v,v}N_v\Sigma_v(\lambda, 2\theta) + M_v)C_n(\lambda, 2\theta) \quad (3.27) \end{aligned}$$

Using the methods described in section 3.4 the term $(A_{v,v}N_v\Sigma_v(\lambda, 2\theta) + M_v)$ is estimated by numerical simulation and divided into the vanadium data:

$$\mathrm{VANCOR}(\lambda, 2\theta) = \frac{\mathrm{SUBBAK}_v(\lambda, 2\theta)}{(A_{v,v}N_v\Sigma_v(\lambda, 2\theta) + M_v)_{\mathrm{est.}}} = (C_n(\lambda, 2\theta))_{\mathrm{est.}} \quad (3.28)$$

To improve statistics, these data are normally smoothed to reduce noise, with the degree of smoothing set by a number in the input file to Gudrun. Hence the final data calibration is in the array

$$\mathrm{SMOVAN}(\lambda, 2\theta) = \text{ smoothed version of } \mathrm{VANCOR}(\lambda, 2\theta) = (C_n(\lambda, 2\theta))_{\mathrm{est.}}. \quad (3.29)$$

A certain amount of smoothing is acceptable since the ratio $\mathrm{VANCOR}(\lambda, 2\theta)$ is expected to be slowly varying with λ. Nonetheless if the smoothing is overdone it can lead to artifacts, particularly at the ends of each spectrum.

IMPORTANT NOTE: For fixed wavelength data, such as from D4C, this smoothing will have no effect, since GudrunN treats each scattering angle as a separate spectrum with just one wavelength bin in it.

When setting up $\Sigma_v(\lambda, 2\theta)$ the positions, widths and heights of the Bragg peaks can be specified in a file with extension **.bragg**. Alternatively the vanadium differential cross section can be input from a file with extension **.dcs** or **.mdcs**.

3.8.2 Data calibration for x-rays

Sadly for x-rays there is no equivalent to the incoherent neutron scattering from vanadium to make an independent estimate of the data calibration. Putting x-ray diffraction data onto an absolute scale is a perennial problem. The method adopted in GudrunX is that developed by Krogh-Moe [1956] and Norman [1957] as it seems to work quite well in practice.

Putting together the results from equation (2.27) and section 2.3.5, the total differential scattering cross section for x-rays is:

$$\begin{aligned}\left(\frac{d\sigma}{d\Omega}\right)_x &= \left(\frac{d\sigma}{d\Omega}\right)_{Th}(\lambda,2\theta)F_x(Q)+\left(\frac{d\sigma}{d\Omega}\right)_{KN}\sum_\alpha c_\alpha S(x,Z_\alpha)\\ &= \sum_\alpha c_\alpha\left(\left(\frac{d\sigma}{d\Omega}\right)_{Th}f_\alpha^2(Q)+\left(\frac{d\sigma}{d\Omega}\right)_{KN}S(x,Z_\alpha\right)\\ &\quad+\left(\frac{d\sigma}{d\Omega}\right)_{Th}\left(\sum_{\alpha\beta\geq\alpha}(2-\delta_{\alpha\beta})\,c_\alpha c_\beta f_\alpha(Q)f_\beta(Q)H_{\alpha\beta}(Q)\right)\\ &= \left(\frac{d\sigma}{d\Omega}\right)_{self}\\ &\quad+\left(\frac{d\sigma}{d\Omega}\right)_{Th}\left(\sum_{\alpha\beta\geq\alpha}(2-\delta_{\alpha\beta})\,c_\alpha c_\beta f_\alpha(Q)f_\beta(Q)H_{\alpha\beta}(Q)\right)\end{aligned}\tag{3.30}$$

The underlying idea is that the Fourier inverse of equation (2.23) is given by

$$h_{\alpha\beta}(\mathbf{r})=\frac{1}{2\pi^2\rho}\int H_{\alpha\beta}(\mathbf{Q})\exp(i\mathbf{Q}\cdot\mathbf{r})d\mathbf{Q}\tag{3.31}$$

so that for $\mathbf{r}=0$

$$\begin{aligned}h_{\alpha\beta}(0) &= \frac{1}{2\pi^2\rho}\int H_{\alpha\beta}(\mathbf{Q})d\mathbf{Q}\\ &= \frac{1}{2\pi^2\rho}\int_0^\infty Q^2H_{\alpha\beta}(Q)dQ\end{aligned}\tag{3.32}$$

Because $g_{\alpha\beta}(0)=0$ (no atomic overlap) then $h_{\alpha\beta}(0)=-1$, i.e. it has a known value.

Suppose, using the procedures described in this chapter, we obtain $\Sigma_x(\lambda,2\theta)$ within our calibration factor, $C_3(\lambda,2\theta)$, namely $\mathrm{SUBBAK}_x(\lambda,2\theta)=C_3(\lambda,2\theta)\Sigma_x(\lambda,2\theta)$. Performing the integrals (3.32) on these data (bearing in mind of course that Q is a function of θ) we obtain

$$\begin{aligned}\int_{Q_{min}}^{Q_{max}}Q^2\left[\frac{\mathrm{SUBBAK}_x(\lambda,2\theta)}{\left(\frac{d\sigma}{d\Omega}\right)_{Th}(\lambda,2\theta)}\right]dQ &= C_3(\lambda,2\theta)\int_{Q_{min}}^{Q_{max}}Q^2\left[\frac{\left(\frac{d\sigma}{d\Omega}\right)_{self}^{(\lambda,2\theta)}}{\left(\frac{d\sigma}{d\Omega}\right)_{Th}^{(\lambda,2\theta)}}\right]dQ\\ &\quad+C_3(\lambda,2\theta)\textstyle\sum_{\alpha\beta\geq\alpha}(2-\delta_{\alpha\beta})\,c_\alpha c_\beta\int_{Q_{min}}^{Q_{max}}Q^2f_\alpha(Q)f_\beta(Q)H_{\alpha\beta}(Q)dQ\end{aligned}\tag{3.33}$$

The approximation that Krogh-Moe and Norman make is that

$$\frac{1}{2\pi^2\rho}\int_{Q_{min}}^{Q_{max}} Q^2 f_\alpha(Q) f_\beta(Q) H_{\alpha\beta}(Q) dQ = -Z_\alpha Z_\beta \tag{3.34}$$

as per (3.32). Given that the electron cloud around each atom is diffuse, and especially within the independent atom approximation, which states that the electron cloud is independent of the surrounding atoms, then there is no guarantee this condition is exact, particularly since the integral can only be performed over a finite Q range. Hence within GudrunX there is the opportunity to add an arbitrary constant to this value, so allowing for possible electron overlap. The revised version of the Krogh-Moe and Norman condition is

$$\frac{1}{2\pi^2\rho}\int_{Q_{min}}^{Q_{max}} Q^2 f_\alpha(Q) f_\beta(Q) H_{\alpha\beta}(Q) dQ = -Z_\alpha Z_\beta + \delta \tag{3.35}$$

where δ is set by the experimenter. Clearly it would make sense that $\delta \geq 0$ but there is no check done to enforce this condition. Inserting (3.35) into (3.33) enables C to be determined:

$$C_3(\lambda, 2\theta) = \left[\frac{\int_{Q_{min}}^{Q_{max}} Q^2 \left[\dfrac{\mathrm{SUBBAK}_x(\lambda, 2\theta)}{\left(\dfrac{d\sigma}{d\Omega}\right)_{Th}(\lambda, 2\theta)} \right] dQ}{\int_{Q_{min}}^{Q_{max}} Q^2 \left[\dfrac{\left(\dfrac{d\sigma}{d\Omega}\right)_{self}^{(\lambda,2\theta)}}{\left(\dfrac{d\sigma}{d\Omega}\right)_{Th}^{(\lambda,2\theta)}} \right] dQ - 2\pi^2\rho \sum_{\alpha\beta\geq\alpha} (2-\delta_{\alpha\beta})\, c_\alpha c_\beta (Z_\alpha Z_\beta - \delta)} \right] \tag{3.36}$$

Since all the terms on the right-hand side of (3.36) are calculable, then in principle $C_3(\lambda, 2\theta)$ can be determined. In practice, since corrections for attenuation, multiple scattering, polarisation, bremsstrahlung scattering, and fluorescence (see later sections) have to be performed on the data, the calibration constant is determined iteratively at the end of each pass through the data. Five such iterations is generally enough to give a good value of the calibration constant. (NOTE: GudrunX actually outputs the value of $\dfrac{1}{C_3(\lambda, 2\theta)}$. In fact, since it is assumed to be the same for all scattering angles, $C_3(\lambda, 2\theta)$ is independent of θ and so is output as a single number.)

3.8.3 Apply data calibration (NORMALISATION in GudrunN and GudrunX)

Having determined the appropriate data calibration constants, (3.24) the data are put on an absolute scale of cross section by dividing by this calibration. For a sample without

container for example, one has

$$\begin{aligned} \mathrm{NORMVAN}_s(\lambda, 2\theta) &= \frac{\mathrm{SUBBAK}_s(\lambda, 2\theta)}{C_n(\lambda, 2\theta)} \\ &= A_{s,s} N_s \Sigma_s(\lambda, 2\theta) + M_s \end{aligned} \tag{3.37}$$

For a sample with container and for the container alone, one has

$$\begin{aligned} \mathrm{NORMVAN}_{s+c}(\lambda, 2\theta) &= \frac{\mathrm{SUBBAK}_{s+c}(\lambda, 2\theta)}{C_n(\lambda, 2\theta)} \\ &= A_{s,sc} N_s \Sigma_s(\lambda, 2\theta) + A_{c,sc} N_c \Sigma_c(\lambda, 2\theta) + M_{sc} \end{aligned} \tag{3.38}$$

$$\begin{aligned} \mathrm{NORMVAN}_c(\lambda, 2\theta) &= \frac{\mathrm{SUBBAK}_c(\lambda, 2\theta)}{C_n(\lambda, 2\theta)} \\ &= A_{c,c} N_s \Sigma_s(\lambda, 2\theta) + M_c \end{aligned} \tag{3.39}$$

Analogous expressions can be written down for the cases where the sample has more than one container.

3.9 Perform attenuation and multiple scattering corrections

Having put the data on an absolute scale and assuming the multiple scattering and attenuation corrections have been estimated, it is now straightforward to remove the multiple scattering:

$$\begin{aligned} \mathrm{MULCOR}_s(\lambda, 2\theta) &= \mathrm{NORMVAN}_s(\lambda, 2\theta) - M_s \\ &= A_{s,s} N_s \Sigma_s(\lambda, 2\theta) I \end{aligned} \tag{3.40}$$

$$\begin{aligned} \mathrm{MULCOR}_{s+c}(\lambda, 2\theta) &= \mathrm{NORMVAN}_{s+c}(\lambda, 2\theta) - M_{sc} \\ &= A_{s,sc} N_s \Sigma_s(\lambda, 2\theta) + A_{c,sc} N_c \Sigma_c(\lambda, 2\theta) \end{aligned} \tag{3.41}$$

$$\begin{aligned} \mathrm{MULCOR}_c(\lambda, 2\theta) &= \mathrm{NORMVAN}_c(\lambda, 2\theta) - M_c \\ &= A_{c,c} N_s \Sigma_s(\lambda, 2\theta) + A_{c,sc} N_c \Sigma_c(\lambda, 2\theta) \end{aligned} \tag{3.42}$$

Performing the attenuation correction is equally straightforward. For the sample without container:

$$\mathrm{ABSCOR}_s(\lambda, 2\theta) = \Sigma_s(\lambda, 2\theta) = \frac{\mathrm{MULCOR}_s(\lambda, 2\theta)}{N_s A_{s,s}}. \tag{3.43}$$

For the sample with one container:

$$\mathrm{ABSCOR}_s(\lambda, 2\theta) = \Sigma_s(\lambda, 2\theta) = \frac{\mathrm{MULCOR}_{s+c}(\lambda, 2\theta) - \frac{A_{c,sc}}{A_{c,c}} \mathrm{MULCOR}_c(\lambda, 2\theta)}{N_s A_{s,sc}} \tag{3.44}$$

For the sample with two containers (s, c, f), then first one has to remove the scattering from the outer container, f, in a manner analogous to (3.44):

$$\begin{aligned} \mathrm{ABSCOR}_{s+c}(\lambda, 2\theta) &= \mathrm{MULCOR}_{s+c+f}(\lambda, 2\theta) - \frac{A_{f,scf}}{A_{f,f}}\mathrm{MULCOR}_f(\lambda, 2\theta) \\ \mathrm{ABSCOR}_c(\lambda, 2\theta) &= \mathrm{MULCOR}_{c+f}(\lambda, 2\theta) - \frac{A_{f,cf}}{A_{f,f}}\mathrm{MULCOR}_f(\lambda, 2\theta) \end{aligned} \tag{3.45}$$

Then the scattering from the innermost container must be subtracted from the sample plus container:

$$\mathrm{ABSCOR}_s(\lambda, 2\theta) = \Sigma_s(\lambda, 2\theta) = \frac{\mathrm{ABSCOR}_{s+c}(\lambda, 2\theta) - \frac{A_{c,scf}}{A_{c,cf}}\mathrm{ABSCOR}_c(\lambda, 2\theta)}{N_s A_{s,scf}} \tag{3.46}$$

In the event that there are more than two containers, the sequence of first subtracting the outermost container using the appropriate attenuation factors, then the next outermost, is repeated until all the containers have been subtracted. The formulae for when there are three containers are left as an exercise for the user!

The final step of (3.43), (3.44) and (3.46) includes the division by the number of atoms in the beam, to give the total differential scattering cross section of the sample per atom of the sample. GudrunN and GudrunX allow the user to choose this value in the event, such as with powder samples, that the container is not fully packed with sample. In the program it is called a "tweak factor" and can be thought of as the inverse of the packing fraction. For example if the packing fraction is 0.5, the corresponding tweak factor would be 2.0. The same packing fraction affects the calculation of the attenuation and multiple scattering: the sample atomic density used for these calculations is equal to the specified atomic density *divided by* the tweak factor. This only applies to the sample itself. If a tweak factor other than 1.0 is used for any of the containers, then the density used in the attenuation and multiple scattering corrections remains that specified in the input file. In those cases the tweak factor is simply the number that the data are multiplied by in the equations prior to subtracting from the corresponding sample-plus-container data.

When comparing the values of ABSCOR with MULCOR, bear in mind that for cylindrical geometry N_s is the actual number of atoms in the beam, whereas for flat plate geometry N_s is the number of atoms per unit area. This is because the multiple scattering and total scattering terms in the calibration (3.28) are calculated per unit area for flat plate samples.

3.10 Post processing

Having finally ended up with the differential scattering cross section of the sample as a function of λ and 2θ corrected for attenuation and multiple scattering, and placed on an absolute scale of barns/atom/sr, the data are still not overly useful, since there are often many hundreds, if not thousands of detectors. It is therefore necessary to combine the

detectors together, initially in groups, finally, if required, into a single spectrum. The latter step may not be useful if the data are sensitive to the intrinsic resolution of the diffractometer, such as with Bragg scattering samples.

3.10.1 Procedures specific to GudrunN: combining detectors in groups

Grouping of the detectors in GudrunN is achieved via a file with extension **.grp**. Normally this will be supplied by the instrument scientist, though the user is entirely at liberty to specify their own groups file. Typically one would group detectors at similar scattering angles together, since these are likely to have similar resolution functions. Equally one might keep separate detectors at the same scattering angle but in different parts of the diffractometer. However the detectors are to be grouped, it is necessary to first specify the common scale of units that the merged data are to be stored on. This might be wavevector change, Q, or d-spacing $= 2\pi/Q$ or simply time-of-flight (μs). Alternatively the detectors can be grouped onto a common wavelength [Å] or energy [meV] scale.

To combine the multiple detectors onto a common scale it is also necessary to specify how this combination will be achieved, i.e. will it simply be the arithmetic mean of the results in each detector and angle, or should the average be weighted by the counting statistics. Throughout the analysis GudrunN and GudrunX keep track of the standard deviation of the cross section values, derived from the counting statistics of the raw data. Hence in the weighted mean the data are multiplied by their corresponding standard deviations before adding to the average, and when adding data to the average is finished, the result is divided by the sum of the standard deviations. In the program this is called *statistical weighting on merge*. Generally using this weighting gives a cleaner result than forming the arithmetic mean, since the statistical weighting down-weights poorly counting detectors.

Before the data can be combined, they need to be put on the common units scale. Converting $(\lambda, 2\theta$ values to the units requested for each detector is stored in the array PREMERGE$(\lambda, 2\theta)$, while the array MERGE$(\lambda, 2\theta)$ contains the same data after rebinning it onto the x-scale common to all groups. The merged data from individual groups are output into the file with extension **.dcs** while the merged data where all the detectors are combined into a single spectrum are stored in the file with extension **.mdcs**.

3.10.2 Procedures specific to GudrunX

In GudrunX it is currently assumed there is only one detector, so there is no provision for detector grouping as such, but if, as for reactor neutron data, each detector angle is regarded as a separate detector, then there is effectively one detector at each scattering angle. These data are merged and rebinned on to a single x-scale, but note that the output units are currently restricted to Q only.

There are three other factors which can affect the x-ray intensity and which require correcting for prior to output of the final differential cross section.

X-ray polarisation corrections

This has already been alluded to in the discussion of x-ray inelastic scattering, Section 2.3.5. There, mention was made of the fact that both the Thomson, (2.61), and Klein-Nishina, (2.56), scattering formulae apply to an unpolarised incident x-ray beam. The polarisation correction arises because an x-ray, being a transverse wave, is scattered by that component of its electric wave vector which is at right angles to its direction of travel. Hence an x-ray scattered at 0° or 180° can be scattered whatever its polarisation because the right angle condition is always satisfied, but for an x-ray scattered at 90° in the horizontal plane, only the vertical component of its electric field vector can scatter, so the intensity drops to 1/2 of its zero angle value. This is what leads to the Thomson formula, (2.61).

As far as we know a laboratory x-ray source is unpolarised, so the Thomson formula should work fine in that case, but with synchrotron x-ray sources, the radiation in the plane of the orbit is horizontally polarised, so that if the detectors move in the vertical plane, as is normally the case, there will be no discernible polarisation effect. At synchrotron instruments the polarization of the beam (after mirrors and monochromators) is often measured directly by looking at the scattering from a piece of Kapton, which would normally be expected to be isotropic in an unpolarized beam.

GudrunX allows for the possibility that the incident beam may be polarised. This case was dealt with in detail by Kahn et al. [1982] for the case of single crystal reflections by a polarised incident beam. Specifically they showed that the polarisation correction for a particular reflection is given by:

$$P(2\theta) = \frac{1}{2}\left[1 + \cos^2(2\theta) - \phi\cos(2\rho)\sin^2(2\theta)\right] \tag{3.47}$$

where ϕ is a measure of the degree of polarisation of the incident beam:

$$\phi = \frac{E_H^2 - E_V^2}{E_H^2 + E_V^2}, \tag{3.48}$$

E_H, E_V are the horizontal and vertical components of the electric field vector, with horizontal defined as the plane formed by the incident beam, the sample, and the detector, and vertical perpendicular to this plane, and ρ is the azimuthal angle of the detecting element out of the horizontal plane. $\phi = 0$ means the horizontal and vertical components of the incident polarisation are equal, corresponding to an unpolarised beam, while $\phi = -1$ corresponds to incident polarisation at right angles to the scattering plane. If $\rho = 0$ and $\phi = -1$ then there will be no polarisation correction. If $\phi = +1$ this corresponds to incident polarisation in the horizontal plane, which means that for $2\theta = 90°$ there will no scattering. Clearly ϕ and ρ play equivalent roles in this formula, and in practice, for unpolarised x-rays we should set both values to zero.

It is worth mentioning that currently in GudrunX the multiple scattering is given the same polarisation factor as the once scattered x-rays. Given the above formula (3.47) this assumption may not be accurate, since, particularly with tall thin cylinders, much of the second scattering involves two scattering events both nearly at right angles. In practice,

for x-rays at moderate energies the impact of multiple scattering is sufficiently small that polarisation in the multiple scattering is unlikely to have a significant outcome on the data analysis.

As shown in section 3.8.2 it is necessary to apply the correction for polarisation *before* estimating the calibration factor for the data.

Bremsstrahlung scattering

In addition to the usual electron transition lines, K_α, K_β, and so on, laboratory x-ray tubes produce a general background radiation caused by the incident electrons being slowed down in the anode material. This has a characteristic spectrum whose maximum energy corresponds to the electron bombardment energy, E_e, McCall [1982]:

$$C\left(\frac{E_e}{E_x}-1\right)^{\alpha} \quad E_x \leqslant E_e \tag{3.49}$$

where C is a constant that depends on the atomic number of the target nucleus and $\alpha \approx 1$. In practice this spectrum will be self attenuated by the target material, so assuming the x-rays have to travel on average a distance, L_T through the anode material before being emmitted, the spectrum will be modified by a factor $\exp\left(-\mu_T\left(E_x\right)L_T\right)$, where $\mu_T\left(E_x\right)$ is the attenuation coefficient of the target material. Futhermore it is normal, in an attempt to reduce unwanted counts reaching the detector, to place a suitable absorbing foil that will stop the K_β radiation. This will introduce its own transmittance factor on the incident beam, $\exp\left(-\mu_F\left(E_x\right)L_F\right)$, where $\mu_F\left(E_x\right)$ and L_F are the attenuation coefficient and thickness of the absorbing foil respectively. Finally it is expected that the detecting system will impose its own cut-off in energy, determined by the discriminating system on the detector. To represent this we use the function $1\Big/\left(1+\exp\left(\frac{E_0-E_x}{w}\right)\right)$, where E_0 is the cut-off energy and w is the width of the cut-off. Hence the overall assumed expression for the bremsstrahlung radiation is given by

$$I_{Br}\left(E_x\right)=C\exp\left(-\mu_T\left(E_x\right)L_T\right)\left(\frac{E_e}{E_x}-1\right)^{\alpha}\exp\left(-\mu_F\left(E_x\right)L_F\right)\frac{1}{\left(1+\exp\left(\frac{E_0-E_x}{w}\right)\right)} \tag{3.50}$$

For the purposes of data analysis the constant C is chosen so that $\int_0^{E_e} I_{Br}\left(E_x\right)dE_x=1$.

Obviously if the diffractometer has a monchromator, the bremsstrahlung correction is not necessary, but otherwise, because bremsstrahlung radiation produces a spread of x-ray wavelengths it has the effect of producing a smeared out version of the structure factor being sought. This smeared out version must be subtracted from the total differential scattering cross section in order to get to the true differential cross section for the specified x-ray wavelength. Fig. 3.4 shows an example of what the resulting incident bremsstrahlung spectrum might look like.

To use this spectrum in the data analysis, it is necessary to convolute the spectrum with the differential cross section, but as usual we don't know the differential cross section! So a process of achieving this iteratively is implemented. After all the corrections and in

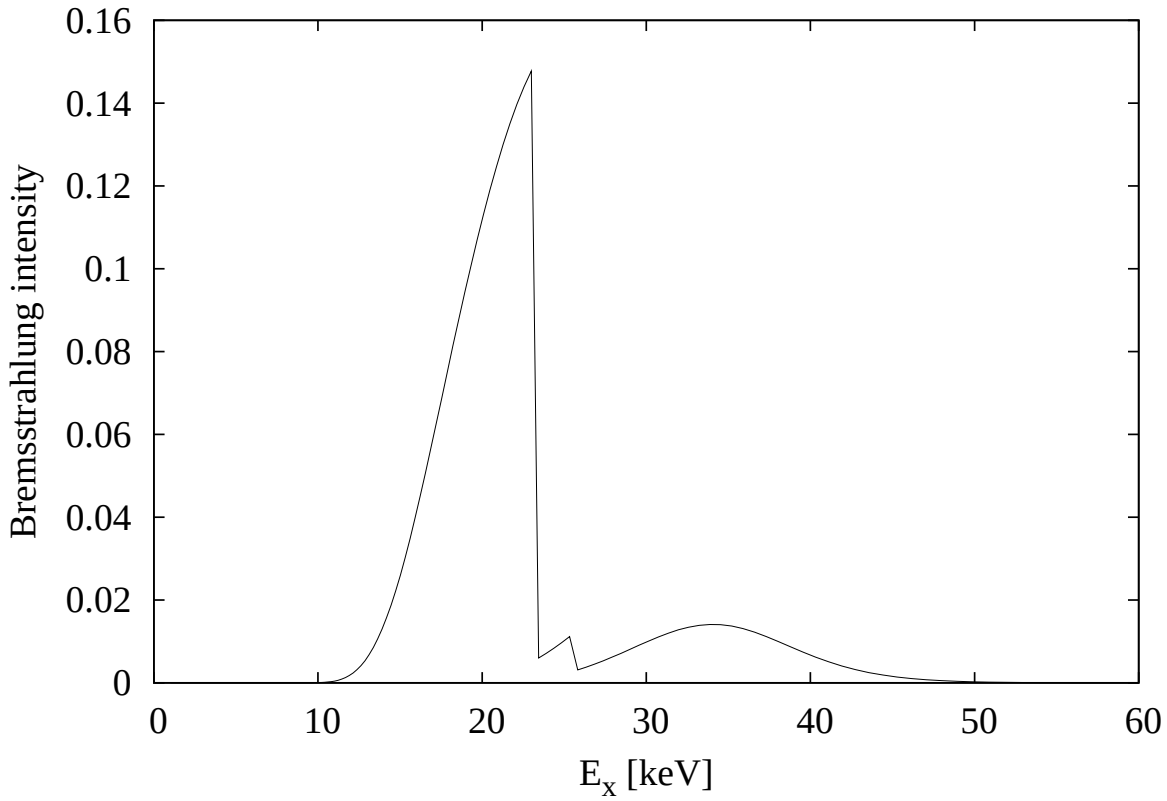

Figure 3.4: Example of the estimated bremsstrahlung spectrum for a silver (Ag) source and assuming a Rh filter of thickness 0.05mm is used. The penetration depth in the Ag anode is assumed to be 0.03mm, and the high energy detector cut-off, E_0, was set at 36keV with a spread (w) of 3keV. The sharp edge near $E_x = 23$keV is caused by the Rh K_α edge, while the smaller edge near $E_x = 25$keV comes from the anode material. Use of the Rh filter prevents most silver K_β x-rays reaching the sample.

the presence of bremsstrahlung radiation, the observed differential cross section, $\Sigma_s(\lambda, 2\theta)$ will be given by

$$\Sigma_s(\lambda, 2\theta) = \left(\frac{d\sigma}{d\Omega}\right)_x (\lambda, 2\theta) + F_{Br} \left(\frac{d\sigma}{d\Omega}\right)_x (\lambda, 2\theta) \bigotimes I_{Br}(E_x) \tag{3.51}$$

where F_{Br} is a factor to be set by the user: if too much bremsstrahlung scattering is subtracted, then $\left(\frac{d\sigma}{d\Omega}\right)_x (\lambda, 2\theta)$ will go negative in some regions, which is unphysical. Therefore F_{Br} can be regarded as a fitting factor, but ideally it should be the same for all samples.

Since we don't know $\left(\frac{d\sigma}{d\Omega}\right)_x (\lambda, 2\theta)$ at the outset it has to be found iteratively. Suppose at the beginning of the n^{th} iteration our current estimate for $\left(\frac{d\sigma}{d\Omega}\right)_x (\lambda, 2\theta)$ is $\left(\frac{d\sigma}{d\Omega}\right)_x^{(n-1)} (\lambda, 2\theta)$. Using (3.51) the next estimate will be:

$$\left(\frac{d\sigma}{d\Omega}\right)_x^{(n)} (\lambda, 2\theta) = \frac{\Sigma_s(\lambda, 2\theta) - F_{Br} \left(\frac{d\sigma}{d\Omega}\right)_x^{(n-1)} (\lambda, 2\theta) \bigotimes I_{Br}(E_x)}{1 - F_{Br}}. \tag{3.52}$$

For the first iteration, $n = 1$, it is natural to set $\left(\frac{d\sigma}{d\Omega}\right)_x^{(0)} (\lambda, 2\theta) = \Sigma_s(\lambda, 2\theta)$ to start the sequence off. Provided $F_{Br} \lesssim 0.5$ this iterative procedure seems to work satisfactorily. Larger values of F_{Br} and it may not converge.

Using the bremstrahlung spectrum shown in Fig. 3.4, Fig. 3.5 shows the extracted $\left(\frac{d\sigma}{d\Omega}\right)_x (\lambda, 2\theta)$, the single atom scattering, and the convoluted bremstrahlung spectrum for Si powder measured on a silver x-ray source. Fig. 3.6 shows the structure factors, after dividing by the single atom scattering, (2.1), obtained with and without the bremsstrahlung correction. It is seen that including the bremsstrahlung contribution makes a big difference to the peak heights, and makes the peak profile cleaner and more symmetric. In addition the background on the data is much flatter when the bremsstrahlung is subtracted. Obviously by measuring or otherwise improving the bremsstrahlung spectrum used in these calculations, these results can be improved still further.

X-ray fluorescence corrections

X-ray fluorescence occurs when an x-ray is absorbed, exciting an electron to a higher orbital, but the electron then decays into a different orbital, emitting a different radiation wavelength than that which caused the excitation. There is a (small) time delay in this process and the emitted photon will know little about the incident photon that caused the

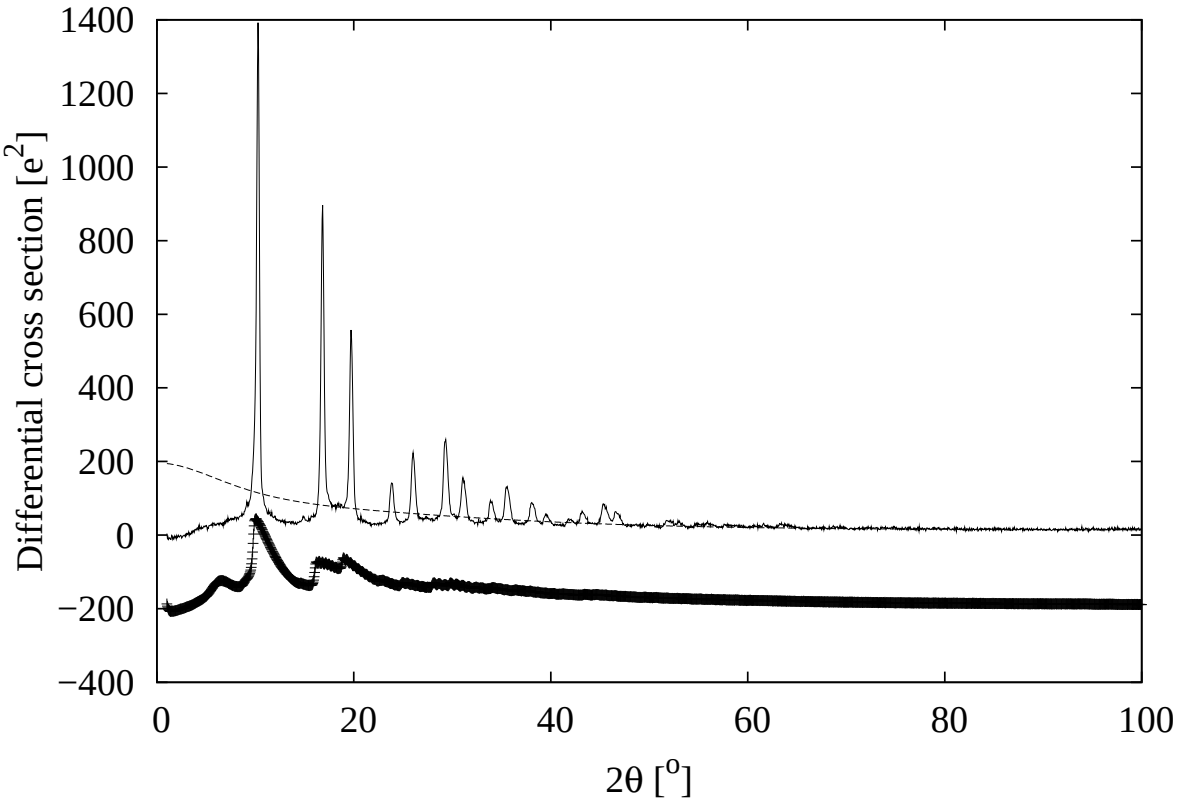

Figure 3.5: Extracted x-ray differential scattering cross section (solid line) for Si powder using Ag K_α radiation with a Rh filter. The dashed line shows the estimated single atom scattering plus Compton scattering and the crosses show the convolution of the differential cross section with the bremsstrahlung specrum from Fig. 3.4. The bremsstrahlung factor, F_{Br}, was set to 0.5 for this calculation.

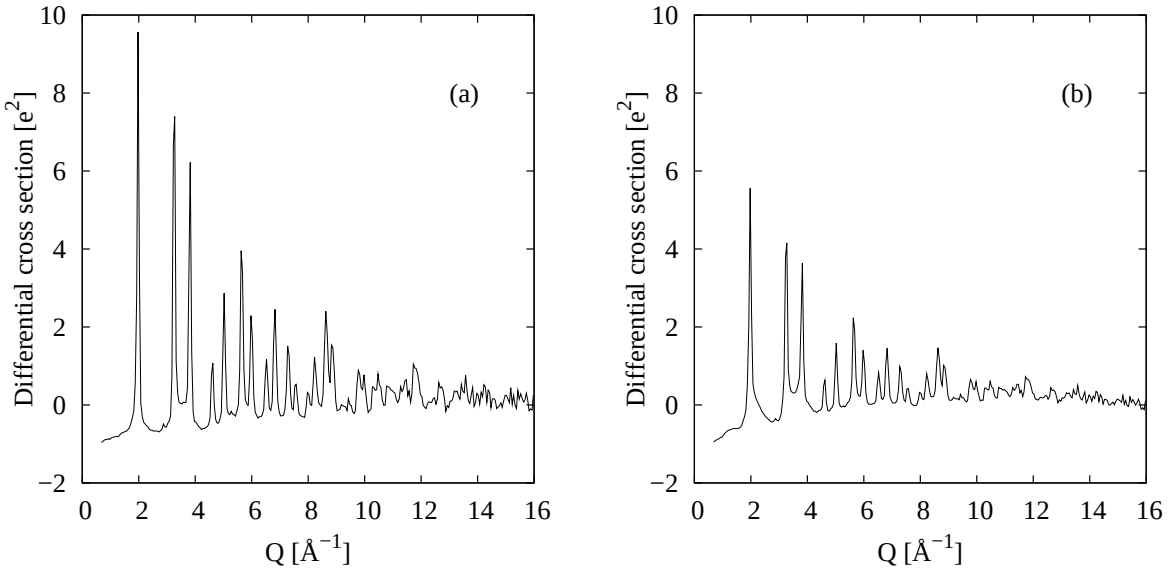

Figure 3.6: Comparison of extracted x-ray structure factors (differential cross section divided by single atom scattering) for Si powder, assuming the bremsstrahlung factor is 0.5 (a), or 0.0 (b).

excitation in the first place. Fluorescence will be a problem whenever there is a fluorescing electron transition near the energy of the incident x-ray. Fluorescence becomes obvious in the data analysis by making it impossible to normalise to the single atom scattering plus Compton scattering in a satisfactory manner.

In GudrunX it is assumed that an element, e, will fluoresce above a characteristic x-ray energy or wavelength, called its fluorescence energy, $E_f^{(e)}$. There are probably few if any cases of a single element fluorescing at more than one energy for a given incident spectrum so only one fluorescence energy is allowed per element. This is because typically it is the K edge in the absorption spectrum that fluoresces, while the L edge is at too low an energy to cause observable fluorescence. However for the heavier elements it may be the L edge that fluoresces, in which case the corresponding K edge is probably at too high an energy to be excited by the incident x-ray spectrum.

It is assumed that the fluorescing x-ray is emitted isotropically in all directions with an intensity proportional to the known photoelectron cross-section for a given incident wavelength. However the observed fluorescence intensity will also be affected by the incident x-ray spectrum - this is assumed to be the same as that used to calculate the bremsstrahlung scattering, $I_{Br}\left(E_x\right)$, as in equation 3.52 - and attenuation in the sample, which in turn depends on the incident x-ray energy, E_x, and the fluorescence energy. Hence it is necessary to calculate the attenuation factor in the sample (plus any containers) for an incident x-ray photon at a series of energies above the fluorescence energy with the emerging photon at the fluorescence energy. These "inelastic" attenuation factors, $A(E_x, E_f^{(e)}, 2\theta)$, are there-

fore distinct from the elastic attenuation factors that have been discussed hitherto, and have to be calculated separately. The sample fluorescence will also depend on the incident intensity at any given energy. If more than one element in the sample fluoresces, it is possible to assign different weights, w_e, to those elements when calculating the fluorescence scattering. Finally, since it is impossible to assign an absolute scale to this fluorescence scattering, the contribution of fluorescence is represented as a user-specified fraction, F, of the sample (elastic) scattering integrated over all scattering angles.

To summarise, the fluorescence is calculated in GudrunX according to the formula:

$$\mathrm{FLUOR}(2\theta) = C_f \sum_e w_e \int_{E_f^{(e)}} I_{Br}\left(E_x\right) \sigma_e^{(PE)}(E_x) A(E_x, E_f^{(e)}, 2\theta) dE_x \tag{3.53}$$

where the sum is over the elements in the sample, and $\sigma_e^{(PE)}(E_x)$ is the photoelectron cross section at energy E_x for element e. The normalising constant C_f is chosen so that the $\int \mathrm{FLUOR}(2\theta) d2\theta$ is a user-defined fraction of $\int \mathrm{NORMMON}_s(\lambda, 2\theta) d2\theta$, and the user has to choose the appropriate fluorescence energy and weight for each element as needed.

This fluorscence scattering is subtracted from the observed x-ray scattering data as a function of scattering angle prior to any processing in terms of normalisation, correction for attenuation and multiple scattering, and background or container subtractions. Fig. 3.7 gives examples of what happens when the fluorescence correction is applied, (a), and when it is not applied, (b).

Bragg-Brentano scanning

For flat plate samples with x-rays it is sometimes necessary to perform Bragg-Brentano scanning. This is the case where both the source *and* the detector are moved, with the angle of incidence and the angle of reflection or transmission kept equal. In this case the footprint of the beam and detector on the sample will vary with scattering angle if the incident and detector slits are held constant. Alternatively the diffractometer in question may have a facility to keep the irradiated area constant as a function of scattering angle by having automatically adjusting slit dimensions. This gives a constant footprint but the scattering volume still changes with scattering angle, depending on the attenuation in the sample. This arragnement gives significant improvement in counting statistics at low angles of incidence, but gives poor performance at high angles of incidence when the beam has become narrow. [2]

[2]IMPORTANT NOTE: Within Gudrun and much of this manual, the angles of incidence, transmission, and reflection are defined as in optical analysis, that is with respect to the normal to the scattering surface and NOT, as in conventional Bragg analysis, see Figure 1.3, with respect to the plane of the scattering surface. Equally the flat plate geometry is defined by stating the rotation angle of the surface normal to the incident beam direction. In reflection geometry a high angle of incidence therefore corresponds to *small* scattering angles, whereas in transmission geometry a high angle of incidence corresponds to *large* scattering angles. The relation between angle of incidence (α) and scattering angle (2θ) is $\alpha = \theta + \gamma_R$, where γ_R is the rotation of the sample normal with respect to the incident beam. A rotation angle $\gamma_R = 0^\circ$

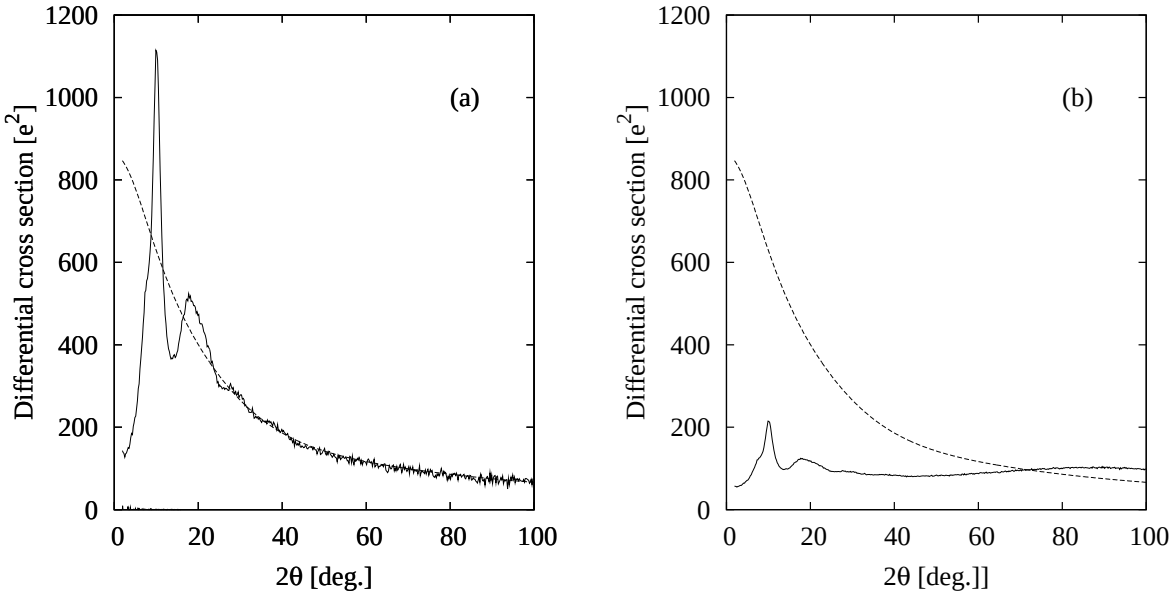

Figure 3.7: Comparison of extracted x-ray differential cross section for amorphous Na_2OTeO_2 powder, assuming the fluorescence fraction is 0.75 (a), or 0.0 (b). The assumed fluorescence energy of Te was assumed to be 31.2keV.

There is an attempt to deal with both these scenarios within GudrunX. The primary object is to calculate the effect of the footprint (if the slits are fixed) or the effect of variable scattering volume in the case of fixed footprint.

Fixed slits - reflection geometry

First we deal with the case of fixed slits and refer to figure 3.8.

From this figure it is straightforward to see that the required volume is

$$V(\alpha) = \begin{cases} 2hf_3t - V_m, & t \leq T \\ 2h(f_1 + f_3)T - V_m, & t > T \end{cases} \tag{3.54}$$

where $f_1, f_2, f_3 \leq R$ and

$$V_m = \begin{cases} 2h\frac{(f_3 - f_1)^2}{\tan\alpha}, & f_3 - f_1 > 0 \\ 0, & \text{otherwise.} \end{cases} \tag{3.55}$$

Since the beam width is fixed in this case, we write

$$f(\alpha) = w/\cos\alpha \tag{3.56}$$

corresponds to TRANSMISSION geometry (sample at right angles to the incident beam at $2\theta = 0$), while a rotation angle of $\gamma_R = -90°$ corresponds to REFLECTION geometry (sample parallel to the incident beam at $2\theta = 0$).

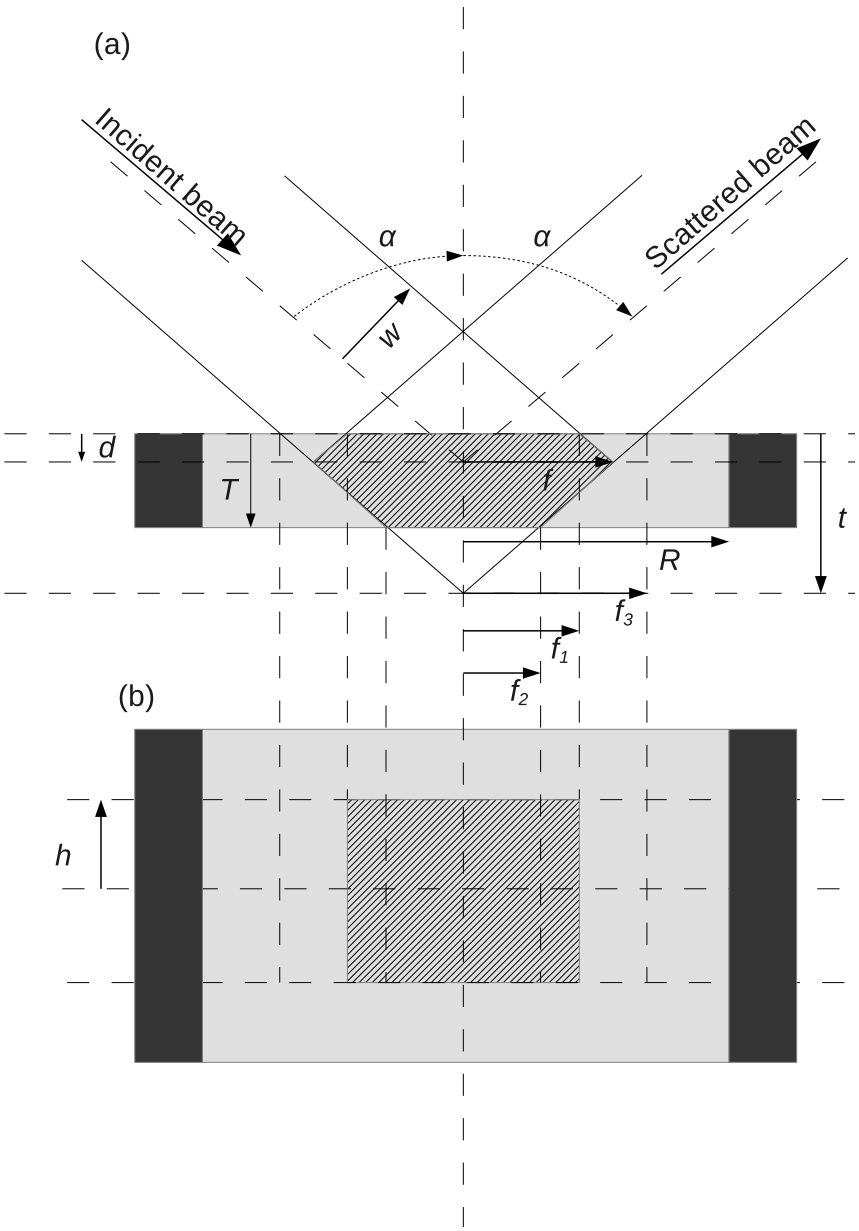

Figure 3.8: Geometry of an x-ray beam of width $2w$ and height $2h$ incident on a rectangular sample of length (along the scattering plane) $2R$ and thickness T at an angle of α to the normal of the sample. The scattering plane is formed by the incident and scattered beam directions. The lateral dimension of the rectangle at right angles to the scattering plane, h, is unimportant for the present calculation. (a) shows a sideways view in the plane of the sample at right angles to the scattering plane while (b) shows the view in the scattering plane, directly above and normal to the plane of the sample. Absorbers (black) are placed at each end of the sample so that x-rays cannot penetrate the sample sides. The surface of the sample is displaced d along the normal to the surface from the beam centre. The shaded area in both diagrams is the beam footprint on the sample whose volume is needed as a function of α.

from which

$$f_1(\alpha) = \begin{cases} 0, & f(\alpha) - |d|\tan\alpha \leq 0 \\ f(\alpha) - |d|\tan\alpha, & f(\alpha) - |d|\tan\alpha < R \\ R, & f(\alpha) - |d|\tan\alpha \geq R. \end{cases} \tag{3.57}$$

and

$$f_3(\alpha) = \begin{cases} f(\alpha) + d\tan\alpha, & f(\alpha) + d\tan\alpha < R \\ R, & f(\alpha) + d\tan\alpha \geq R \end{cases} \tag{3.58}$$

With

$$t(\alpha) = f_3(\alpha)/\tan\alpha \tag{3.59}$$

then

$$f_2(\alpha) = \begin{cases} 0, & t(\alpha) \leq T \\ (t(\alpha) - T)\tan\alpha = f_3(\alpha) - T\tan\alpha, & t(\alpha) > T \end{cases} \tag{3.60}$$

These values are substituted into equation 3.54 to give the sample volume as a function of α. This volume will go to zero in the limit of $w, h \Rightarrow 0$, but the ratio

$$F(\alpha) = \frac{V(\alpha)}{V(0)} \tag{3.61}$$

remains finite at all angles and beam parameters and so can be used as a "footprint" factor to correct for the scattering volume of the sample.

In practice the above calculation only works in the case of a weakly absorbing sample, whereas most samples for x-rays are strongly absorbing. Hence the volumes described need to be modified by the attenuation as a function of depth t and the area of the sample at that depth. This requires an obvious modification to the above formulation which is included in GudrunX but which will not be described further here.

Figure 3.9 gives some examples of the $F(\alpha)$ factor for different values of w, T and d. We see that as w increases the position of the maximum relative volume moves to smaller α (large scattering angles), so limiting the range of the small scattering angle data. Increasing the sample thickness reduces the angular variation quite markedly, while lifting the sample slightly above the beam centre increases the volume available for scattering somewhat. Bear in mind that these solid curves are purely geometric factors and do not include the effect of attenuation which is calculated separately. When attenuation is included (dashed curves) then the trends change quite markedly. Hence it is important to include both the attenuation and volume changes when correcting data measured in this mode.

Fixed irradiated area - reflection geometry

For fixed irradiated area, the value of f is held fixed, and this is achieved by, using equation 3.56, varying w as α changes. As a result we write instead of 3.56:

$$w(\alpha) = f\cos\alpha. \tag{3.62}$$

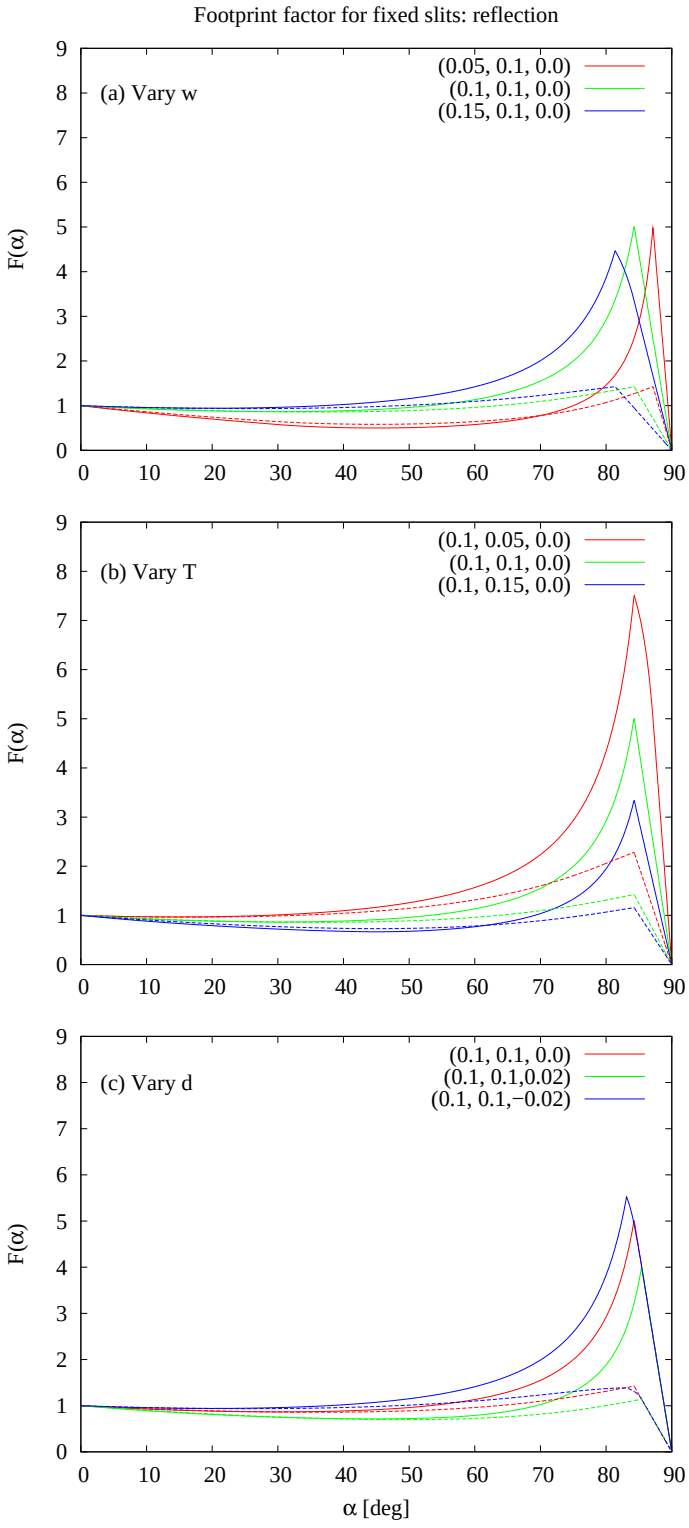

Figure 3.9: Examples of the fixed slit footprint factor in reflection geometry for (a) different beam widths, w, for (b) different sample thicknesses, T and for (c) different sample deviations above or below the beam centre, d. The values of w, T and d are shown in the form (w, T, d) in the legends. All values are expressed as fractions of the lateral dimension R. The dashed lines show the footprint factor when the value of $\mu R = 5$

The rest of the formulation follows exactly as for fixed slits, but the resulting footprint of the sample is quite different, Figure 3.10. In particular it can be seen from (c) that at high angles of incidence (low scattering angles) the footprint is very sensitive to the precise position of the sample with respect to the beam centre. Compared to fixed slit geometry, it will also be seen that at low scattering angles (high angles of incidence) the scattering will be proportionately weaker.

Fixed slits and fixed irradiation area - transmission geometry

Occasionally transmission geometry will be encountered. This is probably relatively unusual for x-rays due to the normally high attenuation of x-rays by most samples. However if high energy x-rays are involved, transmission geometry might be the preferred geometry. Hence the volume correction for transmission geometry is included in GudrunX as for reflection geometry. As before we deal first with the case of fixed slits and refer to figure 3.11.

The areas and volumes that need to be calculated in this case should be fairly obvious from this figure and so will not be written explicitly here. However note that once the incident beam starts to intersect the absorbers placed at each end of the sample, then the centre of scattering will move away from the centre of the sample, so that strictly there should be a correction to the scattering angle. In practice this occurs at high angles of incidence (and therefore at high scattering angles in transmission geometry) so once this intersection starts to occur, it is likely the scattering signal will not be less useful to measure in any case. The attenuation factor is trivial in this case, of the form $\exp\left(-\frac{\mu T}{\cos\alpha}\right)$.

Figures 3.12 and 3.13 give some examples of the $F(\alpha)$ factor for different values of w and T for fixed slit and fixed irradiation length respectively. As stated in the caption to Fig. 3.11 there is little purpose in calculating the effect of moving the sample up and down with respect to the beam, since such movement will have only a slight impact on the footprint factor. Unsurprisingly perhaps we see that the best option is to have the maximum beam width w and lowest sample thickness T depending on the value of the attenuation coefficient for the sample. The limitations in this case occur at high angles of incidence, which in transmission geometry, means high scattering angles. Thus transmission geometry is good for investigating low scattering angles, and poor at high scattering angles, while the reverse is true for reflection geometry. Based on Fig. 3.13 it would appear that using a fixed footprint beam in transmission geometry would be particularly unfavourable since it would mean the scattering signal would be curtailed at high scattering angles which is precisely where the atomic form factors become small.

3.10.3 Converting structure factor to pair distribution function (PDF)

Very often the user would like to see what their data look like when transformed to r-space. Both GudrunN and GudrunX provide facilities to perform a Fourier transform on the extracted structure factors. The method adopted follows that of the top hat convolution

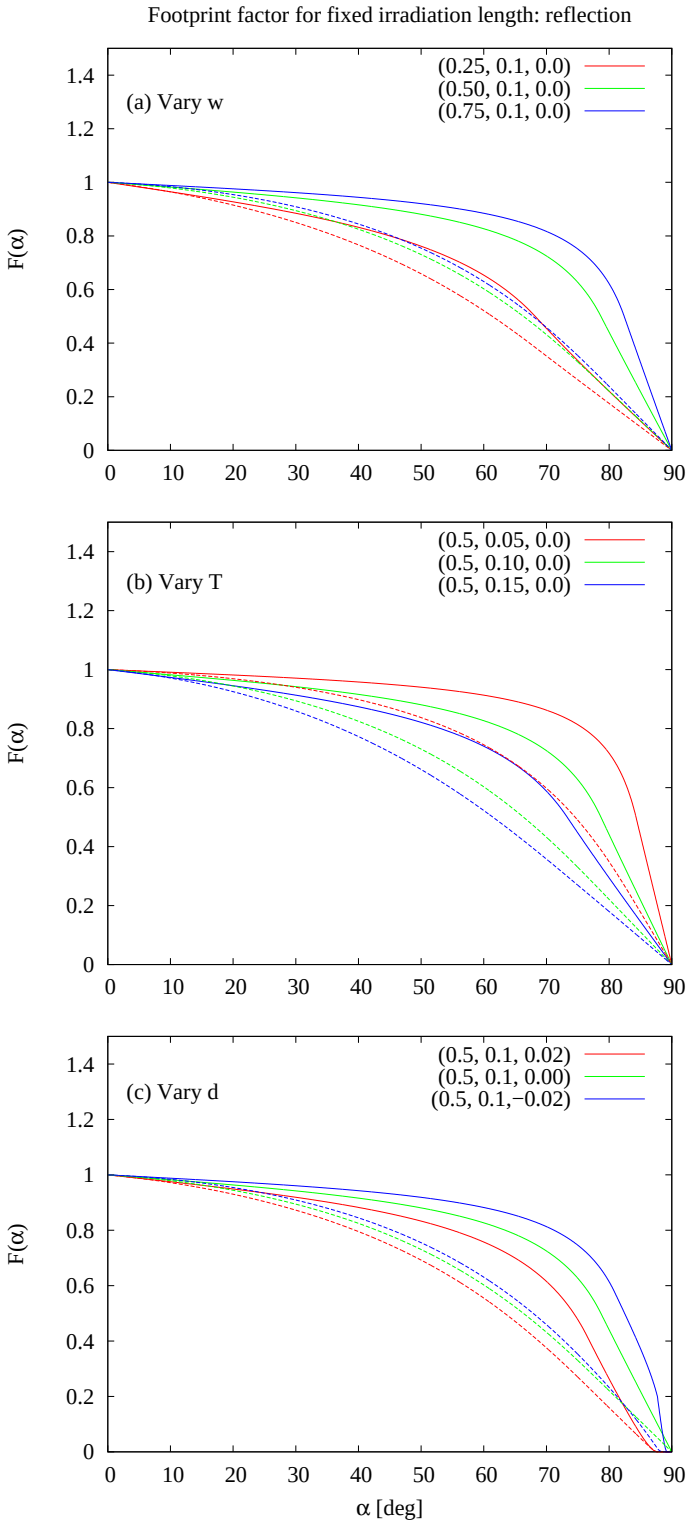

Figure 3.10: Examples of the fixed irradiation area footprint factor in reflection geometry for (a) different footprint widths, f, for (b) different sample thicknesses, T and for (c) different sample deviations above or below the beam centre, d. The values of w, T and d are shown in the form (f, T, d) in the legends. All values are expressed as fractions of the lateral dimension R.

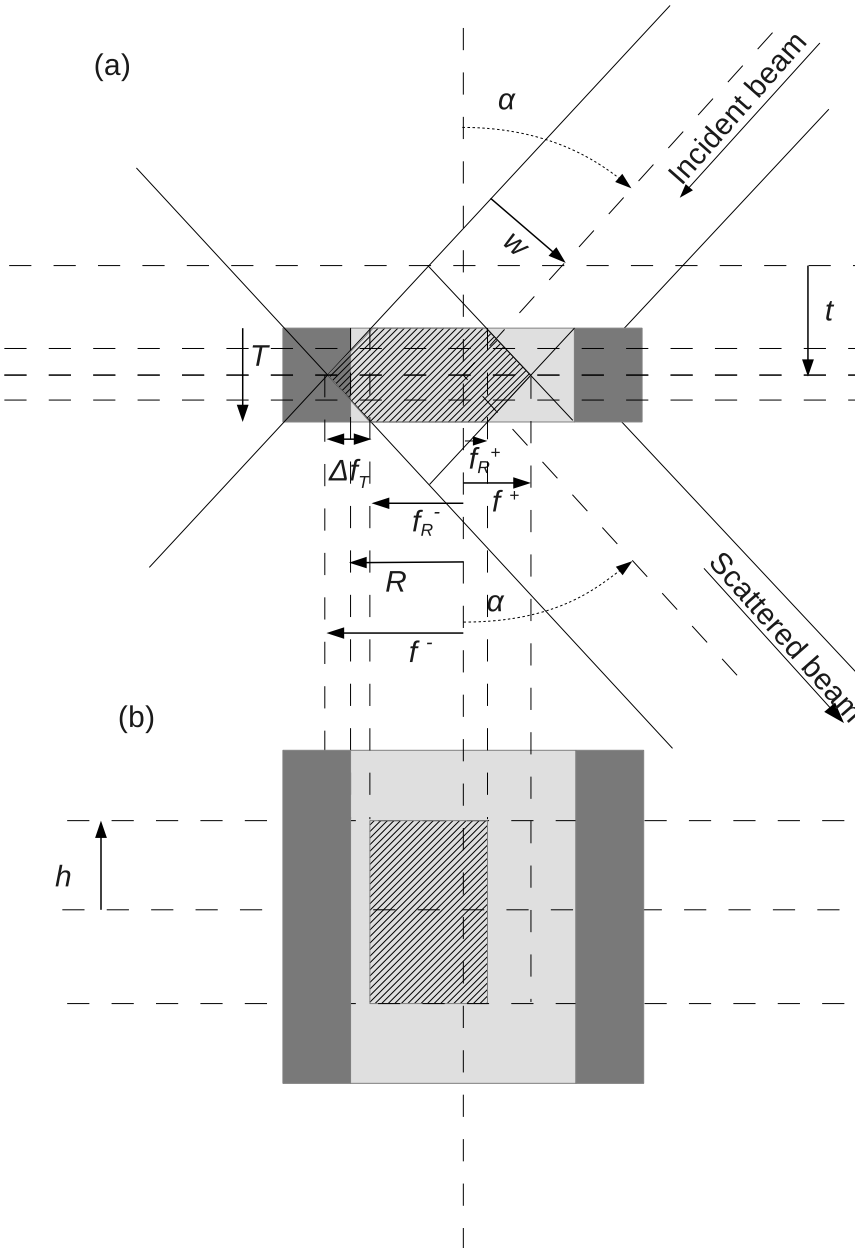

Figure 3.11: Geometry of an x-ray beam of width $2w$ and height $2h$ incident on a rectangular sample of length (along the scattering plane) $2R$ and thickness T at an angle of α to the normal of the sample. The scattering plane is formed by the incident and scattered beam directions. The lateral dimension of the rectangle at right angles to the scattering plane, h, is unimportant for the present calculation. (a) shows a sideways view in the plane of the sample at right angles to the scattering plane while (b) shows the view in the scattering plane, directly above and normal to the plane of the sample. Absorbers (grey) are placed at each end of the sample so that x-rays cannot penetrate the sample sides. It is assumed the intersection of the centres of the incident and scattered beams coincides with the centre of the sample - in this case the effect of an upwards or downwards displacement of the sample relative to this centre will have only a slight effect on the footprint factor. The shaded area in both diagrams is the beam footprint on the sample whose volume is needed as a function of α.

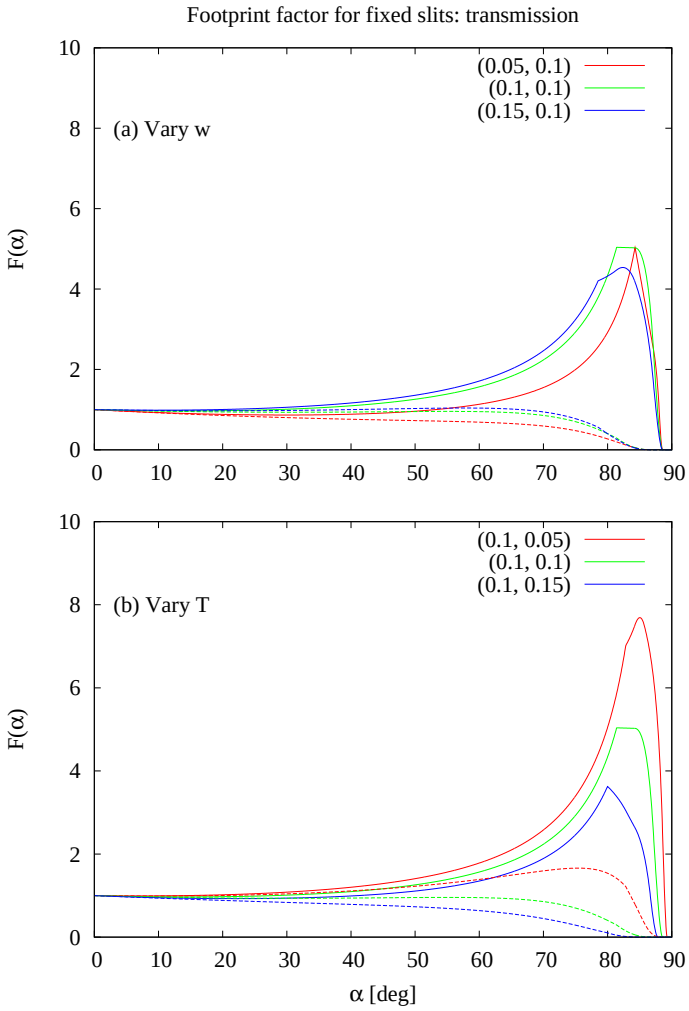

Figure 3.12: Examples of the fixed slit footprint factor in transmission geometry for (a) different beam widths, w, and (b) different sample thicknesses, T. The values of w and T are shown in the form (w, T) in the legends. All values are expressed as fractions of the lateral dimension R. The dashed lines show the footprint factor when the value of $\mu R = 5$

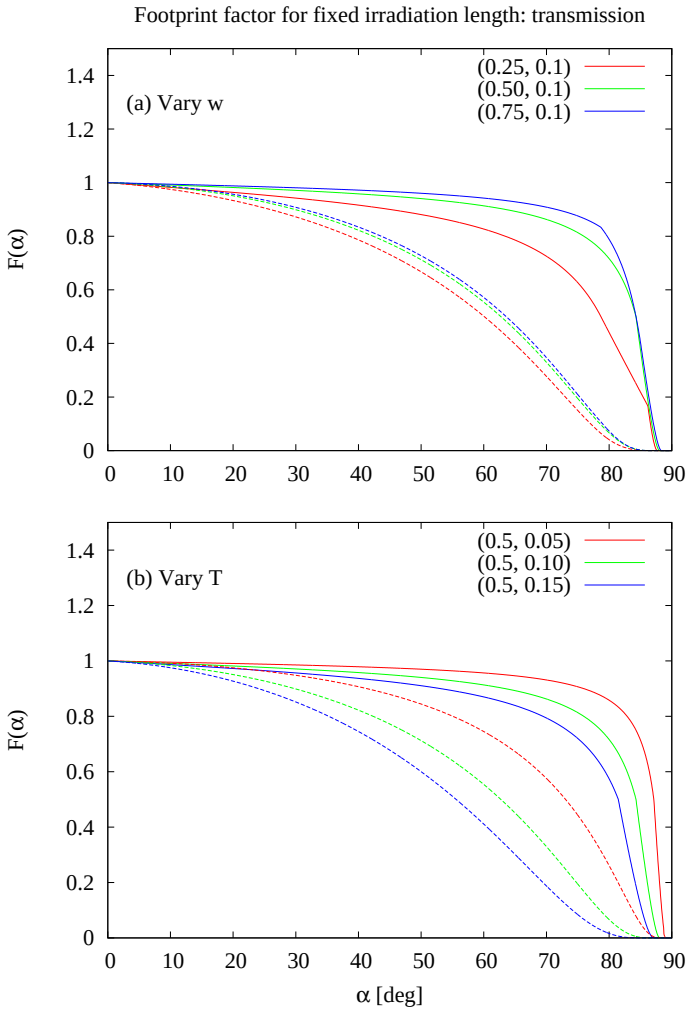

Figure 3.13: Examples of the fixed irradiation length footprint factor in transmission geometry for (a) different beam widths, w, and (b) different sample thicknesses, T. The values of w and T are shown in the form (w, T) in the legends. All values are expressed as fractions of the lateral dimension R. The dashed lines show the footprint factor when the value of $\mu R = 5$

method described in Soper [2009]. Basically the idea is that due to the fact that the data analysis may not have proceeded perfectly, the structure factor is on some kind of Q dependent background. This needs to be removed prior to Fourier transform. The background is generated by convolution of the data with the top hat function:

$$I'(Q_e) = \int_{Q_T} I(|\mathbf{Q}_e - \mathbf{Q}'_e|)\, T(\mathbf{Q}'_e)\, d\mathbf{Q}'_e \tag{3.63}$$

where the integral proceeds over all of reciprocal space for which the data exist, and the top hat function $T(\mathbf{Q}_e)$ is given by:

$$\begin{aligned} T(\mathbf{Q}_e) &= \frac{3}{4\pi Q_T^3}, \quad |\mathbf{Q}_e| \leq Q_T \\ &= 0, \qquad\quad |\mathbf{Q}_e| > Q_T \end{aligned} \tag{3.64}$$

The effect of the convolution therefore is to smear $I(Q_e)$ only in the region near Q_e.

The aim is to now make the Fourier transformation of the difference

$$D'(Q_e) = I(Q_e) - I'(Q_e) \tag{3.65}$$

instead of Fourier transforming the intensity function itself, $I(Q_e)$, namely:

$$d(r) = \frac{1}{(2\pi)^3 \rho} \int_{Q_{min}}^{Q_{max}} D'(Q_e)) \exp[i\mathbf{Q}_e \cdot \mathbf{r}]\, d\mathbf{Q}_e \tag{3.66}$$

where Q_{min}, Q_{max} is the range of Q_e values for which data are available. Making the use of the fact that the Fourier transform of a convolution is the product of the respective Fourier transforms, it is straightforward to show that

$$d(r) = [G_{self}(r) + h_{exp}(r)]\,(1 - t(Q_T r)) \tag{3.67}$$

where

$$G_{self}(r) = \frac{1}{2\pi^2 \rho r} \int_{Q_{min}}^{Q_{max}} Q_e I_{self}(Q_e) \sin(Q_e r)\, dQ_e \tag{3.68}$$

$$h_{exp}(r) = \frac{1}{2\pi^2 \rho r} \int_{Q_{min}}^{Q_{max}} Q_e I_{int}(Q_e) \sin(Q_e r)\, dQ_e \tag{3.69}$$

and

$$t(x) = \frac{3}{x^3}[\sin x - x \cos x] \tag{3.70}$$

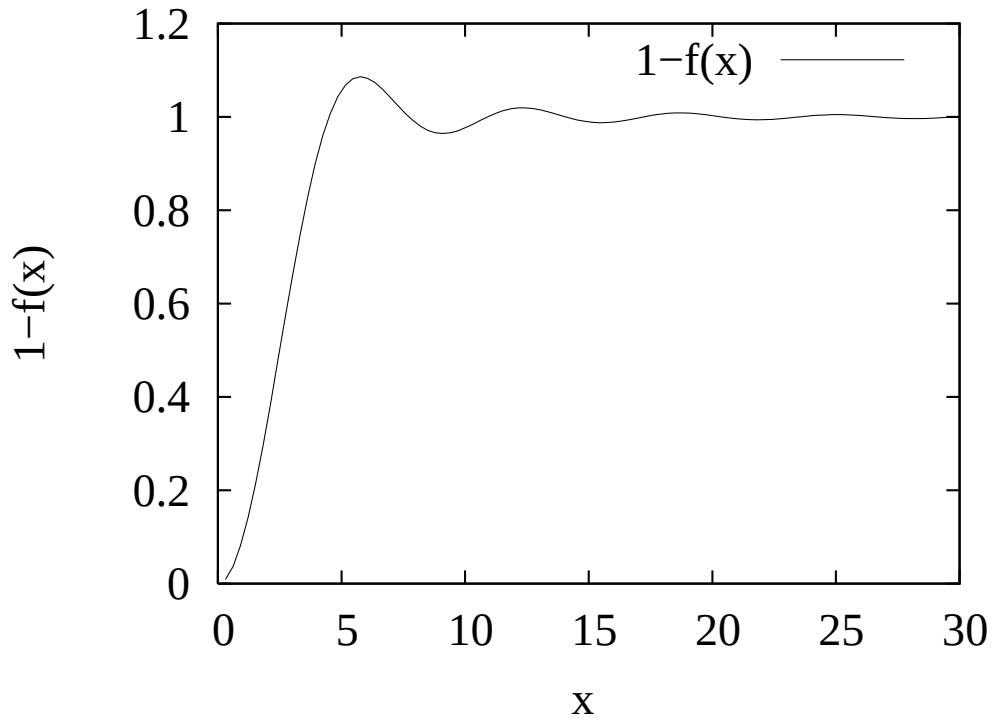

Figure 3.14: The convolution function $1 - f(x)$ which is defined in equation (3.70).

The function $1 - f(x)$ is shown in Fig. 3.14. It is close to zero at low x, then rises close to unity for $x >\sim 4$. In other words it will heavily suppress low frequency structure in Q-space, but leave the higher frequency structure relatively intact. Precisely which frequency is cut off depends on the value of Q_T. For $x << 1$ $f(x) \approx x^2/10$ so that for small enough r and Q_T the structure in $d\,(r)$ at a distance of say $r = r_0$ will be 4 times more suppressed than structure at $r = 2r_0$ and so on.

Written in the form (3.67), it will be apparent that the convolution can easily be reversed in r space because the result (3.66) simply needs to be divided by $(1 - f\,(Q_T r))$. By itself however this would achieve little since it would lead to the same function as would be derived by direct Fourier transform of the data. Instead the technique is to introduce constraint (2) at this point and assume that for some $r < r_{min}$ we know $g(r)$ precisely, i.e. $g(r) = g_0(r)$ while for larger r $g(r)$ is derived by inverting the convolution in (3.67):

$$\begin{aligned} d_{exp}(r) &= g_0(r) - 1\ , \quad r < r_{min} \\ &= d\,(r)\,/\,(1 - f\,(Q_T r))\,, \quad r \geq r_{min} \end{aligned} \tag{3.71}$$

with the assumption that $G_{self}\,(r)$ makes an insignificant contribution for $r \geq r_{min}$. If it does make a contribution in this region then the present method will not remove it, but it will remove it for $r < r_{min}$.

The object is to obtain an interference function in Q_e space which has minimal contributions from the self scattering background and which satisfies our specified constraints.

In principle one could simply Fourier transform (3.71) back to Q_e space to achieve this, but if $g(r)$ is structured to high r doing so might introduce further truncation effects. In addition unless the reverse transform is done carefully, this procedure will lose the statistical quality of the original data. A better plan is to generate an additional background function, $b(r)$, such that the function

$$d_{exp}(r) = d(r) - b(r) \tag{3.72}$$

This leads to

$$\begin{aligned} b(r) &= d(r) - g_0(r) + 1, \quad r < r_{min} && (3.73)\\ &= -d(r) f(Q_T r) / (1 - f(Q_T r)), \quad r \geq r_{min} && (3.74) \end{aligned}$$

Fourier transforming this to Q_e leads to:

$$B(Q_e) = 4\pi\rho \int r^2 b(r) \frac{\sin Q_e r}{Q_e r} \tag{3.75}$$

This extra background in Q_e space is then subtracted from $D'(Q_e)$ to yield an estimate of the interference differential cross section:

$$I_{int}^{(exp)}(Q_e) = I(Q_e) - I'(Q_e) - B(Q_e) \tag{3.76}$$

Because the function $f(Q_T r)$ is short ranged in r the likelihood of truncation oscillations being transferred to $B(Q_e)$ is small. By this method the statistical quality of the original data is left intact, the specified constraints (1) and (2) are applied, and the effects of truncation in both Q_e and r-spaces are held to a minimum, even when the data have a large self scattering component.

Setting the width of the top hat function, Q_T, can be tricky since if the data have a large background component then it would be desirable to make Q_T small to follow the shape of the background accurately. However when applied to (3.74) if the product $Q_T r_{min} \lesssim 3$ then the denominator is likely introduce a large spike at the cut-off, r_{min}. Therefore to avoid this, a useful rule of thumb is to set $Q_T > \dfrac{3}{r_{min}}$.

Note that when data are binned logarithmically as can now be done in GudrunN the top-hat method will not work since it relies on having equally spaced data value. In these cases (and even when the spacing is constant) it is now possible to simply subtract a constant from the data, based on the average value over some specified Q-range. This is in effect the same as setting $Q_T = \infty$. However the rest of the algorithm works as above, but the convolution function, (3.70), is of course zero over all finite values of x.

3.10.4 A revised Lorch function

In his famous paper (Lorch [1969]), E. Lorch attempted to derive a function which would suppress the traditional truncation oscillations that bedevil direct Fourier transform of diffraction data. The success of his approach is marked by the almost universal adoption of his truncation function, $\dfrac{\sin Q\Delta}{Q\Delta}$, where $\Delta = \dfrac{\pi}{Q_{max}}$. (Note I have dropped an unnecessary factor of 2 in the definition of Δ compared to Lorch's definition.) The derivation of this function however contains an obvious flaw which can be shown simply by performing the integral that he claimed to have performed. The equation concerned is not numbered, but it occurs in section 3 of that paper, so I quote it verbatim below:

$$\int_{r-\Delta}^{r+\Delta} 4\pi\ r^2\{g(r)-g_0\}\ dr = \frac{2}{\pi}\int_{r-\Delta}^{r+\Delta}\int_0^{Q_{max}} Qi(Q)\sin Qr\ dQ\ rdr \tag{3.77}$$

The idea here was to form the *average* of $g(r)-g_0$ over the region $r\pm\Delta$. Performing the r integral in (3.77) directly as instructed, we obtain:

$$\begin{aligned}\frac{1}{2\Delta}\int_{r-\Delta}^{r+\Delta} Q\sin Qr\ rdr &= \frac{1}{2Q\Delta}\Big[\sin Qr - Qr\cos Qr\Big]_{r-\Delta}^{r+\Delta} \\ &= \cos Qr\left(\frac{\sin Q\Delta}{Q\Delta}-\cos Q\Delta\right)+Qr\sin Qr\frac{\sin Q\Delta}{Q\Delta}\end{aligned} \tag{3.78}$$

from which it can be seen that the Lorch function is only retrieved when $Q\Delta \ll \pi/2$, but this condition cannot be satisfied at $Q = Q_{max}$ by definition! Moreover this function certainly does not go to zero in that limit. So the function that has been used by researchers all over the world for more than 40 years to perform Fourier transforms of diffraction data was based on faulty mathematics!

Notice however the similarity between eq. (3.78) and the Fourier transform of the top hat function in section 3.10.3, eq. (3.70). This suggests a simple revision to the Lorch function in keeping with his original idea of averaging $g(r)$ over a region of space. In effect we will instead *smear* $g(r)$ uniformly over the region $|\mathbf{r}\pm\mathbf{\Delta}|$ by performing the same convolution of the top hat function as previously in Q-space, but now in r-space. Writing

$$\begin{aligned}L'(\mathbf{r},\Delta) &= \frac{3}{4\pi\Delta^3}, \quad |\mathbf{r}|\le\Delta \\ &= 0, \qquad\quad |\mathbf{r}|>\Delta\end{aligned} \tag{3.79}$$

the convolution of the radial distribution function with the top hat function is

$$\langle h(\mathbf{r})\rangle_\Delta = \int_\Delta L'(\mathbf{r}-\mathbf{r}',\Delta)\,h(\mathbf{r}')\,d\mathbf{r}'. \tag{3.80}$$

Introducing the Fourier transform

$$h(\mathbf{r}) = \frac{1}{(2\pi)^3\rho}\int_{\mathbf{Q}} h(\mathbf{Q})\exp\left[i\mathbf{Q}\cdot\mathbf{r}\right]d\mathbf{Q} \tag{3.81}$$

and the independent variable $\mathbf{r}'' = \mathbf{r} - \mathbf{r}'$ then

$$\begin{aligned}\langle h(\mathbf{r})\rangle_\Delta &= \frac{1}{(2\pi)^3\rho}\int_{\mathbf{Q}}\int_{\Delta} L'(\mathbf{r}'',\Delta)\exp\left[-i\mathbf{Q}\cdot\mathbf{r}''\right]d\mathbf{r}'' h(\mathbf{Q})\exp\left[i\mathbf{Q}\cdot\mathbf{r}\right]d\mathbf{Q} \\ &= \frac{1}{(2\pi)^3\rho}\int_{\mathbf{Q}} L'(|\mathbf{Q}|,\Delta)\,h(\mathbf{Q})\exp\left[i\mathbf{Q}\cdot\mathbf{r}\right]d\mathbf{Q}. \end{aligned}\tag{3.82}$$

where

$$L'(Q,\Delta) = \frac{3}{(Q\Delta)^3}\left(\sin Q\Delta - Q\Delta\cos Q\Delta\right). \tag{3.83}$$

Hence $L'(Q,\Delta)$ is the modified Lorch function, but note that it does not go to zero at $Q = Q_{max}$. In fact the form (3.83) suggests there is nothing to stop Δ being a width specified by the user, and moreover that width could in principle be a function of r, i.e. $\Delta = \Delta(r)$. In GudrunN and GudrunX a form for this variation is allowed:

$$\Delta(r) = \Delta_0\left(1 + r^\beta\right) \tag{3.84}$$

with β specified by the user, so the degree of broadening in r-space can vary distance.

3.10.5 Towards accurate Fourier transforms

One final note concerns the evaluation of the integral (3.81). Normally $h(Q)$ is measured as a histogram with each value representing the average value for each measurement bin. Hence the exact integral is normally replaced by a sum over values:

$$h(r) = \frac{1}{2\pi^2\rho r}\sum_{Q_{min}}^{Q_{max}} h(Q)Q\sin Qr\ 2\Delta_Q(Q) \tag{3.85}$$

where $2\Delta_Q(Q)$ is the width of the bins which may in general be a function of Q. Comparing this with (3.81), and again in keeping with the spirit of Lorch, it would make sense to average the function $Q\sin Qr$ over the bin width, i.e. instead of (3.85) we perform the average

$$\begin{aligned} h(r) &= \frac{1}{2\pi^2\rho r}\sum_{Q_{min}}^{Q_{max}} h(Q)\int_{Q-\Delta_Q}^{Q+\Delta_Q} Q\sin Qr\ dQ \\ &= \frac{1}{2\pi^2\rho r}\sum_{Q_{min}}^{Q_{max}} Qh(Q)\left[\cos Qr\left(\frac{\sin\Delta_Q r}{\Delta_Q r} - \cos\Delta_Q r\right) + Qr\sin Qr\frac{\sin\Delta_Q r}{\Delta_Q r}\right]2\Delta_Q \end{aligned}\tag{3.86}$$

This reverts back to (3.81) in the event $\Delta_Q \to 0$. This expression is useful in time-of-flight work when the Q bins often increase in width with increasing Q.

Chapter 4

Running Gudrun

Gudrun comes in two flavours, **GudrunN** (for neutrons, previously called simply "Gudrun"), and **GudrunX** (for x-rays). In **GudrunN** most of the analysis is done via two supplied Fortran executables, gudrun_dcs.exe and purge_det.exe. The graphical user interface (GUI) in this case acts primarily as a guided editor to help the user write the input files to these routines, and to also provide some graphics capabilities for looking at the outputs. The input file has to be written in a particular format, so in practice it is much easier to write these input files from the GUI. The latter is a Java program and so requires Java Runtime Environment (JRE) to be installed on your computer, but this is normally not a problem since Java is often present to run applets in web browsers. If you do choose to run the Fortran programs directly, it is a good idea at least to write the first input files from the GUI to make sure they have the format of the current version of GudrunN, since the GUI can sometimes tolerate older versions of the input file and still write a sensible output file, but the Fortran program will almost certainly not tolerate an older format input file.

In **GudrunX**, most of the analysis is done within the GUI itself, with just two calls to Fortran executables, corrsx_in_out.exe and tophatsub.exe, the former performing the attenuation and multiple scattering calculations and the latter performing the final Fourier transform of the differential cross section. Hence there is no choice but to run within the Java framework: the GUI has been developed to make use of the high speed string processing methods that are available within Java.

The underlying framework for the two versions of the GUI is common so that operations such as copying and pasting tabs, and creating and saving files are the same.

The GUI is normally started in a Windows system with the commands:
copy Gudrun{N,X}_windows.syspar GudrunGUI.syspar{N,X}
java -cp "..\GudrunGUI" -jar "..\GudrunGUI\GudrunGUI_4.jar" {N,X}
copy GudrunGUI.syspar{N,X} Gudrun{N,X}_windows.syspar
For a Linux system the equivalent commands are:
cp Gudrun{N,X}_linux.syspar GudrunGUI.syspar{N,X}
java -cp "../GudrunGUI" -jar "../GudrunGUI/GudrunGUI_4.jar" {N,X}
cp GudrunGUI.syspar{N,X Gudrun{N,X}_linux.syspar

while for the Mac they are:
cp Gudrun{N,X}_mac.syspar GudrunGUI.syspar{N,X}
java -cp "../GudrunGUI" -jar "../GudrunGUI/GudrunGUI_4.jar" {N,X}
cp GudrunGUI.syspar{N,X Gudrun{N,X}_mac.syspar
Here '{N,X}' means N *or* X. Note that since the GudrunGUI.syspar file will be different for the x-ray version compared to the neutron version they have to be given different names.

Both these commands are contained in scripts: *gudrunn.bat, gudrunx.bat* (Windows), *gudrunn.sh, gudrunx.sh* (Linux) or *gudrunnmac.sh, gudrunxmac.sh* (Mac), which come with the current distribution of Gudrun.

In either case what happens here is that first the appropriate version of GudrunGUI.syspar is generated, then the GUI is started, and in this example it is assumed the .jar file resides in a folder called "GudrunGUI" which is in the main Gudrun folder. If the folder sequence in your case is different from this, you will need to modify the Java command appropriately. Finally when the GUI is closed (using either the "Exit" option in the file menu, or else by clicking the x button at the top of the GUI) the GudrunGUI.syspar file is copied back to the original file in case it has been changed in any way.

4.0.6 Files you need to run Gudrun

Gudrun is normally supplied as a .zip file - the current version is Gudrun4.zip. For non-Windows users it is also necessary to obtain the auxilliary file, Gudrun4files.zip, which contains the Fortran source code which will need to be built using the supplied commands before attempting to run Gudrun. It is suggested you create a folder called something like "GudrunDistribution" in which to unzip these files. This should ideally be in the main directory (C:\ for Windows, /home/¡username¿/ for Linux), although can in principle be anywhere. If you subsequently download a later version of Gudrun it would be a good idea to rename this folder to something else, just in case the newer version doesn't perform as expected! Follow the supplied readme.txt to do this. Unzipping the .zip file will create a folder called **Gudrun#**, where the # represents the current version of the GUI (currently # = 4) and in this folder should be the files shown in Fig. 4.1. [1]

The folder **bin** contains the binary executables for both Linux and Windows, as well as the GNUplot plotting routines used in the Windows version. Windows binaries are denoted by the extension (file type) .exe, while Linux or Mac binaries normally have no file type. As noted elsewhere the Linux binaries will need to be re-built for each Unix-based operating system on which Gudrun is installed. The GNUplot routines will not be discussed extensively here as they appear exactly as downloaded from the GNUplot website. For Linux or Mac versions it will be necessary to install GNUplot separately in order to make use of the plotting features within Gudrun (but note that this is strictly optional - if you have a preferred plotting program the output files can be plot just as easily with other packages.) If you intend to use the in-built GNUplot plotting option it

[1] In this manual the files are shown for a Linux operating system. However the format in Windows should be identical, even if the appearance is slightly different.

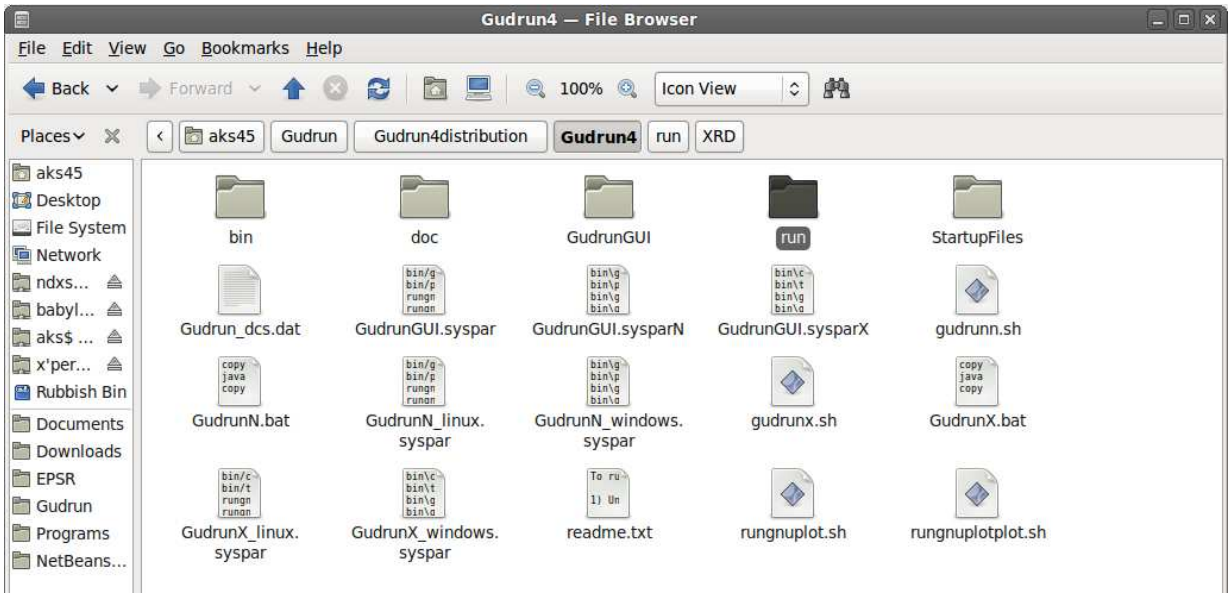

Figure 4.1: Appearance of the main Gudrun folder

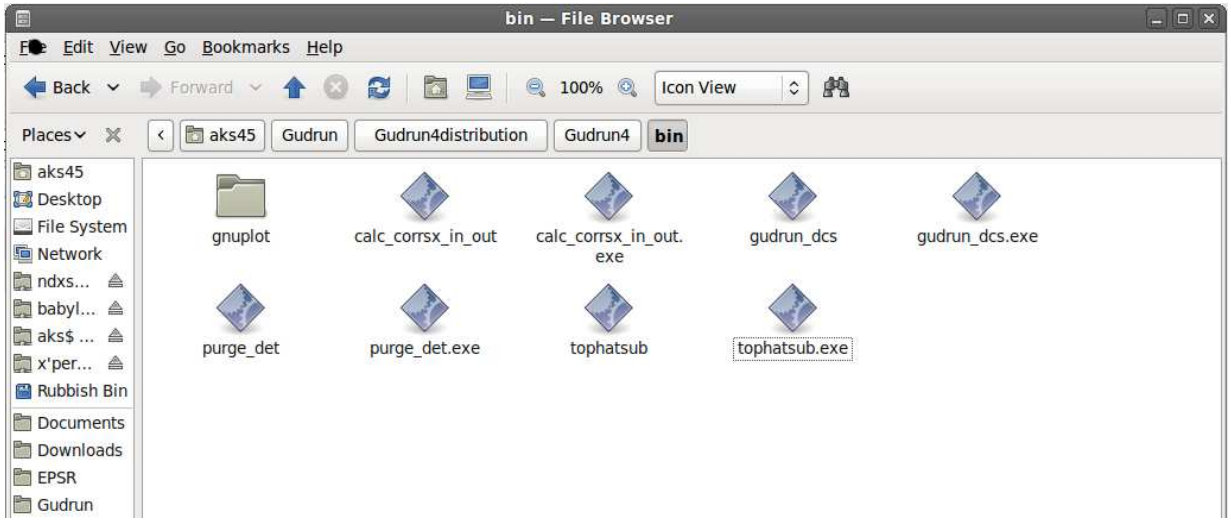

Figure 4.2: Appearance of the Gudrun bin folder

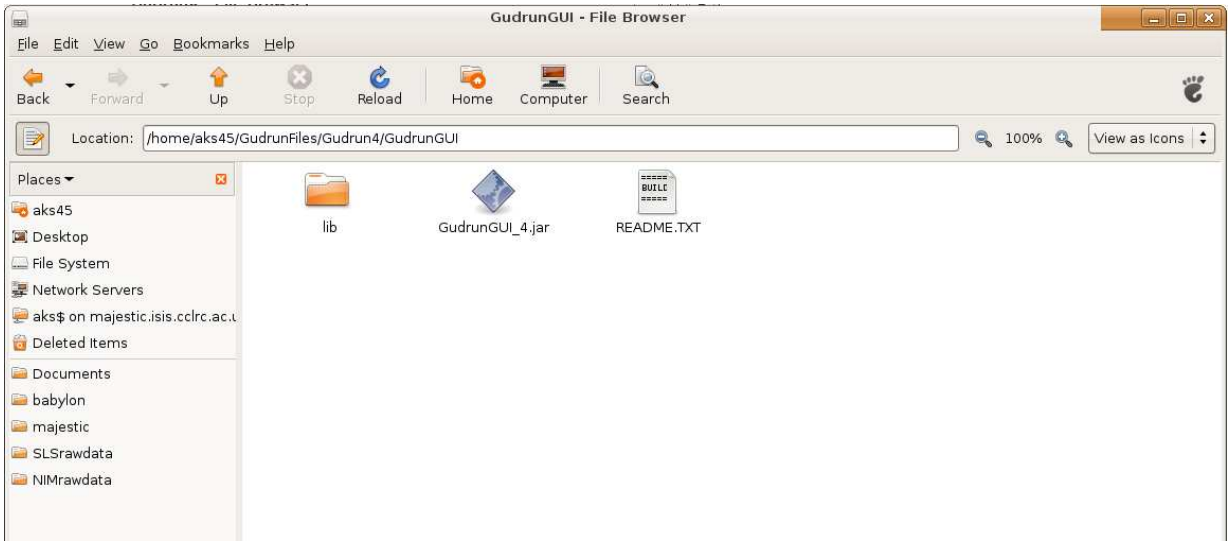

Figure 4.3: Appearance of the GudrunGUI folder

will be necessary to refer to it when setting up Gudrun to run.

The folder **GudrunGUI** contains the Java executable that will be used. Fig. 4.3 shows what this folder should contain. Since these executables are the ones that can change from time to time, probably it is a good idea not to store any of your own run files in this folder since the entire folder will be updated with new versions. The executables with extension **.ex** or **.exe** are the Windows executables, whereas those with no extension are the Linux versions. Since these are not compiled as static executables under Linux it means they will probably need to be recompiled for each operating system on which they run. Contact the authors for information on how to do this. The Java executables (**.jar** file and **lib** folder) should of course be common to all operating systems on which Java is installed.

Next are shown the contents of the *run* and *startupfiles* folders in Figs. 4.4 and 4.5.

The *run* folder contains three folders to enable to check that the routines have been installed and run correctly. The D4C and SLS folders were written by GudrunN, while the XRD folder was written by GudrunX so be sure you start the correct version of the GUI before attempting to open these files.

The *StartupFiles* folder contains various files needed to define basic parameters for particular instruments. These may not be completely up to date, so do check with an instrument scientist if you are not sure about this. In the current version of the GUI there are also some standard containers available. The data for these are stored in the files "ContainerTemplatesN.txt" and "ContainerTemplatesX.txt". If you want to add to or modify these files, this is simple to do using a standard text editor, but be sure to preserve the exactly the format as supplied - otherwise the files may not be read correctly.

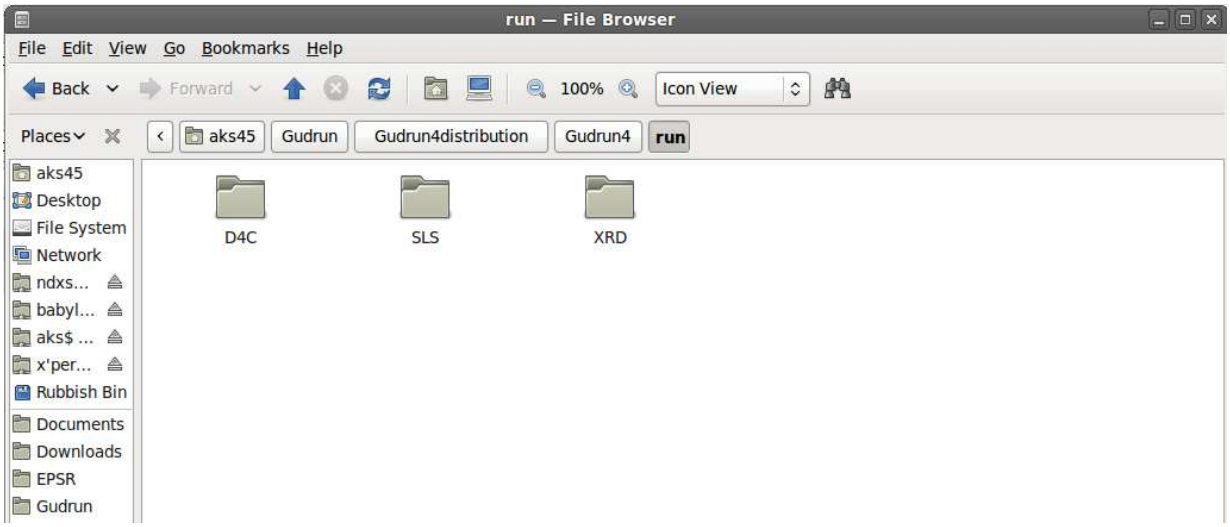

Figure 4.4: Appearance of the Gudrun *run* folder (as supplied)

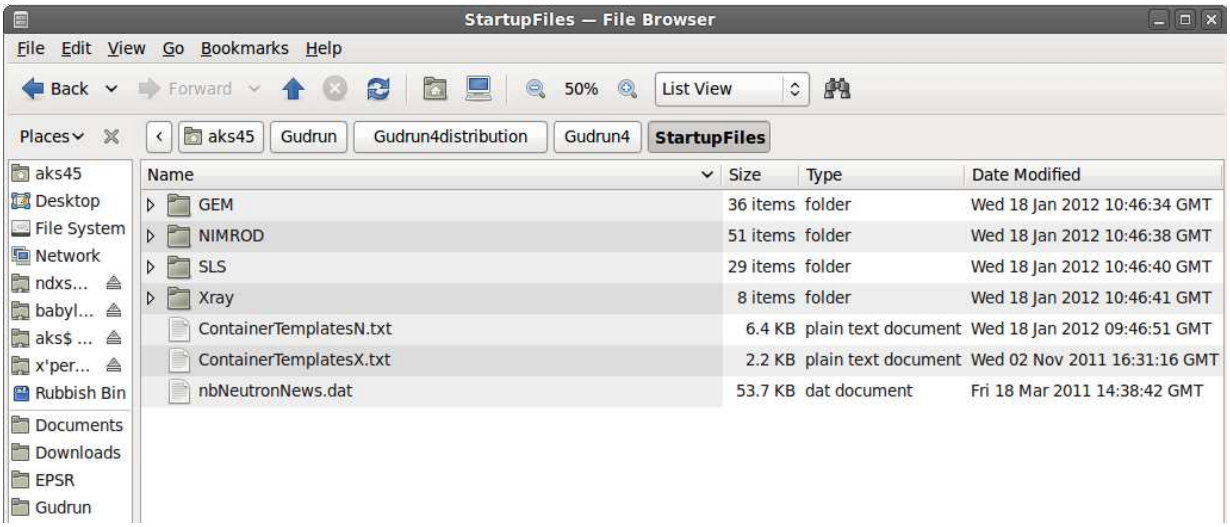

Figure 4.5: Appearance of the Gudrun *StartupFiles* folder

4.0.7 Starting GudrunN - neutrons

The easiest way to start the GUI for neutrons is go to the folder **Gudrun4** and double click on the **GudrunN.bat** file in Windows, or run the corresponding shell script in Linux. Probably it is better at the beginning, until you are confident in what you are doing, to do this from the command prompt at the beginning as it will list any error messages that Java produces if one or more files are not in place. If you do double click on the file icon and nothing happens, you will be none the wiser as to what happened, so try starting from the command prompt.

When it starts it should load the startup file which is specified in the **Gudrun_windows.syspar** or **Gudrun_linux.syspar** files. This filename is displayed along the top of the GUI, Fig. 4.6. If it does not load this file correctly check the system parameters to make sure they point to the correct places. This is done by clicking the *System* menu item in the GUI, then *Set system path names*, Fig. 4.7. You can get the required files by clicking the appropriate browse buttons. This is also a good time to check that the executables are correctly specified. Note that in order for these new values to take effect the GUI has to be exitted, then restarted.

When the GUI starts a green box appears on the top left stating that "No program running" - see Fig. 4.6. When purge_det or GudrunN are running this box turns red with an appropriate message to signify which program is running. It turns green again once the particular program has finished. This feature enables you to continue to work in the GUI (e.g. plotting) while a program is running. However do not attempt to save an input file while this box is red, otherwise you may corrupt the current run.

Another check you can do at regular intervals to ensure that all the files you have specified do indeed exist is press the *Run* menu item, then *Check files exist*. If all the files you have specified in each tab are found where specified it will give an OK message, otherwise it will list the missing files, Fig. 4.8. If lots of data files appear to be missing, make sure the *Data file directory* specified on the INSTRUMENT tab is set correctly.

4.0.8 Setting the "Look and Feel" of the GUI

When GudrunGUI is started it adopts the "Look and Feel" that is specified for Java in the particular operating system where it is running. This is mostly OK, but for Apple Mac in particular this can be confusing and unfamiliar. So under the system menu it is now possible to change the look and feel. This is achieved by clicking system > Set look and feel > select Look and Feel from drop-down menu
The "metal" look and feel is the cross-platform standard. The system menu also allows you to change the tab placement between LEFT (default) and TOP.

4.0.9 Features of the GudrunN GUI

As can be seen from Fig. 4.6, GudrunN (and GudrunX) are tabbed windows, with one tab for each of INSTRUMENT, BEAM, NORMALISATION and SAMPLE BACKGROUND.

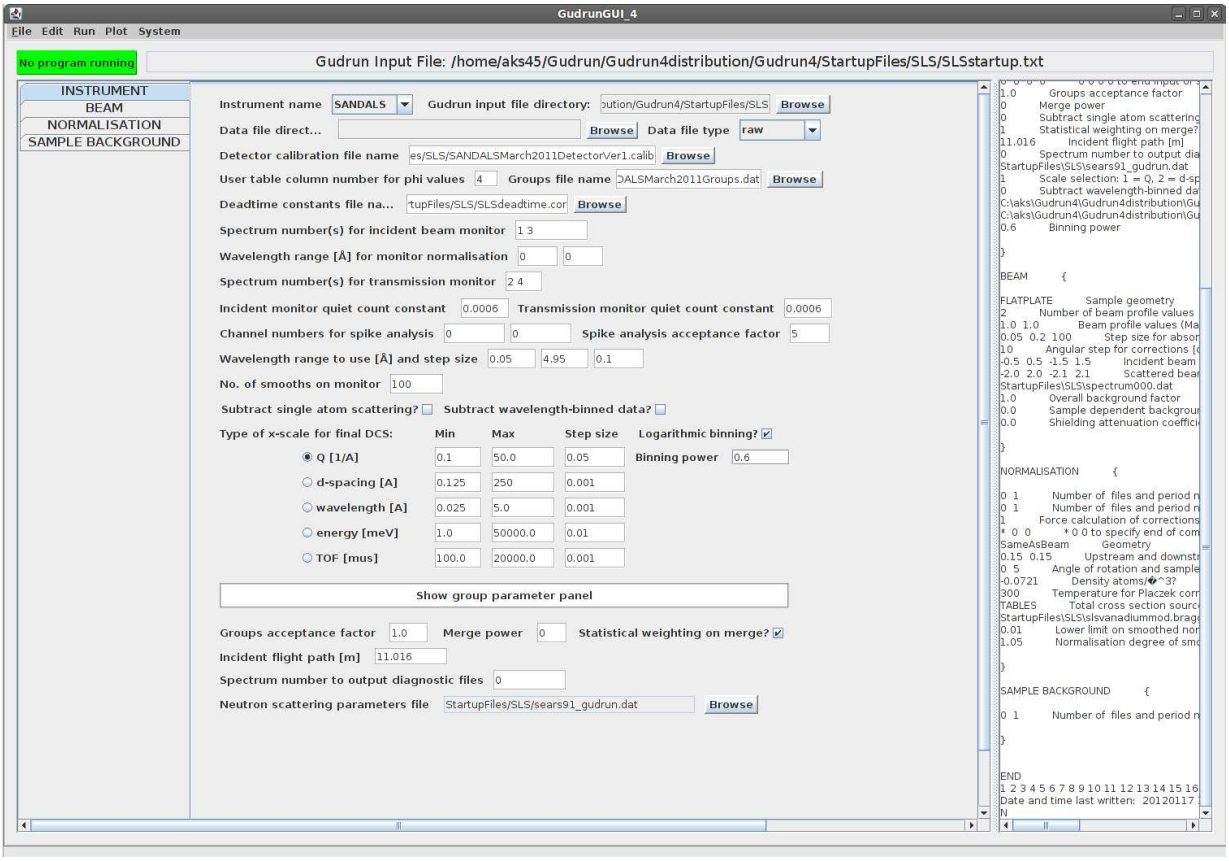

Figure 4.6: Layout of the GUI when it starts. If the start up file has loaded correctly, then four tabs should be displayed, INSTRUMENT, BEAM, NORMALISATION and SAMPLE BACKGROUND.

Figure 4.7: Layout of the system menu, achieved by clicking *System* then *Set system path names*

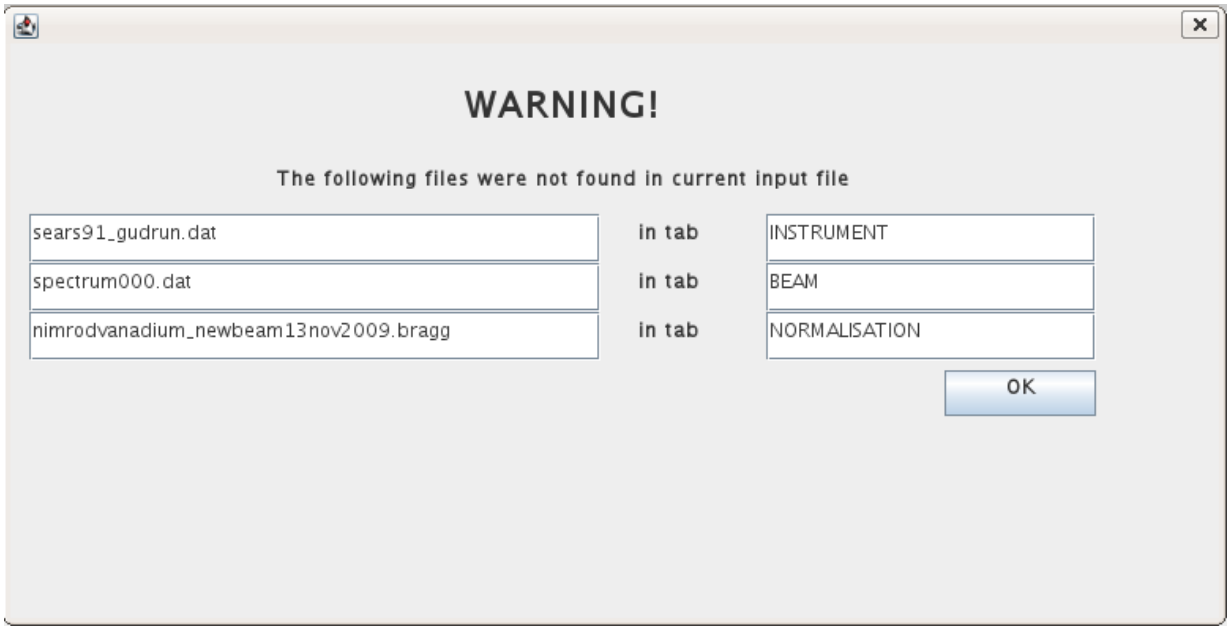

Figure 4.8: Layout of *Check files exist* warning menu, achieved by clicking *Run* then *Check files exist*

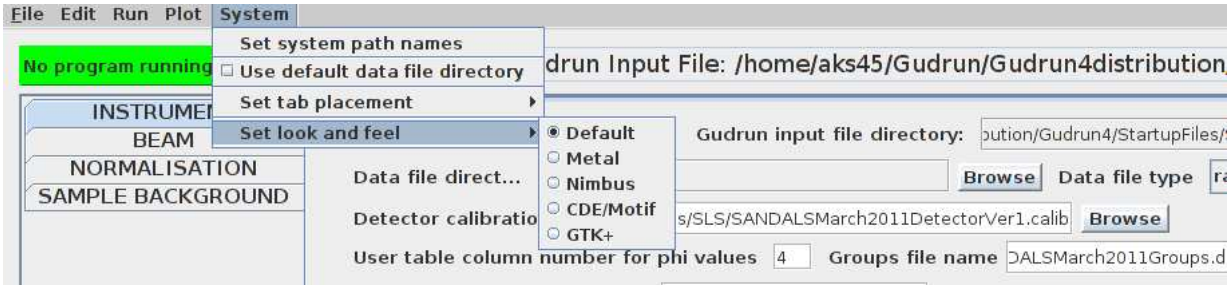

Figure 4.9: Setting the look and feel with the drop-down menu.

If the startup file has been set up correctly, these four tabs should be correct for the instrument you intend to analyse and for the operating system in which you are running. You are only allowed to have one each of the INSTRUMENT, BEAM and NORMALISATION tabs - these cannot be removed, but you can have as many SAMPLE BACKGROUND tabs as you wish. Hence if you need to run with different INSTRUMENT, BEAM or NORMALISATION tabs you will have to generate separate input files for each configuration. Two additional types of tabs are possible, namely one or more SAMPLE tabs, and up to three CONTAINER tabs for each sample. The CONTAINER tabs can only be inserted after a SAMPLE tab, and they must be specified in the order in which they occur in the experiment, namely innermost first, outermost last.

SAMPLE, SAMPLE BACKGROUND and CONTAINER tabs can added as required. To insert a SAMPLE or CONTAINER, simply click on the tab immediately BEFORE where you want to insert the new tab to highlight it. Then insert either from the *Edit* menu, or by typing Ctrl-A (for SAMPLE), or Ctrl-B (for SAMPLE BACKGROUND). To insert a CONTAINER you can only use the Edit menu, from which one or two more drop-down menus can be accessed to insert either an arbitrary container (Other) or a standard container - select one from the list supplied. (As noted above these standard containers are defined by the files ContainerTemplates{N,X}.txt stored in the StartupFiles folder.)

The samples are processed in the order supplied by the list of tabs. The CONTAINERS associate with each sample are listed after the particular sample: if several samples have the same container, that container MUST be listed after each sample, otherwise the sample will be treated as if it had no CONTAINER(S). Each SAMPLE must be inserted after a SAMPLE BACKGROUND tab or after the last CONTAINER of the previous SAMPLE. There is no limit to the number of SAMPLE tabs that can be inserted, but obviously the more tabs, the slower will be the analysis. If a sample has no container, then simply specify the SAMPLE tab. When starting a new SAMPLE or a non-standard CONTAINER you will be asked to specify a name. This name is just used within the GUI to help keep track of samples and containers.

Fig. 4.10 shows what this should look like. Here there are three samples, only the middle one of which has a container.

In addition to the tabs, there is an editor panel on the right hand side of the GUI which shows the current GudrunN Input File exactly as it has been read in. This editor panel is

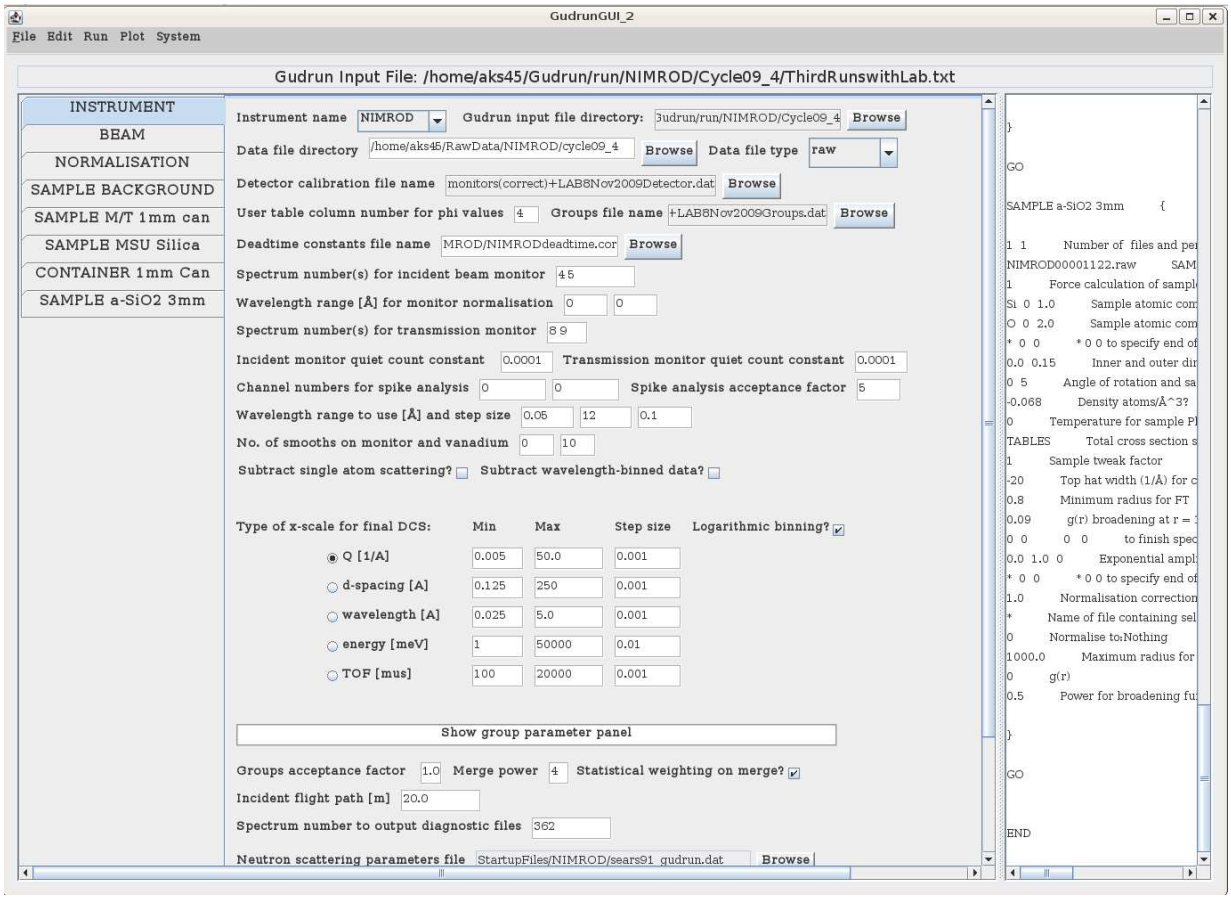

Figure 4.10: Layout of the GUI after loading three samples. The second sample, MSU silica, has a container. The first sample is in fact the empty container on its own.

useful for checking that what is shown in the GUI does indeed appear in the input file. It can be read into and out of the GUI using the *Transfer in* and *Transfer out* options under the *File* menu without changing any of the input files. It is possible to edit the GudrunN Input File directly in the panel, but note that if you do so, it must be first read into the GUI using the *Transfer in* option before saving, otherwise any changes not in the GUI will be overwritten when the GUI is saved to the GudrunN Input File. It should be mostly straightforward to identify which parts of the GudrunN Input File correspond to in the GUI as the comments in the Input File are the same as those appearing in the GUI.

4.0.10 GudrunN menus

File menu

This allows you to open and save Gudrun Input Files. It is important that you Save your current input file BEFORE opening another because no checking is done to see if a file has been changed. If you fail to save a file, before opening another, a message bar appears asking if you want to save it.

In addition to *Open*, *Save* and *Save As* options, there is a *Reload* option in this menu. This is so that if at some point you wish to discard any changes you have made without saving, the original Gudrun Input File can be reloaded again as it was since the last time it was saved. (Note that it is not necessary to save the Input File before running the GudrunN executable since the GUI writes a separate file, **Gudrun_dcs.dat**, directly from the GUI before running Gudrun.

Edit menu

This allows you to perform the various operations of adding, removing, and renaming SAMPLEs, SAMPLE BACKGROUNDs and CONTAINERs. Note that you need to highlight a particular tab, sometimes requiring two clicks, before these options will work. The menu also lists the corresponding short cut keys for most of these operations. If you wish to remove a tab it is better to *Cut* it rather than *Delete* it since the former method makes a copy before deleting, whereas the latter does not. That way if you delete a tab by mistake it can always be restored with a *Paste*.

This menu also has commands to convert a SAMPLE to a CONTAINER and vice versa. This can be useful when checking an empty container, treating it has a sample before running it as a container. Note that the original SAMPLE or CONTAINER are lost when performing this operation, so if you wish to keep the original it is important to make a copy of a SAMPLE or CONTAINER *first* before converting it. In addition, since the first tab after the first SAMPLE BACKGROUND must always be a SAMPLE, if you attempt to convert the first SAMPLE to a CONTAINER it will in fact leave the original in place and put the new CONTAINER immediately after that SAMPLE.

In GudrunN (only) it is also possible to convert the NORMALISATION tab to a SAMPLE or CONTAINER. In that case the new SAMPLE or CONTAINER is added at the

end of the list of tabs, but of course the original NORMALISATION tab is not deleted in that case.

Run **menu**

The *Run* menu has several items. The first has already been described, namely *Check files exist*. This runs through the GUI and for each filename found checks to see that it exists in the location specified.

The second item in this menu (neutron version only) is *Write purge file*. This brings up a separate box to allow you to specify the allowed variation in detector performance within each group of detectors, as specified in Section 3.3. On pressing the *Press to write* ***purge_det.dat*** button a file of that name is created in the current folder, and can be used to *Run purge*, which is the next item in this menu.

At that point it is a good idea to check the Command Prompt to be sure that *purge_det* ran correctly: at the end of lots of output it should say how many good detectors were found. If any errors occurred, the program will not complete properly and the important **spec.bad** file will not be written. It is crucial that this file exists BEFORE attempting to run GudrunN itself. **spec.bad** lists all the spectra found in the input file. A 0 means the detector is good, that is it is within the specified range, a -ve number means it is low counting, +ve means it is high counting. Generally speaking it is not necessary to run this check repeatedly as new runs appear, but if you are worried about detector stability it is a good idea to check the bad detectors regularly: a steadily reducing number of good detectors may indicate a problem with the detectors or their electronics. Perhaps more important is to run this check near the beginning of a set of runs so that you are aware and can get fixed detector problems before you attempt to accumulate data.

The last item in this menu is to run *Gudrun{N,X}* itself - actually the program is called *Gudrun_dcs*. If everything has run correctly up to now, this should execute satisfactorily, depending on what values are in the various tabs as described below.

Note that when *purge_det* and *Gudrun{N,X}_dcs* are running the GUI freezes and cannot be accessed. This is to prevent values being changed while the programs are running. When the GUI becomes free to use again is your signal that the execution has finished.

If any of the tabs that are to be included in the execution contain errors, the run GudrunN,X command will not operate, but a message box appears instead listing the errors. Currently error checking is limited to checking that data files exist in all the boxes where these are required. More elaborate error checking may be incorporated in the future, e.g. to ensure all text boxes have some text in them!

Plot **menu**

This menu has two items. The first produces a new plotting window called *Plot Data* which allows you to set up and save a GNUplot plot file. This is described in a separate section below, 4.2. The second item will simply run GNUplot in the current GudrunN Input File folder. I will not describe how to use GNUplot here since there is already comprehensive

documentation both in GNUplot itself and on the Internet. For Windows it is important to use the correct version, so this is distributed with both GudrunN and GudrunX. The GNUplot window allows you to enter GNUplot commands directly.

System menu

The main item in this menu is the box to enter the system values as already described in Section 4.0.7 and shown in Fig. 4.7. In addition to the items already described, it is possible to specify a default folder where the raw diffraction data are stored. This is useful when running a GudrunN Input File from another machine, but you want to use the raw data in your own folder.

The bottom line of the *System* box also allows you to supply a plotting sequence when plotting multiple groups of detectors. This is so that the groups can be shown (say) in order of increasing scattering angle.

The second item in this menu allows you to use this default data directory (instead of the one shown in the INSTRUMENT tab). When this is set a red warning message appears in the top left of the GUI to remind you of this.

4.0.11 GudrunN GUI tabs

INSTRUMENT tab

The INSTRUMENT tab, Fig. 4.10, allows you to specify a number of parameters for a particular run. Normally much of this will come from the startup file for a particular instrument, but some values may need to be adjusted depending on the particular circumstances. The ones highlighted are those you should check and pay attention to:-

1. The Instrument name.
2. Where the raw data are stored (meaning the files containing the actual neutron counts).
3. The type of dataset (currently only ISIS RAW and SAV formats and D4C format are supported - NEXUS format is being contemplated but is not currently supported. Note that all the data files for a given GudrunN Input File must be stored in the same folder and must have the same format, so it is not possible to mix RAW and SAV formats for example.)
4. The detector calibration file, (**.dat**, or **.calib**. If the latter, then this is strictly a *spectrum* calibration file - at ISIS spectrum and detector numbers are not necessarily the same.)
5. The groups file (**.grp, .dat**, which describes how the detectors are to be grouped);
6. The deadtime correction parameter file.

7. Spectrum numbers for the incident and transmitted beam monitors (if more than one monitor is to be included separate their spectrum numbers by spaces);

8. The minimum and maximum wavelength range to calculate the monitor normalisation for (use 0 and 0 for this range to use point-by-point normalisation - this is the default).

9. The channel numbers for spike analysis and the spike acceptance factor (these values are normally not changed. In recent years the occurrence of spikes, caused by sudden detector noise in particular time channels, has become extremely rare.);

10. The wavelength range to be used in the data analysis - this will vary from instrument to instrument and may also depend on the sample. At the same time the step in wavelength at which the corrections will be calculated is also specified on this line. Normally this is 0.1Å.

11. The number of smooths on the monitor (three-point smoothing). With the current version of Gudrun the value you type is immaterial, other than if it is zero, no smoothing on the incident monitor is performed, while smoothing is performed if it is non-zero. The number of three-point smooths is now determined from the statistical error bars on the monitor spectrum. The smoothing is repeated until the mean standard deviation of the data from the smoothed line is equal to or greater than the mean square deviation given by the error bars. This serves to limit the possibility of over-smoothing the monitor values, which can have a serious impact on the final data. N.B. the NORMALISATION smoothing is now controlled by two items in the NORMALISATION tab.

12. The "Subtract single atom scattering" and "Subtract wavelength binned data" boxes should be left unchecked unless you know what you are doing!

13. The units of the output DCS files, the minimum, maximum and linear step size in the requested output units, and whether the binning is to be linear or logarithmic. If the binning is logarithmic then in addition to the linear step size you need to signal the logarthmic step size. Starting from the smallest x value the binning is then logarithmic until the bin size reaches the linear bin size, after which it becomes linear: if you want to ensure the binning is logarithmic throughout, simply make the linear bin size very large so that this transition is never reached. The binning in Q and r spaces is discussed in a separate section below.

14. Whether you wish to specify particular x-ranges and background factors for specific groups;

15. The groups acceptance factor (normally 1.0. A value less than this may mean some groups do not appear in the final merge of groups. The (revised) operation of this value is described further below.), the merge power (normally 4, this value controls

the weighting on Q for estimating the assymptotic level of the DCS. Hence a value of 4 means the weighting goes as Q^4. A revised method of estimating the level of each group has been implemented in the current version.), and whether statistical weighting in the merge is to be used - this means each group is weighted by its relative statistical accuracy when forming the merge. (The alternative is to form the arithmetic mean of the groups, but this tends to worsen the statistical quality of the final result, although this is sometimes unavoidable for hydrogenous samples.)

16. The incident flight path in m. This should not be changed unless you know it is incorrect. For reactor data (D4C) you also need to specify the incident radiation wavelength.

17. The spectrum number for diagnostic files. If this is 0 no diagnostic files will be output. If it corresponds to a spectrum found in the data files, it will show the analysis step-by-step as given in sections 3.2, 3.6, 3.7 - 3.9 and 3.10.1 for that particular spectrum. A comprehensive list of outputs is given in Chapter 5.

18. The file name containing the neutron scattering lengths, total cross sections, and capture cross sections.

Groups acceptance factor

In the past whether a group would be included in the final merge could be decided by specifying an acceptance factor less than 1.0. In that case the group was accepted if its high Q level was within the specified fraction of the expected scattering level. With the advent of wide-Q diffractometers such as NIMROD with often vastly different scattering levels between low angle groups and higher angle groups, this method did not work, and in general values of the acceptance factor other than 1.0 were never used in practice. In the current implementation a new role for this parameter has been adopted, basically still to help eliminate poorly performing groups of detectors, or more precisely poorly performing regions of groups of detectors.

To guage an idea of how this factor now works, Fig. 4.11 shows a plot of the ratio of RMS deviation to differential scattering cross section for a particular group on NIMROD. It can be seen that this ratio has a minimum, corresponding to the peak in the incident neutron flux, then rises either side of this. The groups acceptance factor now selects that region of this group either side of the minimum such that the ratio is equal to or less than the specified acceptance factor. This is the region used in the merge. The horizontal arrrowed bar in this figure shows approximately the region that would be selected for the merge using a criterion of 10% (acceptance factor = 0.1). The region outside this bar will be ignored in the merge, and if none of the data from this group lies within the specified criterion, then the group is completely ignored in the merge. The region of acceptance is measured from the minimum in the RMS deviation to DCS ratio and is defined once this ratio exceeds the specified value: if beyond the maximum or below the minimum values the ratio drops below the limit, those regions will nonetheless still be excluded. This

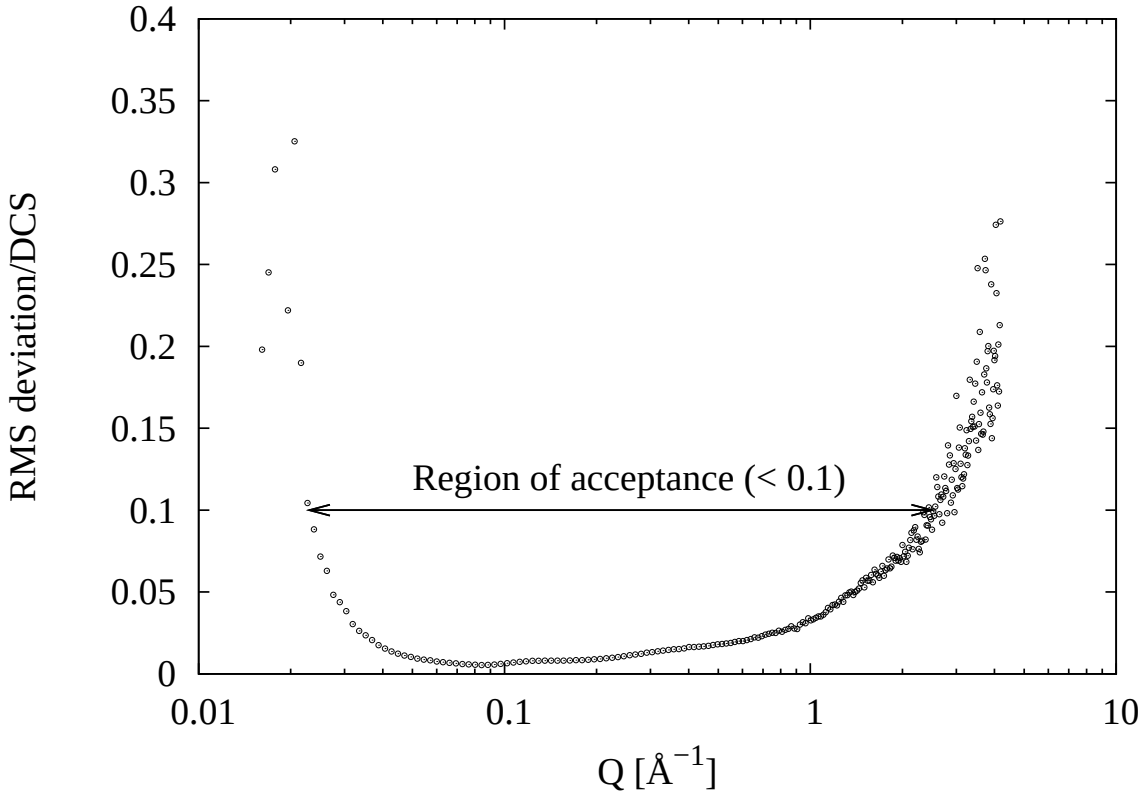

Figure 4.11: Ratio of RMS deviation to differential cross section for a particular group of detectors on NIMROD. The horizontal arrowed bar indicates the region accepted for the merge with the acceptance factor set to 0.1.

exclusion will take place irrespective of whether or not statistical weighting is to be used when merging detectors. This acceptance test is only performed if the acceptance factor is below 1.0: if the acceptance factor is larger than or equal to 1.0 the whole range of every group will be accepted.

Data binning in Q and r spaces with GudrunN (from March 2012)

Traditional x-ray and neutron diffractometers have a limited range of Q so that it is common to bin the data on to a linear scale. This is useful for such tasks as Fourier transforming the scattering data to r-space. The main exception to this rule is for performing Rietveld refinement when a logarithmic x-scale (d-space) is common. As noted above Gudrun has the option to output the data either on a linear or logarithmic x scale. With the advent of new pulsed source instrumentation it is possible to obtain data over 4 orders of magnitude in Q, which can make purely linear or logarithmic binning over the entire Q range highly inefficient, leading to a large number of points. If the binning is purely linear, then one

needs a fine grid of points to accommodate the rapid variations in structure factor at low Q, but this then leads to inefficient sampling at high Q. On the other hand if the binning is purely logarithmic, then for a useful sampling frequency at low Q you will like end up with too crude a binning at high Q. Hence a scenario where you have logarithimic binning at low Q and linear binning at high Q would be more in keeping with the information content of wide Q-range data.

To accommodate this requirement the current version of Gudrun uses a composite binning regime, accessed when the "logarithmic binning" box is ticked. With this regime, the width of the x-bin at any given x value is given by

$$\Delta(x) = \Delta_0 \tanh\left(\frac{\Delta_L}{\Delta_0} x\right) \tag{4.1}$$

where Δ_0 is the constant step size that occurs at large x, and Δ_L is the logarthmic step size that occurs at small x. In the limit $x \to 0$ this expression reduces to $\Delta(x) = \Delta_L x$, while at large x we have simply $\Delta(x) = \Delta_0$. If you want to ensure the binning is logarithmic throughout simply set the linear step size $\Delta_0 \gg \Delta_L x$ for all x values that occur in the final output file. The same binning method is applied whatever units of the output data are chosen.

In r space, when the range of distances over which correlations occur becomes very large, the opposite of these trends is required, namely typically you might require *linear* binning at low r, where the atomic detail is important, but *logarithmic* binning at high r where the structure becomes progressively less detailed, but longer ranged. To this end the integral of 4.1 is required, namely

$$\Delta(r) = \frac{\Delta_{r,0}}{\ln(2)} \ln\left(2\cosh\left(\frac{\Delta_{r,L}}{\Delta_{r,0}} \ln(2) x\right)\right). \tag{4.2}$$

$\Delta_{r,0}$ is the constant step size that occurs at small r, and $\Delta_{r,L}$ is the logarthmic step size that occurs at large r, where the expression reduces to $\Delta(r) = \Delta_{r,L} x$. Currently $\Delta_{r,L}$ is not setable by the user and is internally set to 0.01. $\Delta_{r,0}$ is set by the user in the SAMPLE tab, and is given a negative value if logarithmic binning is required, but it always represents the step size in the linear portion of the output data.

The methods described in section 3.10.4 and 3.10.5 ensure that this variable bin size is treated correctly when transforming between Q and r space.

BEAM tab

The BEAM tab, Fig. 4.12 allows you to specify aspects of the incident neutron beam, the sample geometry, and the scattering detector. In order, you need to specify (or at least check)

1. The sample geometry (CYLINDRICAL or FLATPLATE);

2. The beam profile, $N(x)$, discussed in Section 3.4.2. Referring to Fig. 3.3, $N(x)$ is the number of neutrons per unit width measured at position x in a direction at right angles to the direction of the beam. For the corrections programs contained in Gudrun, the value of x is measured from the centre of the sample, with +ve x along a direction at right angles to the incident beam and to the left when facing away from the neutron source. For cylindrical sample, the z-aixis will go along the axis of the cylinder. This beam profile does not need to be normalised since the corrections programs do this normalisation in any case.

3. The step sizes for the CYLINDRICAL attenuation and multiple scattering corrections and the number of slices for the FLATPLATE multiple scattering correction. Note there is no step size for the flat plate attenuation correction because this correction is analytic. IMPORTANT NOTE: for cylindrical samples it is necessary to set the attenuation step size to approximately 1/25th of the outer radius of the sample and the multiple scattering step size to about 1/5th of the outer radius. These values are not set automatically, but if they are too large, then teh calculated corrections will not be accurate, and if they are too small, the programs will print a message to say some array specifier is out of bounds, and not calculate any corrections. In GudrunX GUI these step sizes are set automatically by the program, but this has not been implemented so far within Gudrun. For the FLATPLATE multiple scattering corrections setting the number of slices to 100 seems to give stable results in all cases.

4. The step in angle at which to calculate the corrections [degrees]. Note the GUI has an error here - the number input is NOT the number scattering angles at which to calculate the corrections!

5. The edges of the incident beam. These are defined as $a1$ and $b1$ in Fig. 3.3 and are measured from the centre of the sample. Also required are the top and bottom positions where the incident beam intersects the sample along its axis if cylindrical. These positions are also measured from the centre of the sample. Note that these values ONLY affect the calculation of the cylindrical corrections, since the flat plate corrections assume the sample is larger than the beam;

6. The edges of the scattered beam (assumed parallel) as defined in Fig. 3.3. These values might be useful where there is heavy collimation on the scattered beam which restricts the view of the sample by the detector.

7. The filename containing the incident beam spectrum parameters;

8. A background factor which will be applied to the background for all detectors, except where it has been changed at step 14 in Section 4.0.11.

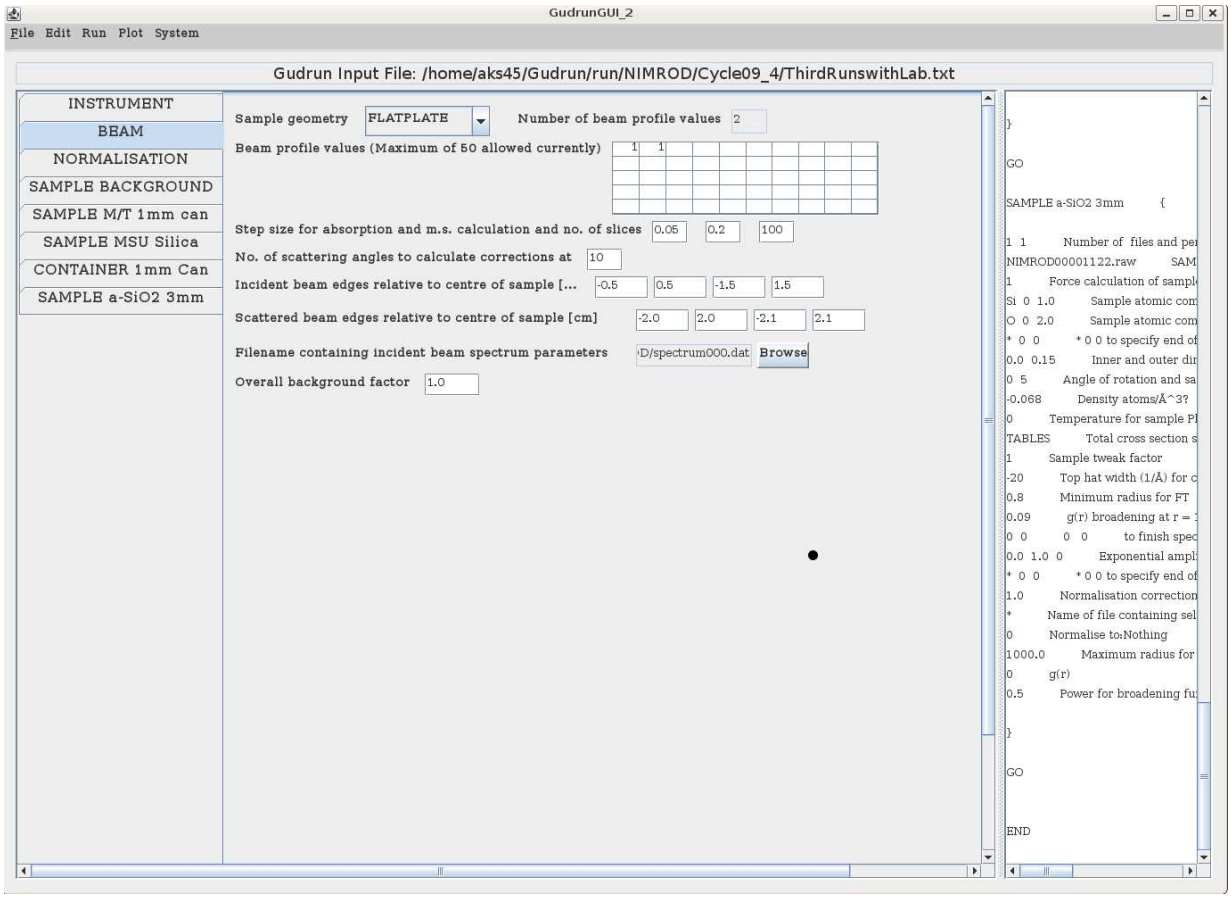

Figure 4.12: Layout of the BEAM tab in GudrunGUI

NORMALISATION tab

The word "normalisation" here in GudrunN refers to the process of putting the data on an absolute scale of cross section per unit solid angle, as described in Section 3.8.1. For this a sample of vanadium of the same geometry as the sample is normally used due to its large and flat incoherent differential cross section. For GudrunN to work correctly it is expecting the vanadium to have the same geometry as the sample, i.e. cylindrical vanadium with cylindrical sample, flat plate vanadium with flate plate sample. In principle it is possible to mix the two, but GudrunN will not recognise a flat plate vanadium with a cylindrical sample because the units of the calculated cross sections are different. For cylindrical samples the cross section is the actual cross section per steradian, expressed in the units of cm^2 per sr, but for flat plate samples the cross section calculated in the corrections programs is per unit area of beam, and so is dimensionless. It is possible to fool the program into thinking the vanadium is cylindrical (for example) when in fact it was flat plate, by using a "normalisation" factor described in the SAMPLE tab, however this will not give an absolute scale and the appropriate factor can only be guessed at best. Note that in GudrunN it is possible to select a vanadium geometry *different* from that for the samples (as defined in the BEAM tab). This is for those rare cases where a suitable vanadium measurement with the correct geometry is not available.

The NORMALISATION tab allows you to

1. Define the data files for the vanadium data and its corresponding background files. Note that in the past multiple periods have been used on SANDALS so there is the option of specifying the period number for these data files, but normally the period number is 1. Data files are added to the windows by pressing *Add*, then selecting the required files from the window that pops up. If no files are shown, it probably means the data file directory in the INSTRUMENT tab has not been set correctly, or else, if the data file directory is being accessed across a network, there is a delay in the network. Data files are removed by first highlighting those to be removed, then press *Remove*. The normalisation background is normally a run with the beam on but no sample or sample environment at the sample position, as explained in Section 3.7.

2. The composition, dimensions and density of the vanadium. Note that when typing in the composition window it is important to press "enter" when finished in a box, or use the arrow keys to move to another box, otherwise the typed value may not be transferred correctly to the GudrunN Input File. Note also that as of 17-01-2012, for flat plate geometry the upstream and downstream thickness is specified, rather than the "inner and outer" dimensions as previously. For a solid slab the total thickness can appear in one of these boxes with 0.0 in the other box, or half the total thickness can be specified in each box.

3. The temperature for the Placzek (inelasticity) correction on the vanadium. If this is zero, then no inelasticity correction on the vanadium will be performed.

4. Whether the vanadium total cross section is to be obtained from cross-section tables, the transmission monitor (if it exists) or read from a file. Normally the table values are sufficient for this purpose. Note that for this tab, and also the SAMPLE and CONTAINER tabs if the transmission monitor is used to estimate the transmission crossection of the NORMALISATION, SAMPLE or CONTAINER, then a low order polynomial is used to generate a smooth version of the transmission ratio prior to calculating the cross section. This to avoid noise in the transmission ratio being sharply accentuated in the transmission cross section and so causing spurious effects on the attenuation and multiple scattering corrections. This is particularly important when the run time is short so that statistics are poor. The order of the polynomial is selected automatically by the program and depends on the range of wavelengths being sampled, with roughly 1 order being given for each unit wavelength range.

5. It possible to specify either a differential cross section (DCS) file for the vanadium or else specify a list of Bragg peaks, (**.bragg** file, for vanadium as a function of Q with their (Gaussian) heights and widths. Normally the weak Bragg peaks from vanadium are not visible in data with high signal to noise ratio, but for samples with weak coherent signal, such as hydrogenous samples removing these peaks prior to normalisation can be crucial to obtaining useful data.

6. At the end of the tab are two numbers that are used to control the smoothing on the NORMALISATION and whether each detector is to be accepted. The first number, the "normalisation degree of smoothing", affects how much smoothing is performed. After each smoothing the ratio $R = \sum_i (D_i - F_i)^2/\sigma_i^2$ is formed, where D_i are the data, F_i are the smoothed data, and σ_i is the RMS deviation of each data point (from the counting statistics). If the data are undersmoothed, then $R < 1.0$, while if they are oversmoothed, then $R > 1$. Oversmoothing could result in distortions appearing in the smoothed result, but obviously will give a cleaner normalisation. Hence the smoothing is continued until $R >$ "Normalisation degree of smoothing", so you can control the degree of smoothing on the NORMALISATION data using this value. Normally values in the region 1.05 - 1.2 are useful to give a reasonably smoothed normalisation without overly distorting it.

7. The second number controls whether each particular detector is used at all. Basically if R from the previous item drops below the specified value (usually 0.01) then the detector will be ignored completely, since it suggests there is something wrong with the signal from this detector (e.g. too much background, or very weak signal). This works in addition to any previous assignment of this detector as good or bad from purge_det, but currently the fact is not recorded so that each time you run the analysis the detector will be re-checked for compliance with the required minimum ratio.

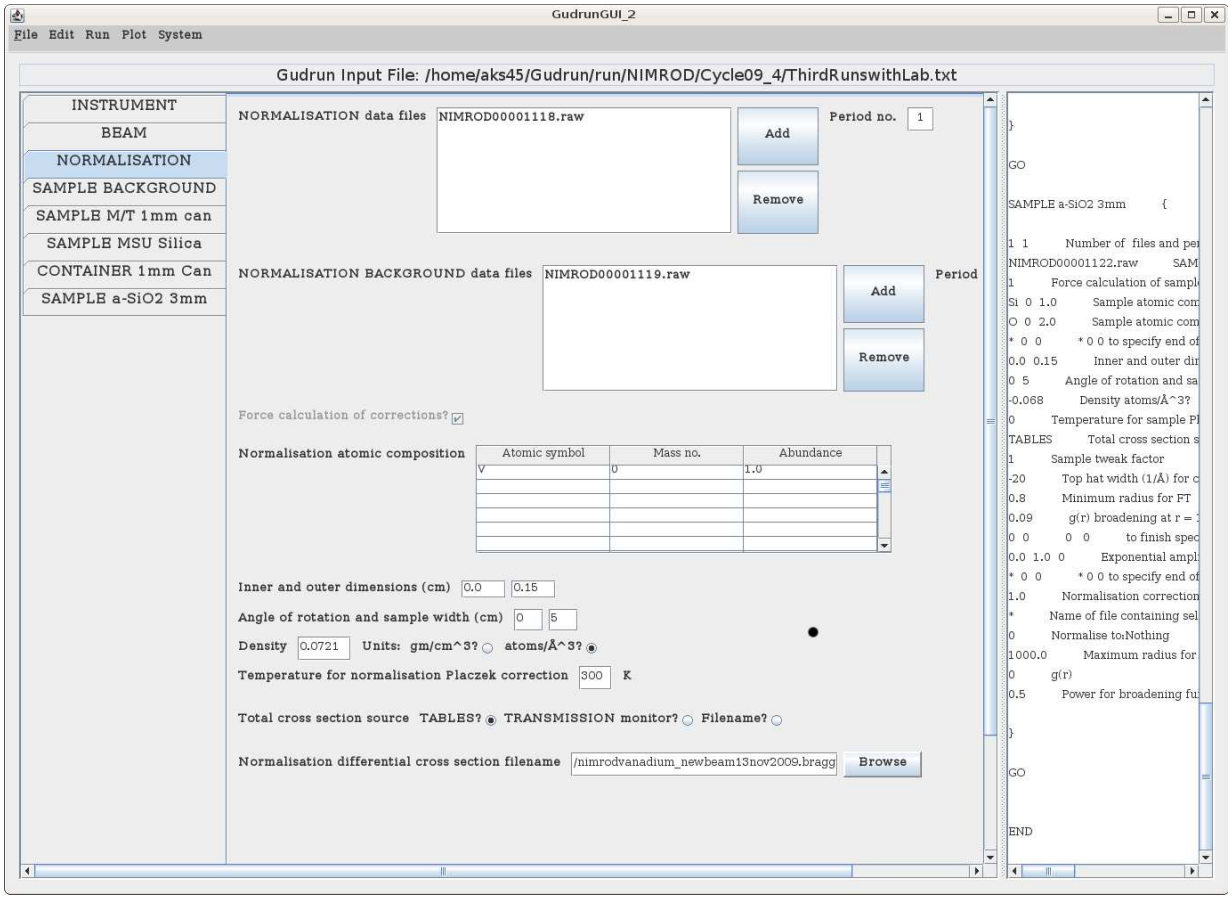

Figure 4.13: Layout of the NORMALISATION tab in GudrunGUI

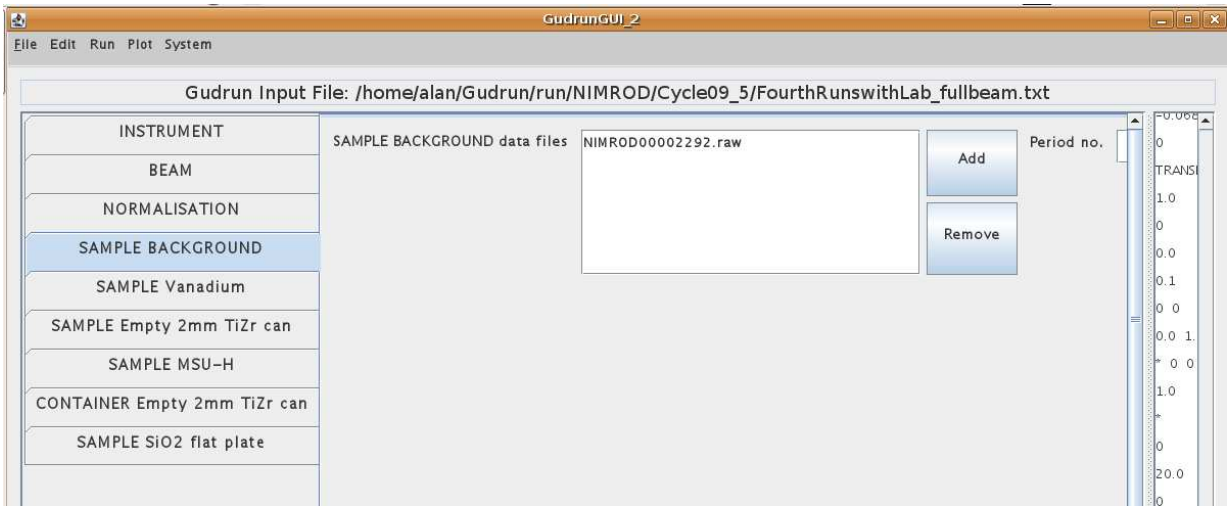

Figure 4.14: Layout of the SAMPLE BACKGROUND tab in GudrunGUI

SAMPLE BACKGROUND tab

As already explained you can have as many SAMPLE BACKGROUNDs as you wish: for any given SAMPLE the one used will be that closest and prior to that sample in the list of tabs. The sample background may be different from the normalisation background since the latter is normally the background with nothing in the beam, while the sample background may include the background from a furnace or cryostat which surrounds the sample. It is for this reason that multiple sample backgrounds are allowed, since one sample may be measured in a container in a cryostat, while another may have been measured just in its container. The cryostat could have been treated as a second container, but if it is not strongly scattering it is probably sufficient to treat it simply as a background.

The only parameters for the SAMPLE BACKGROUND tab are the data files which store the data for this background, Fig. 4.0.11.

SAMPLE tab

The top half of the SAMPLE tab, Fig. 4.15, down to the cross section source specification, is almost identical to the top half of the NORMALISATION tab, with two exceptions:-

1. Obviously there is no sample background specified here since this is already specified in the SAMPLE BACKGROUND tab.

2. Below the data files box there are two extra tick boxes, one to force each run file to be analysed separately, and the other to avoid analysing this sample altogether. The first option is useful if you want to compare separate runs on the same sample, looking for stability or changes of structure with time. The second allows you to have multiple samples in the GUI, but you do not have to analyse all of them everytime you run Gudrun. Only those that are ticked will be analysed.

Neither of these tick boxes will affect what is saved to the GudrunN Input File, but note that in addition to writing the file specified at the top of the frame, the GUI writes a second file, called **Gudrun_dcs.dat** which is the file actually input into Gudrun_dcs. It is this second file that contains the schedule of samples and containers that are actually put through the analysis.

Note also that as of 17-01-2012, like for the NORMALISATION tab, for flat plate geometry the upstream and downstream thickness is specified, rather than the "inner and outer" dimensions as previously. For a solid sample the total thickness can appear in one of these boxes with 0.0 in the other box, or half the total thickness can be specified in each box.

Below this main section comes the details of other parameters that can be specified for particular samples, Fig. 4.16. Reading from left to right, top to bottom:

1. The sample "tweak" factor. (Horrible name!) This is really the reciprocal of the packing fraction: a packing fraction of 0.5 would translate to a tweak factor of 2, and so on. Basically this factor was invented to correct for the fact that with powdered samples it is not possible to fill the container completely, or for liquids in awkward shaped containers such as those made from fused silica, it was not always possible to know the sample dimensions precisely. The sample tweak factor is to be distinguished from the container tweak factor because it is used to modify the specified number density (which is assumed to be that for the sample with 100% packing) by dividing that density by the tweak factor. It is this modified density that is used to calculate the attenuation and multiple scattering corrections, and the number of atoms in the beam for the final normalisation of the cross section to b/sr/atom, Section 3.9. However if a Fourier transform is done on the data, then it is the unmodified density that is used, since this corresponds to the local density.

2. Normalisation correction factor. This was mentioned in the NORMALISATION tab and is used (very rarely in fact) to correct for the fact that the normalisation geometry may not be consistent with that of the sample.

3. The final normalisation to either nothing, $\langle b \rangle^2$, or $\langle b^2 \rangle$.

4. The top hat width for removing the single atom background scattering, see Section 3.10.3, prior to Fourier transform. If this value is zero, no background is subtracted and no Fourier transform is performed. If the value is negative, the final differential cross section is averaged from that Q value to the maximum Q value, and that average level subtracted from the data prior to Fourier transform. The top hat convolution will only be performed if there is linear binning and the units are Q, but the constant subtraction and subsequent Fourier transform will be performed with both log and linear binning. However the data units always have to be Q.

5. Both $h(r)$ and $d(r) = 4\pi\rho r h(r)$ are produced if the Fourier transform is being performed. These outputs are given alternative extensions **.mgor01** and **.mdor01** respectively.

6. The minimum radius used for cleaning up the Fourier transform. This is the value of r_{min} as described in Section 3.10.3, equation (3.71).

7. The maximum and step in radius for the Fourier transform are specified. If the step size is negative, then logarithmic binning in r space is adopted according to the procedure described in section 4.0.11.

8. The broadening in r-space is defined as described in Section 3.10.4.

9. The minimum and maximum wavelength of any resonances that are to be avoided when merging the detectors are specified. Up to 5 pairs of values are allowed for each sample.

10. Up to 5 pairs of exponential amplitudes and decay constants can be specified. This is mainly used with hydrogenous samples to subtract the residual low Q behaviour which is not removed by the top hat function. The formula for this background function in Q-space is $B(Q) = \sum_i A_i \exp(-Q/\gamma_i)$, where the sum is over the number of exponentials specified, A_i is the amplitude of each exponential, and γ_i is the decay constant for each exponential. The amplitudes A_i can have both positive and negative values.

11. The last line of this tab should be ignored at this stage as it is related to work in progress, and may eventually disappear.

CONTAINER tab

As already mentioned each sample can have up to three containers, listed in the order innermost to outermost. The format is very similar to the SAMPLE tab down to the cross section specification, Fig. 4.17, but there are no tick boxes since whether this container is included or not is governed by the directions given in the preceding SAMPLE tab. There is just one extra factor, a container tweak factor, normally unity, which is used to adjust the container scattering up or down in cases where normal application of the attenuation correction either unde- or over-subtracts the container scattering.

Note that neither in the GUI nor when the corrections are calculated in Gudrun_dcs is any check done that the dimensions of each container are consistent with the sample and other containers, that is there are no overlaps. The corrections programs will produce results even if there are overlaps between containers or with the sample, but corrections will of course be incorrect in that case! Hence this check needs to be done by the user before running the analysis.

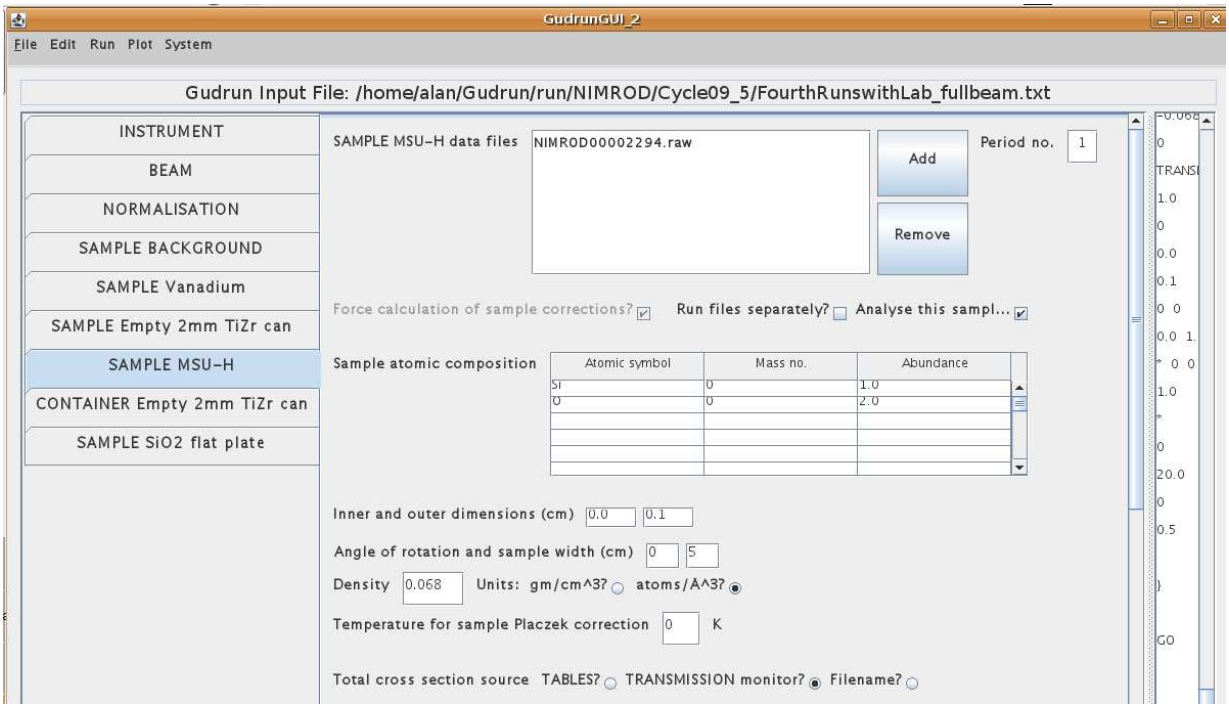

Figure 4.15: Layout of the top half of the SAMPLE tab in GudrunGUI

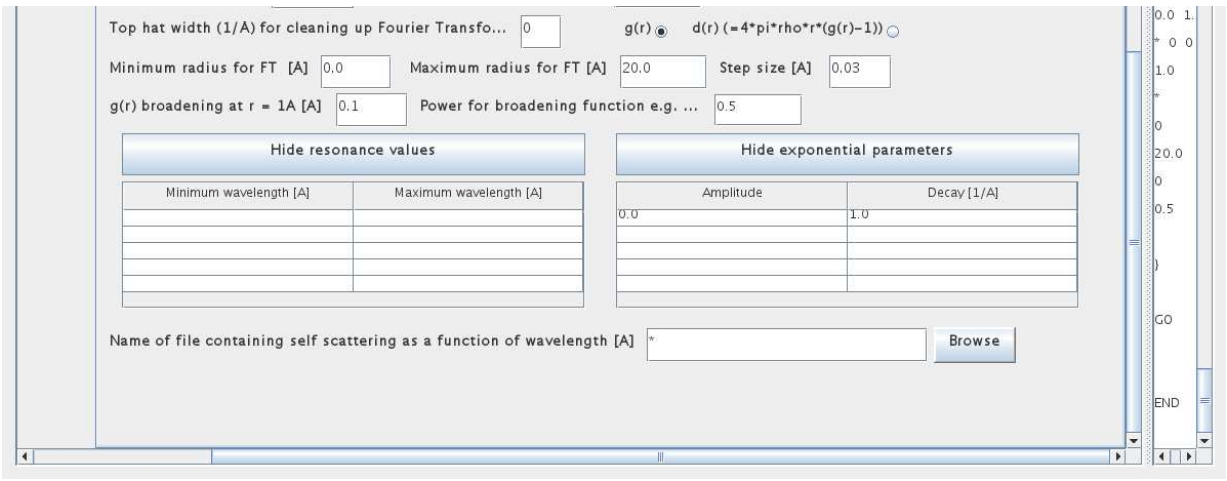

Figure 4.16: Layout of the bottom half of the SAMPLE tab in GudrunGUI

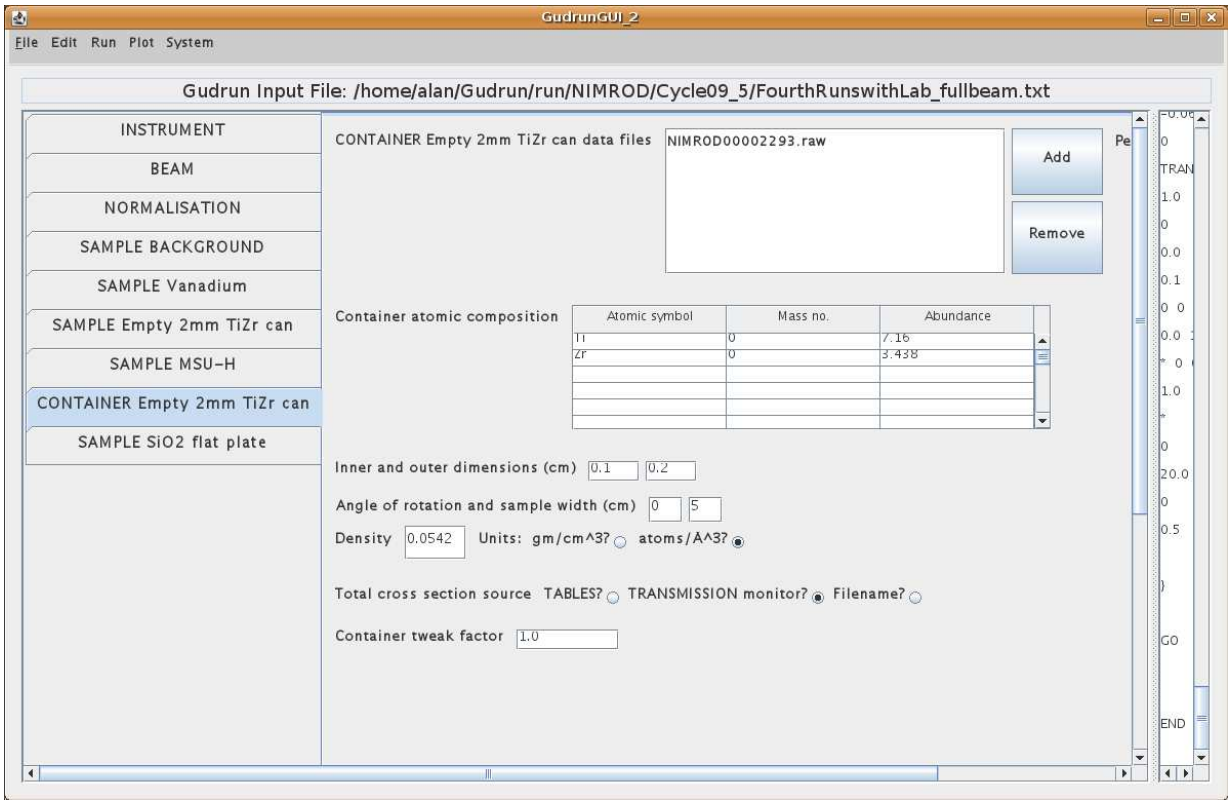

Figure 4.17: Layout of the CONTAINER tab in GudrunGUI

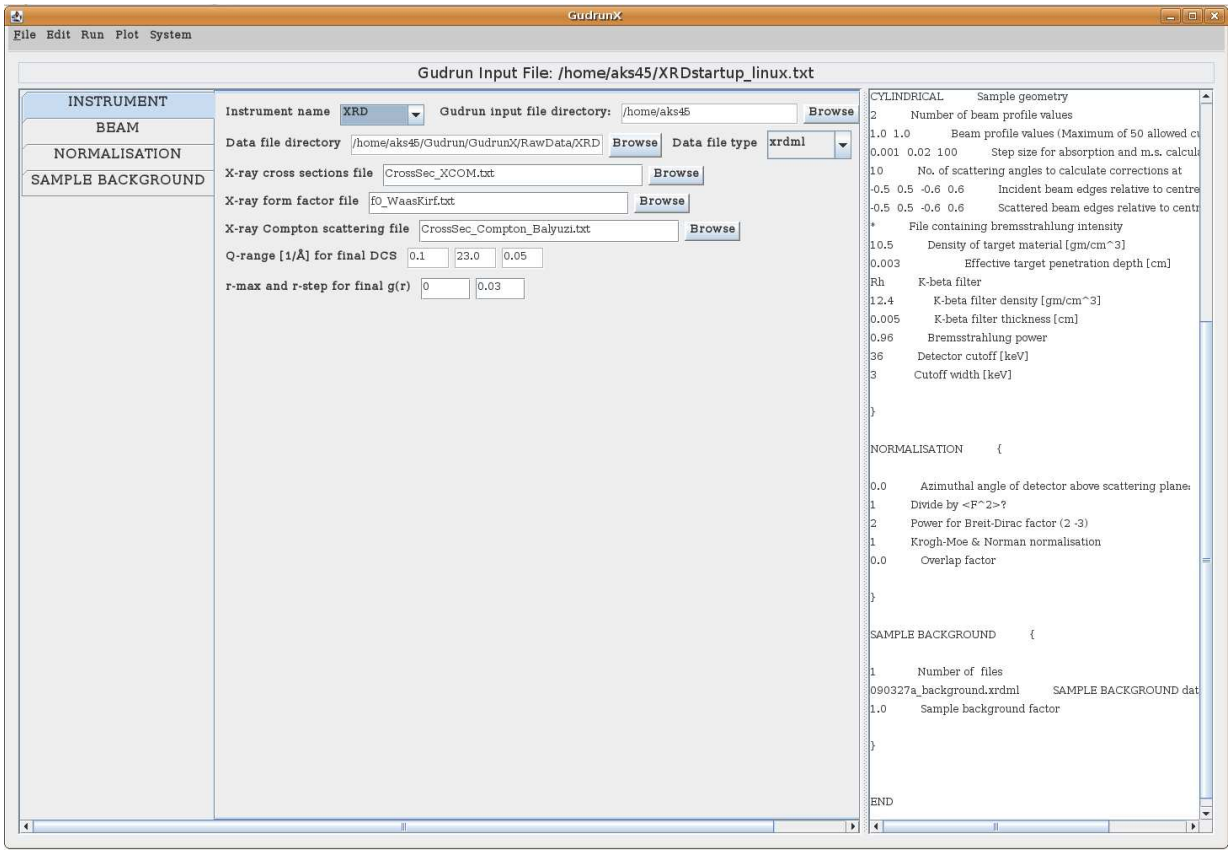

Figure 4.18: Layout of the GudrunX GUI when it starts. If the start up file has loaded correctly, then four tabs should be displayed, INSTRUMENT, BEAM, NORMALISATION and SAMPLE BACKGROUND.

4.1 Running GudrunX from the GUI

4.1.1 Starting the GudrunX GUI

The GudrunX GUI is started either by double clicking on **gudrunx.bat** (in Windows) or running the corresponding shell script, **gudrunx.sh** in Linux. When it opens it should look like Fig. 4.18. Note that there are INSTRUMENT, BEAM, NORMALISATION and SAMPLE BACKGROUND tabs as before, but their formats are often different from the corresponding neutron versions.

Currently a major difference between GudrunN and GudrunX is that in GudrunN all the processing is done in separate, Fortran compiled, executables, namely **purge_det.ex** and **Gudrun_dcs.ex**. In GudrunX most of the processing is done in the Java routines behind the GudrunX GUI. The exceptions are the routine to calculate the attenuation and multiple scattering corrections, **calc_corrsx_in_out.exe** and the routine to calculate the Fourier transform, **tophatsub.exe**. These latter two routines are Fortran compiled and are run by an external call from Java. Hence these need to be specified correctly in the

Figure 4.19: Layout of the GudrunX *System* box, achieved by clicking *System* then *Set system path names*

System box, Fig. 4.19 if Java is to be able to find them when it wants to them run.

4.1.2 Features of the GudrunX GUI and menus

These are pretty much identical to those already described in Sections 4.0.9 so will not be repeated here. Equally the menus are almost identical to GudrunN, Section 4.0.10. The only exceptions are that in the *Edit* menu it is not possible to convert the NORMALISATION tab to a SAMPLE or CONTAINER, and the *Run* menu which has only two items, namely the *Check files exist* item and the *Run GudrunX* item. There is currently no *Purge* option with GudrunX. Note also that GudrunX will require a different GudrunGUI.syspar file compared to GudrunN because the executables are different, as already noted.

Fig. 4.20 shows what this should look like once a sample and its container are loaded.

4.1.3 GudrunX GUI tabs

INSTRUMENT tab

The first two lines of the INSTRUMENT tab in GudrunX, Fig. 4.21, are exactly the same as for GudrunGUI. Currently there are two types of data format supported. These are

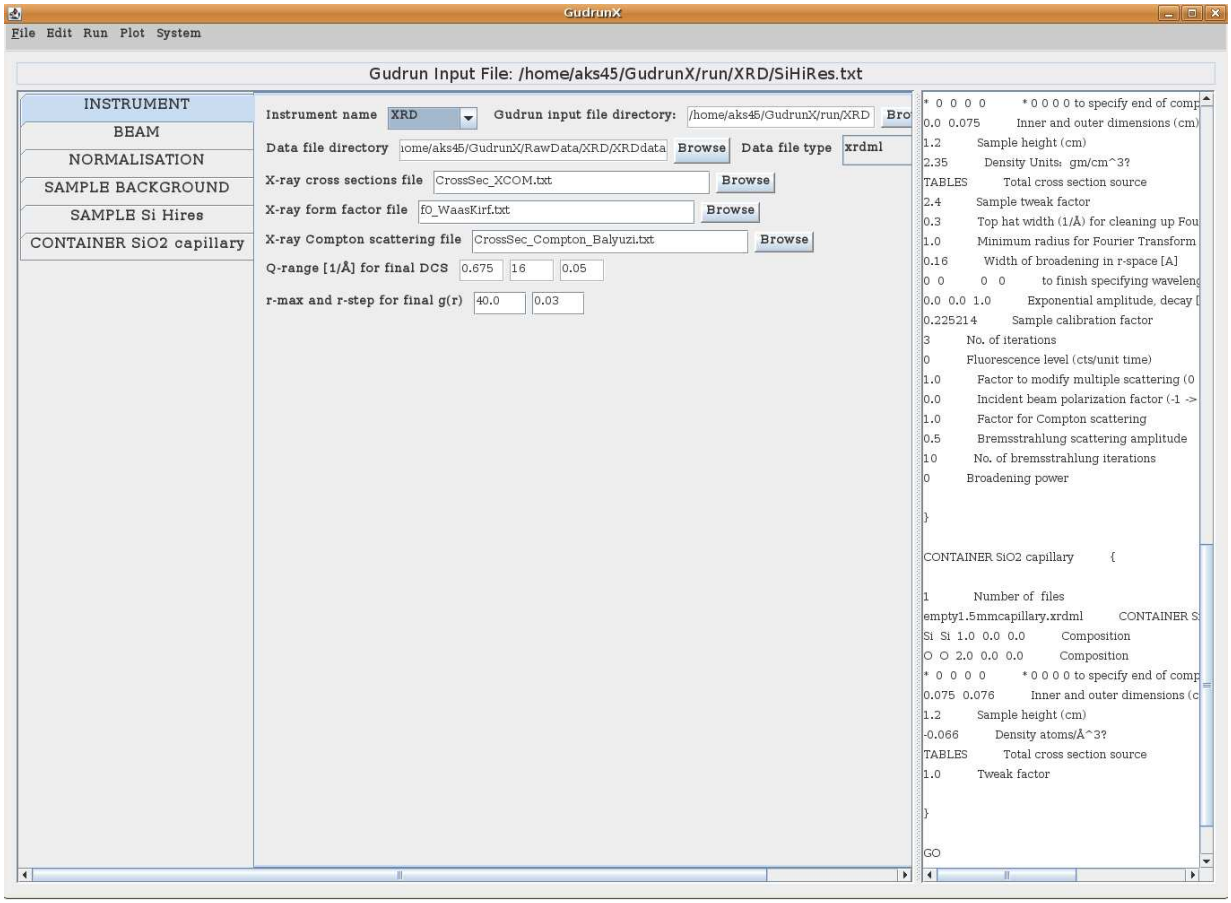

Figure 4.20: Layout of the GudrunX GUI after loading a sample with its container.

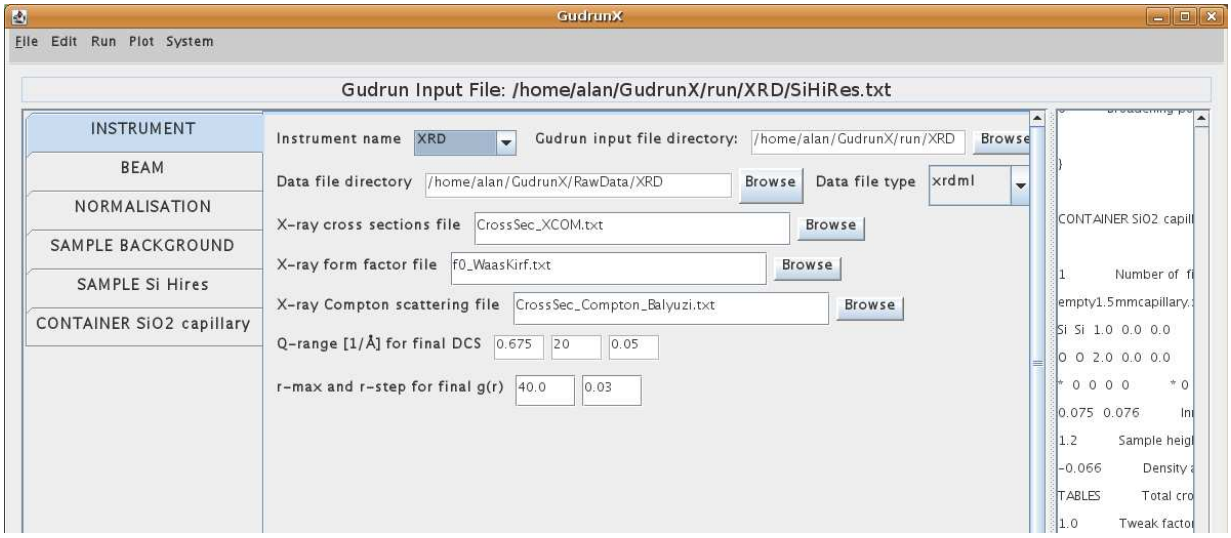

Figure 4.21: Layout of the GudrunX INSTRUMENT tab.

.xrdml, which is the standard PANalytical XML data file format, or .xye or .dat (you can have one or the other but not both) which is x,y,e format, with x the scattering angle, y the intensity (in arbitrary units) and e the RMS error on the value of y. These latter extensions were set up for synchrotron data. In addition data in the form x,y,m, where m is the monitor value, or simply x,y are can be used. If the latter, then it is assumed the monitor value is the same for all data points.

Below these lines are:

1. The names of the total cross section, form factor coefficients, and Compton scattering coefficients files. These are normally stored in the directory where GudrunX begins. They have a particular format that is recognised by the GUI.

2. The lowest, highest and step in Q values for the output files

3. The maximum and step in r values for the output $g(r)$, if required.

BEAM tab

As with the INSTRUMENT tab, the first part of the BEAM tab in GudrunX, Fig. 4.22 is identical to that in GudrunGUI. A notable difference however is that the GUI will set the attenuation and multiple scattering step sizes based on the outer dimension of the sample so there is no need to worry about these values in GudrunX.

The next part of this tab defines the bremsstrahlung spectrum. This is defined according to equation (3.50, and can be specified either as a file, containing entries in the order $E_x(MeV), I_{Br}(E_x)$, or else the parameters to this intensity equation can be specified in the tab itself, in hopefully an obvious format. To use the values in the GUI it is necessary

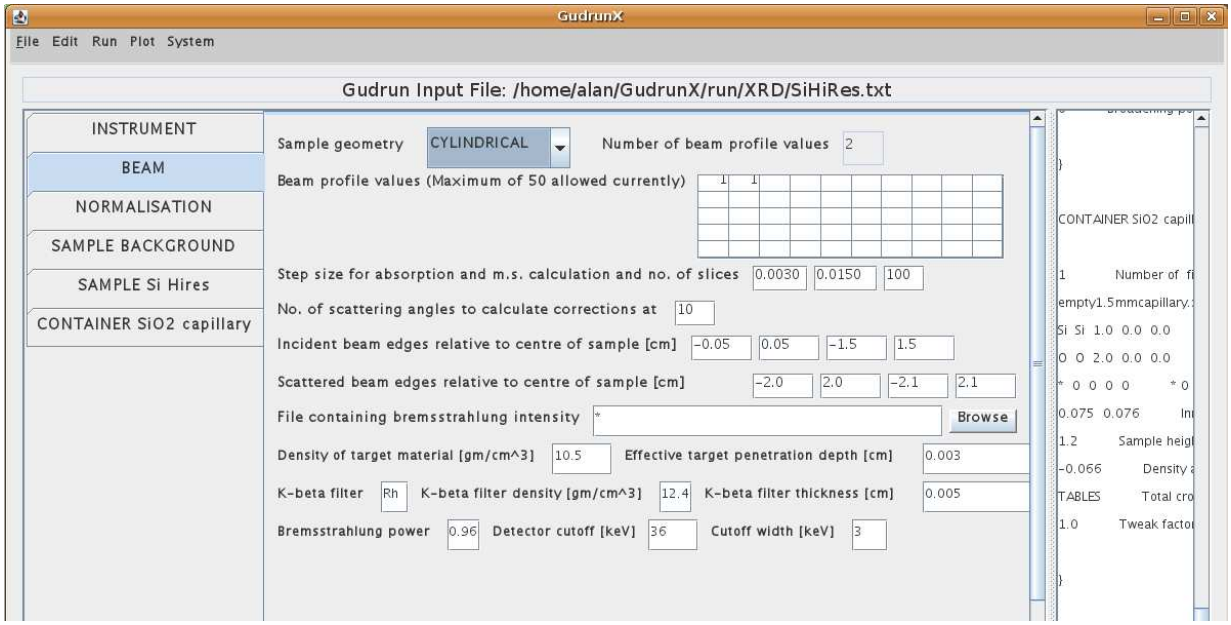

Figure 4.22: Layout of the GudrunX BEAM tab.

to give the filename for the bremsstrahlung spectrum as an asterisk, as shown here. The target material and tube voltage are obtained from the SAMPLE tab, see below.

Bragg-Brentano scanning

For flat plate samples with x-rays it is sometimes necessary to perform Bragg-Brentano scanning. This is the case where both the source *and* the detector are moved, with the angle of incidence and the angle of reflection or transmission normally kept equal. In this case the footprint of the beam and detector will vary with scattering angle if the incident and detector slits are held constant. Alternatively the diffractometer in question may have a facility to keep the beam and detector footprints constant as a function of scattering angle by having automatically adjusting slit dimensions. This gives significant improvement in counting statistics at high angles in reflection geometry, but since the x-ray flux across the slit may not be constant it means there is an unknown variable as a function of scattering angle that can be difficult to estimate or calibrate. It also gives very poor performance at low angles in reflection geometry as then the beam has become extremely narrow.

There is an attempt to deal with both these scenarios within GudrunX. Thus when FLATEPLATE geometry is selected a new section appears in the BEAM tab which allows you to state whether you are using "theta-theta" (= Bragg-Brentano) scanning, and if so, it allows you to specify certain parameters to calculate an angle dependent factor to compensate for the beam and detector footprint, see Figs. 4.23 and 4.24.

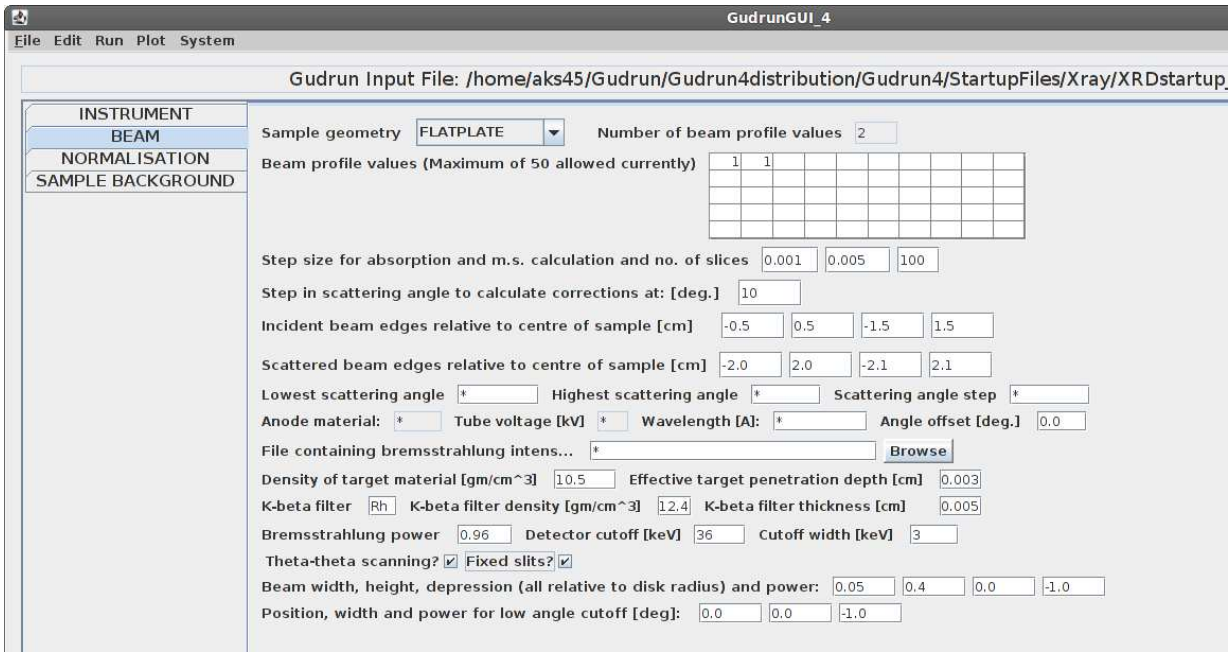

Figure 4.23: Layout of the GudrunX BEAM tab when "theta-theta" (Bragg-Brentano) scanning and fixed slits are selected.

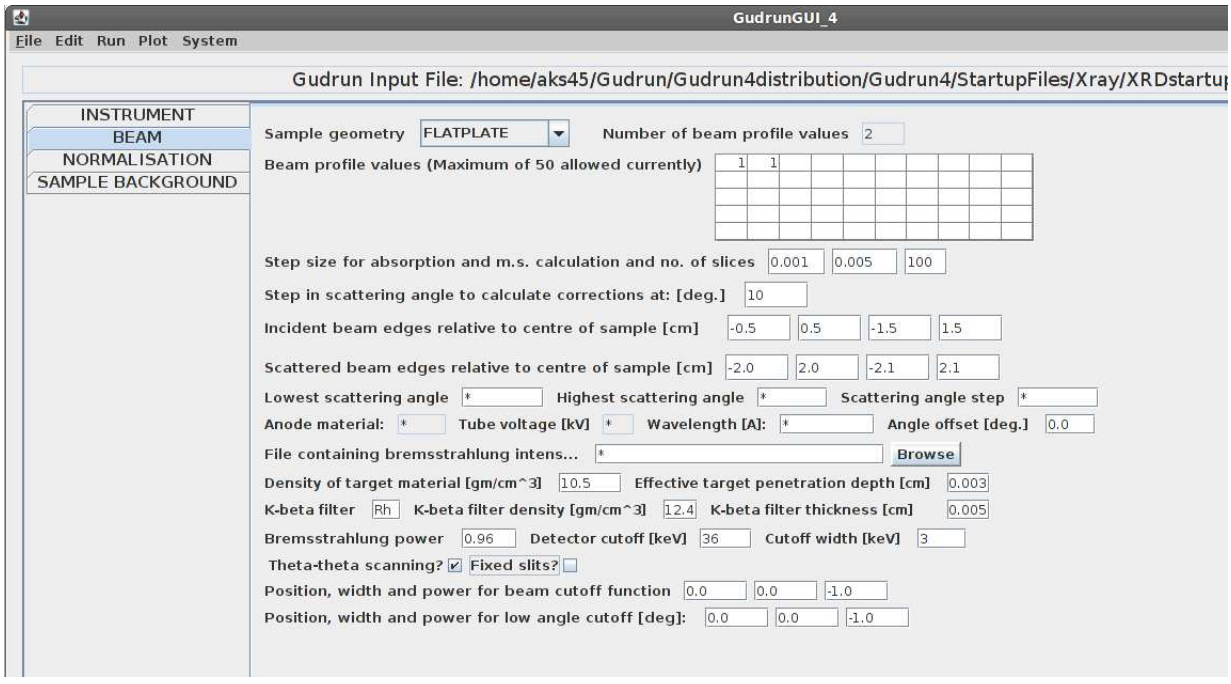

Figure 4.24: Layout of the GudrunX BEAM tab when "theta-theta" (Bragg-Brentano) scanning and fixed footprint are selected.

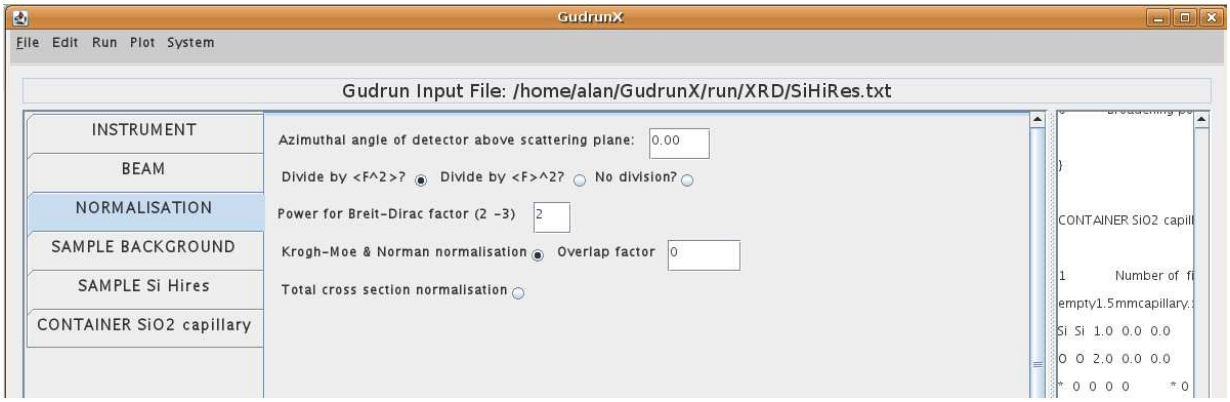

Figure 4.25: Layout of the GudrunX NORMALISATION tab.

NORMALISATION tab

As already mentioned there is no equivalent to the vanadium sample in an x-ray experiment, so the NORMALISATION tab, Fig. 4.25, in GudrunX simply specifies what type of normalisation is to be performed and how the data are to be calibrated to put them on an absolute cross section scale. The items to be specified are:

1. The angle ρ from equation (3.47). This is normally zero unless you have good reason to believe otherwise.

2. The type of normalisation of the data required. This was specified in the SAMPLE tab in GudrunGUI.

3. The power for the Breit-Dirac factor, equation 2.57 in the Klein-Nishina formula, equation 2.56. Strictly speaking this power should be 2, according to equation 2.56, GudrunX gives the option of changing this power to improve the subtraction of the single atom scattering. The power mostly affects the higher angle part of the scattered spectrum. This might be a reasonable thing to do if the detector is not the "black" detector that is traditionally assumed.

4. If using the Krogh-Moe and Norman method for data calibration, you can specify an overlap factor, δ, as desctibed in Section 3.8.2, equation (3.35.

5. If using calibration to the single atom scattering, the program simply forms the average value of the data in the range from half Q_{max} to Q_{max} and the same average value of the single atom scattering over the same range of Q values, and uses the ratio of these two numbers as the data calibration factor. Generally speaking this method is less satisfactory than the Krogh-Moe and Norman method.

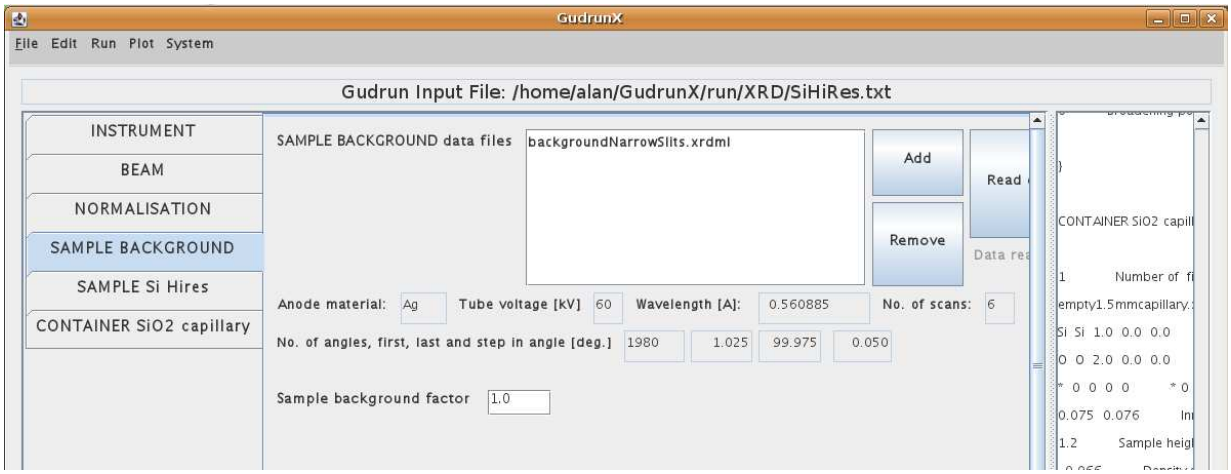

Figure 4.26: Layout of the GudrunX SAMPLE BACKGROUND tab.

SAMPLE BACKGROUND tab

This is very similar to the GudrunN SAMPLE BACKGROUND tab, except that some new (non-editable) boxes appear which give details of the x-ray tube and angles when the data have been read in. The data can be read in at any time by pressing the *Read data* button.

There is also the option to specify a sample background factor if so required. This is in place of the background factor that appeared in the BEAM tab in GudrunGUI.

SAMPLE tab

The top half of the SAMPLE tab in GudrunX, Fig. 4.27, is very similar to that found in GudrunGUI, with the changes to the data file specification area as already noted for the SAMPLE BACKGROUND tab. Also note that you can tick the *Run files separately* box and enable the cross-section filename button, but these do not currently do anything, and the program will proceed as if they had been left unchecked. The sample tweak factor is used in exactly the same way as for GudrunN.

The bottom half, Fig. 4.28, however has some differences, namely:

1. Fluorescence counts. As explained in Section 3.10.2, this is subtracted from the sample data prior to any processing. If fluorescence is present in the sample, then the "Specify Fluorescence Levels" needs to be pressed and a separate table will appear where the fluorescence energies and relative weights for each element can be set. In addition it is necessary to set the overall relative level of fluorescence scattering compared to the total scattering from the sample. The correct value for this level to subtract can only be determined by trial and error. Subtract too much and the data will have negative intensity in some regions, which of course is physically impossible. Subtract too little and you will have a hard time fitting the single atom scattering to the data. The fluorescence scattering, equation 3.53, is time consuming

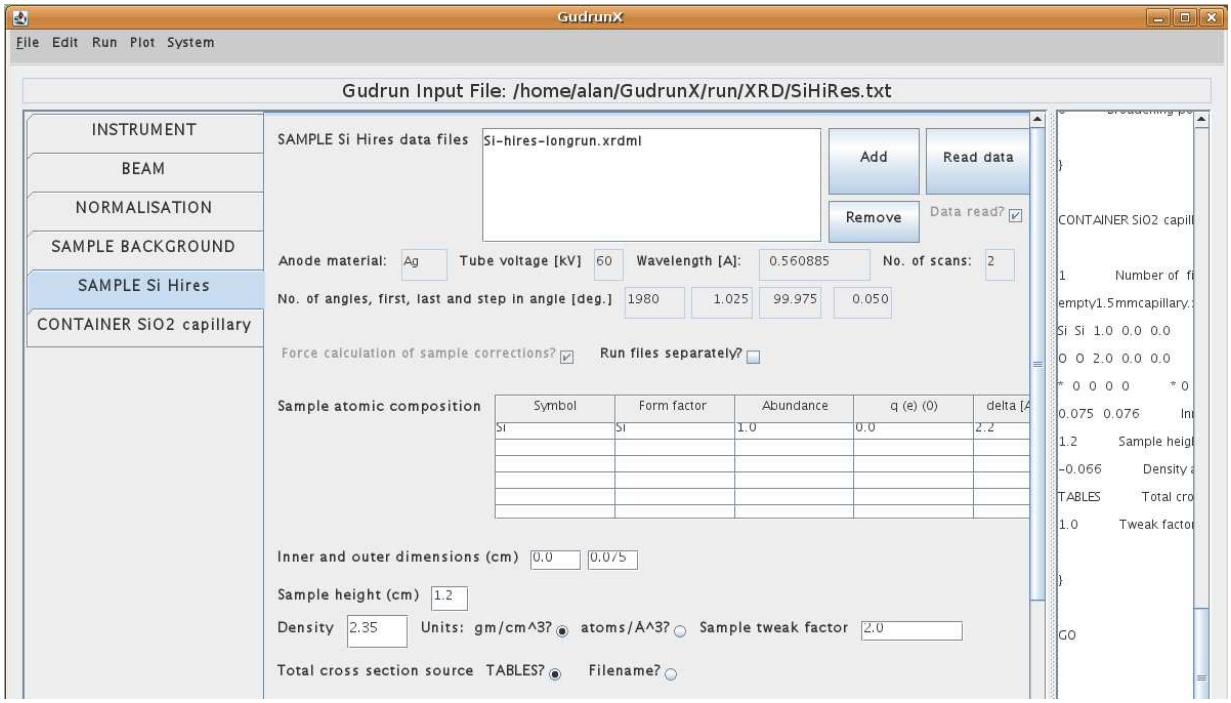

Figure 4.27: Layout of the top half of the GudrunX SAMPLE tab.

to evaluate, so if the only thing that is changed between each run of GudrunX is the overall fluorescence level it is not necessary to recalculate the fluorescence scattering, so normally the "Force fluorescence calculation" box is left unchecked. However if you want to force this calculation you can check the box. If either the individual atom fluorescence energies or weights are changed, then the fluorescence scattering is automatically recalculated from scratch.

2. Factor to modify multiple scattering. While it is often assumed multiple scattering in an x-ray experiment is a small component, calculations with GudrunX at high energies suggest this is not so. However given the very large change in x-ray scattering cross section with angle plus the effect of the polarisation correction, it is not clear that the isotropic approximation used in the correction programs is really valid. (This approximation assumes that for the purposes of calculating the multiple scattering the once scattered x-rays radiate isotropically with scattering angle, an assumption which is clearly not true in this case.) Hence you have the option of multiplying the multiple scattering above or below its calculated level, to try to improve the behaviour of the large Q data after subtracting the single atom scattering.

3. Incident beam polarisation factor. This is ϕ the polarisation factor defined in equation (3.48.

4. Compton scattering factor. As for the muliple scattering, you are allowed to multiply

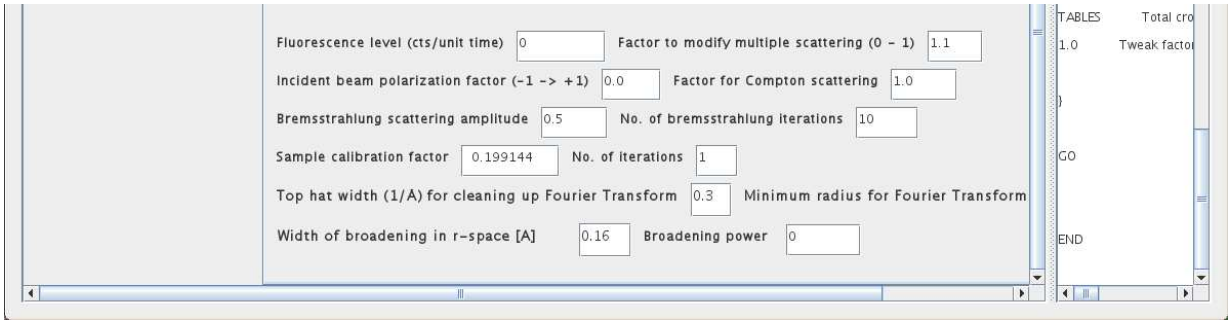

Figure 4.28: Layout of the bottom half of the GudrunX SAMPLE tab.

the Compton scattering by the specified value so help improve the subtraction of the single atom scattering, if necessary.

5. The bremsstrahlung amplitude and the number of bremsstrahlung iterations. The deconvolution of the differential cross section from the bremsstrahlung spectrum has to be performed iteratively, as described in Section 3.10.2, and generally 10 iterations is sufficient to get a good deconvolution. The bremsstrahlung amplitude defines that fraction of the overall intensity that occurs as bremsstrahlung radiation. Normally a value of ~ 0.4 works well for the Ag tube on PANalytical XRD, if there seems to be a problem this relative amplitude can be modified if needed.

6. The sample calibration factor is determined by the program using one of the normalising options specified in the NORMALISATION tab, so does not need to be set.

7. The number of iterations required to calculate this calibration is normally in the region of 3-4, but if the number of iterations is set to zero, the program will use the value shown in the tab. Hence in that case the user can set their own calibration constant.

8. The top hat width for removing the single atom background scattering, see Section 3.10.3, prior to Fourier transform. If this value is zero, no background is subtracted and no Fourier transform is performed. The option of using a negative value for the top hat width is currently not available within GudrunX.

9. The minimum radius used for cleaning up the Fourier transform. This is the value of r_{min} as described in Section 3.10.3, equation (3.71).

10. The broadening in r-space is defined as described in Section 3.10.4. Note that in GudrunX the maximum r value and step size are defined in the INSTRUMENT tab rather than in the SAMPLE tab.

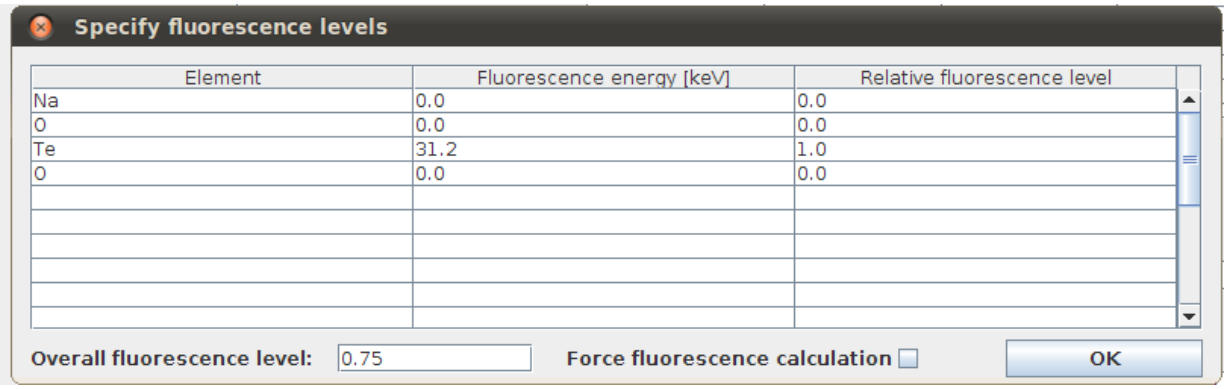

Figure 4.29: The table used to set the fluorescence levels.

CONTAINER tab

This follows the CONTAINER tab in GudrunN closely, with the same changes in the data files area as already noted for the SAMPLE BACKGROUND and SAMPLE.

4.2 Plotting options

Chapter 5 will indicate the files that are output by GudrunN and GudrunX. These include diagnostic files as well as output files containing the analysed data. Most likely you will use your own method of presenting these data in a form ready for publication, but both GUIs provide a simple interface to generate GNUplot plot files to be used to interogate the data and diagnostic files produced. In fact with the postscript option GNUplot can easily produce publication quality graphs, so this is normally my preferred method of graphing data, but others may not agree!...

The simplest way to do this is to start GNUplot from the *Plot* menu: this opens GNUplot in the current input file folder and you can enter commands by hand. However if plotting lots of files, this can become tedious, so now there is a separate plot dialogue to allow you some flexibility in the way the plots are produced. The same dialogue will allow you save and reload a previous list of plot commands. The GNUplot commands are shown in files with extension **.plt**, while the saved plotting commands that can be read back into the plot dialogue are stored in a file with extensinn **.aux**.

4.2.1 Plot dialogue

The plot dialogue is shown in Fig. 4.30 and is started by pressing *Plot*, then *Generate GNUplot plotting file*.

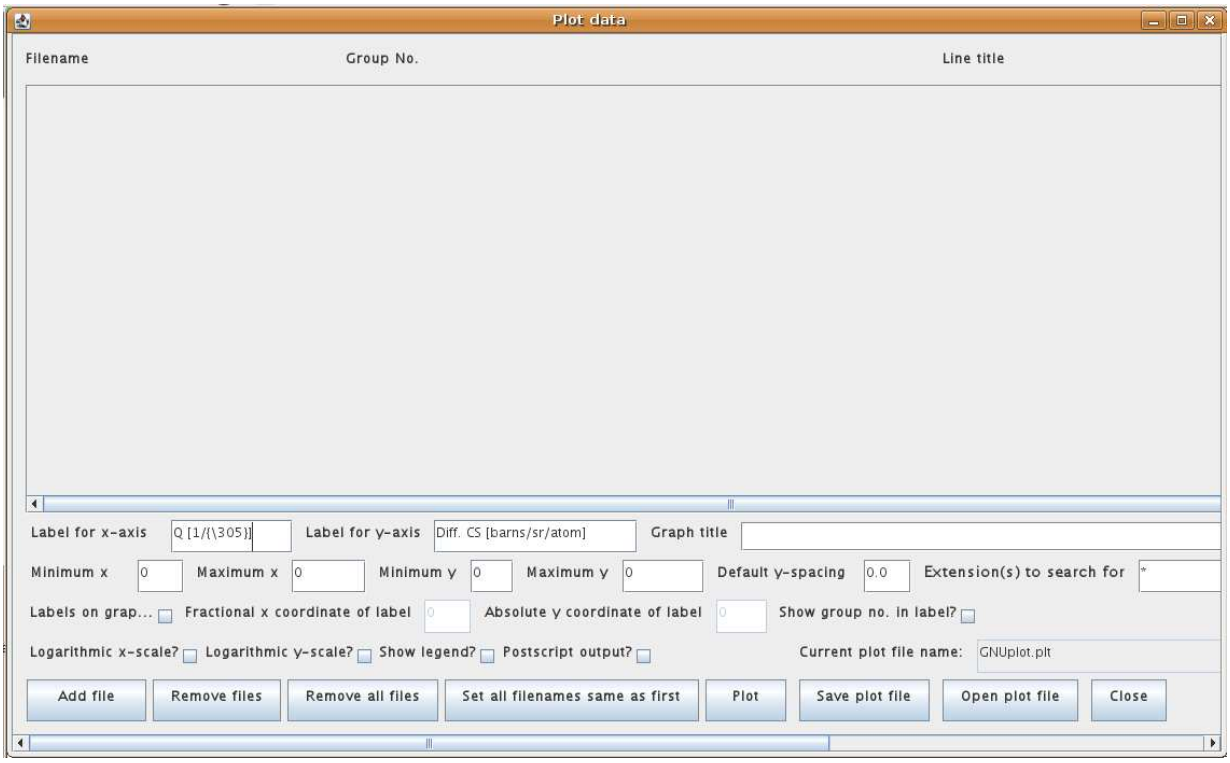

Figure 4.30: Layout of the Plot dialogue. In this view no plotting files have been inserted so far.

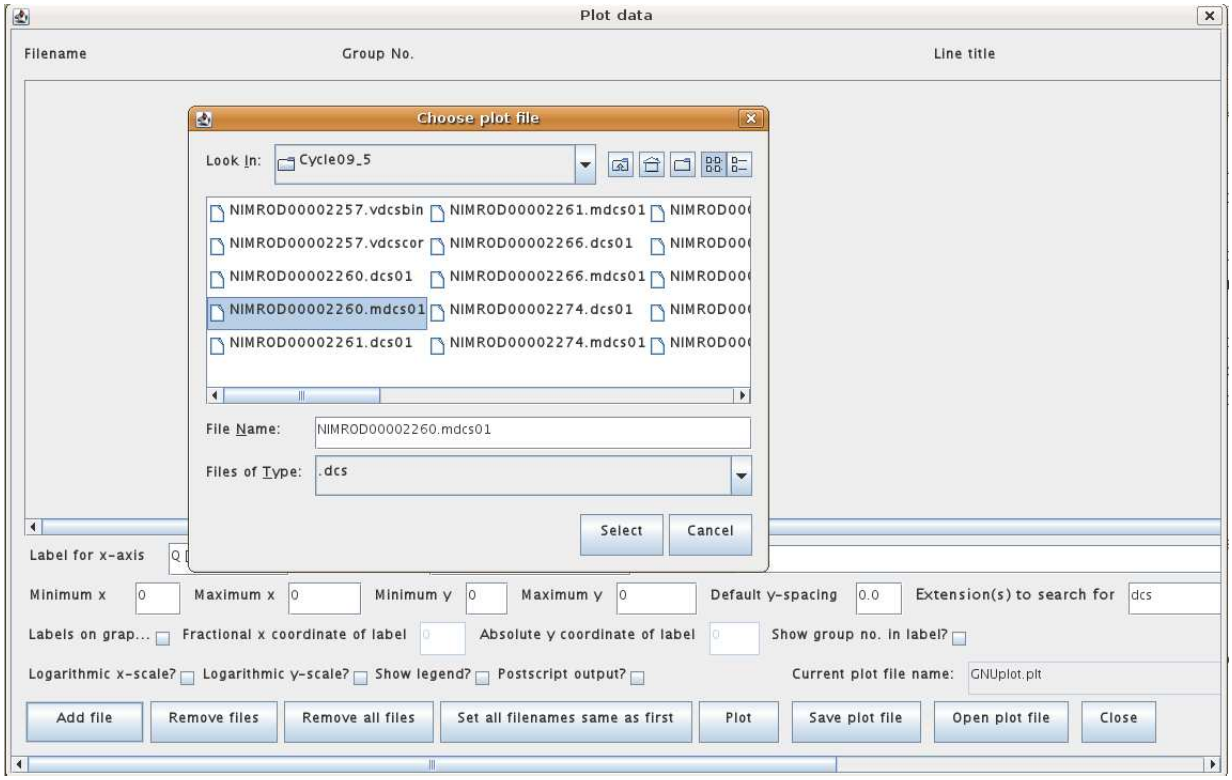

Figure 4.31: Layout of the Plot dialogue. In this view the *Add file* button has been pressed after typing "dcs" in the extension box.

Adding files to and removing files from the Plot dialogue

On the lower right hand side of the dialogue is a text box with the label "Extension(s) to search for". This is useful when the data analysis folder has lots of files in it. By typing in this box you can select which files you want to list. If the specified extension is preceded by a dot, then only files of that specific extension will be listed, while without the dot, files with extensions that *contain* the typed text will be listed. Fig. 4.31 shows what happens when you type *dcs* in this box, then press *Add file*. Finally Fig. 4.32 shows what it looks like after the file has been selected.

Each line in the list of files has several parameters to be assigned.

1. The filename is the first: this can be changed either by typing in the filename box or pressing the *Browse* button.

2. The filename is followed by the Group number. For files with multiple groups, such as the **.dcs01** files from Gudrun, each group occurs as a pair of columns, intensity versus root mean square deviation on this intensity. The left most column is the x-scale (e.g. Q, wavelength, energy, d-spacing, or TOF. Hence group 2 for example would correspond to columns 4 and 5 in the **.dcs01** file.

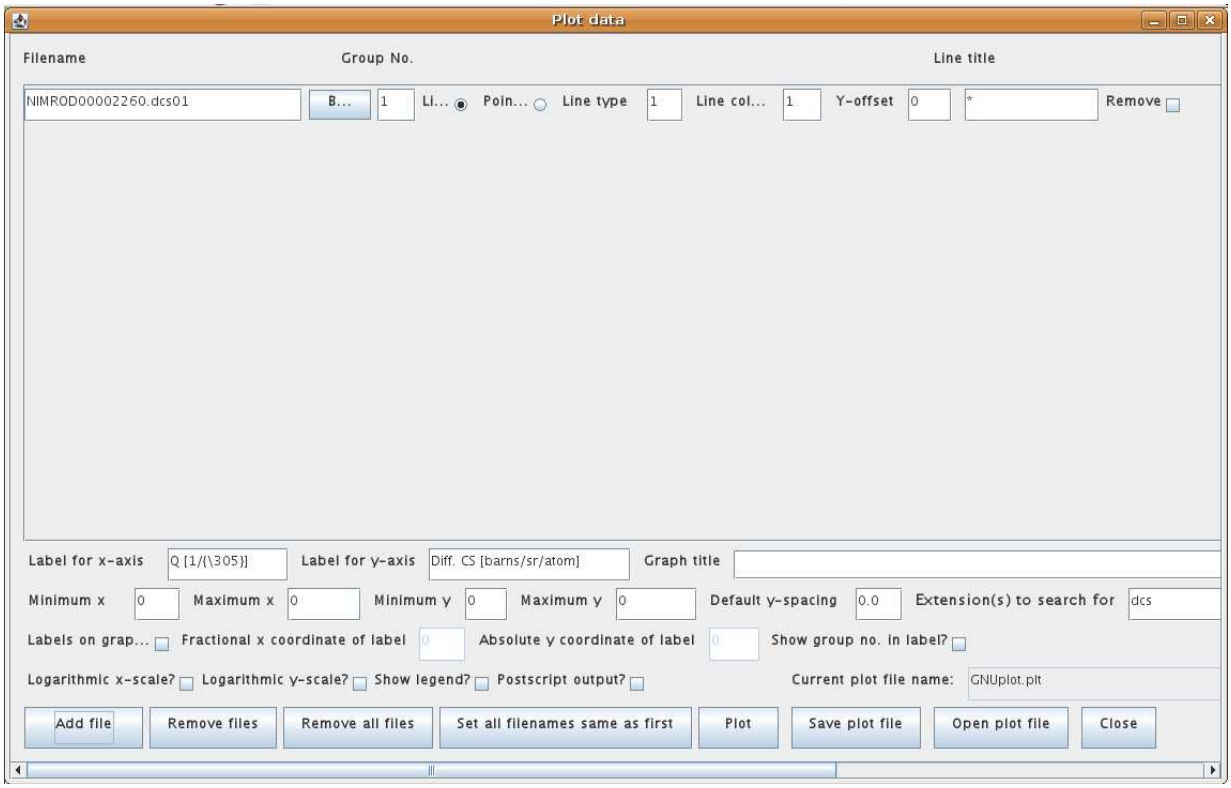

Figure 4.32: Layout of the Plot dialogue. In this view the *Add file* button has been pressed after typing "dcs" in the extension box, and a file has been selected (by pressing *Select* in the file selection dialogue).

3. Following the Group number, you have the option to plot the data as a line or as points. The type of line or point is specified in the next text box, *Line type*. The line colour can also be specified in the box *Line colour*.

4. Next in this line is a box to specify the offset of this curve from the previous curve (if there is more than one. If a * is given, then the offset will be generated automatically from the value of *Default y-spacing* further down the box. A value of 0 for the spacing is normally assigned to the first file of the list.

5. The next box gives this line a label. A * will indicate a default label will be generated if required, while if the box contains nothing, no label will be generated. Note that labels will only be plotted if specifically asked to do so if the *Labels on graph?* box is checked.

6. Finally there is tick box at the end of the line to signal you want this line deleted when the *Delete files* button at the bottom of the dialogue is pressed.

If you press *Add file* again it will add another line to the list of files which will be a carbon copy of the previous line, except that the line colour will be incremented by 1 (to give a different colour), and, if the *Group plotting sequence* in the *System path names* box, Fig. 4.7, has been given a list of group numbers, the next group number appearing in this sequence will be set for the next file added. If you don't want these numbers you can always delete the *Group plotting sequence* or else simply edit the Group number box.

Files can be removed from the list by ticking the *Remove* box on the right hand side, then pressing *Remove files* at the bottom of the dialogue. Alternatively you can delete all files by pressing the *Remove all files* button.

Other features of the Plot dialogue

Below the list of files to plot there are a number of additional options which control the appearance of the plot. Mostly these are self explanatory. If both of either the x or y limits are zero, then GNUplot will use the full range of data found in the plotting files. If only one of the limits is zero, it will set that limit as zero, not the minimum x value in the file.

Other buttons to note are:-

1. The *Plot* button instigates the actual plotting, depending what values have been set in the Plot dialogue. To do this it uses the command given on the *Full path for GNUplot plot command* line in the System box. Note that the file actually input to GNUplot is called **GNUplot.plt**.

2. The *Set all filenames same as first* button will do exactly that, but it won't change the filename extensions, assignment of group numbers, line types and colour, and the other parameters on each line.

3. The *Set all extensions same as first* button will do exactly that, but it won't change the filenames themselves, nor assignment of group numbers, line types and colour, and the other parameters on each line.

4. The *Postscript output?* check box will produce an encapsulated postscript file if checked, but there will be no corresponding graphic window (although in some versions a command prompt window may appear - this should be closed if it does appear).

5. Plot files can be saved and opened with the corresponding buttons at the bottom of the Plot dialogue. This is useful if you want to revert to a previous plot and change it in some way.

6. Finally the *Close* button will close the Plot dialogue window, but will not erase its contents, so that if you open it again it will come up looking as it was when you last closed it.

4.2.2 Plotting problems

When the *Plot* button is pressed then a GNUplot graph window should appear with the required graph on it. If it does not, it almost certainly means there is some problem with the command used to start GNUplot, e.g. the executable does not exist or is not in the path specified. Sometimes the problem can be simple in that an input file directory (found on the INSTRUMENT tab) must be specified in order for GNUplot to know where to start. This can happen if you are using the GUI simply to plot data without running any actual data analysis.

The easiest thing to do in case problems occur is open a terminal or command prompt and go to the folder where the current input file is stored, and practice the GNUplot plot command, such as that found in the file **rungnuplotplot.bat** (for Windows) or file **rungnuplotplot.sh** (for Linux). If that works in a command prompt, it should work from the GUI, provided the command is typed correctly in the System box. In Windows for example the command might be:

C:\GudrunX\gnuplot\binary\wgnuplot.exe GNUplot.plt -

This command tells the terminal to start GNUplot in the current folder and load the file **GNUplot.plt**. The hyphen at the end tells GNUplot to pause after plotting the file rather than closing immediately. This allows you to inspect the plot after it has been plot. You then have to close the plot window (and any associated terminal window) manually.

Occasionally it will happen that the graphics screen just flashes when you press *Plot* then immediately disappears again. This is almost certainly because there are no files to plot, or the requested Group number does not exist in the file specified, or an older version of GNUplot is being run. If after inspection you cannot figure out what is wrong, start GNUplot from the *Plot* menu, and then type: "call '**GNUplot.plt**"'. This will run the plot file, but not delete the GNUplot command prompt so that you can hopefully see what

is wrong with your plot file. Usually GNUplot will give a message indicating which part of the plotting script it doesn't understand.

4.3 Problems running the GUIs

Normally, provided Java is correctly installed on your machine, you should not encounter problems starting the GUI. In recent editions of Windows there seems to be some reluctance to allow Java to install the correct path, so that when you type: "Java" or "Java -version" in a command prompt, the command is not recognised. If this happens you will need to find the path to your installed version of Java. Normally it can be found in the *Program Files* folder on a Windows system. So instead of typing simply "Java" as above, you would need to type something like:-

"C:\Program Files\Java\jre6\bin\java"

This command would have to replace the Java command in the Windows batch file that starts the GUI, usually **GudrunGUI.bat**.

For users running on European computers, a comma is used in place of a period (full stop) to signify the decimal point. This can throw off reading the data into the GUI. To avoid this problem insert the following qualifier after the Java command:

"Java -Duser.language=en -jar ..."

Having got the GUI started however is not necessarily the end of the problems, since it is necessary to load the correct **Gudrun.syspar** file. There are normally two versions of this file in the directory containing the GudrunGUI.bat files, one for Windows and one for Linux. The **.bat** or shell script **.sh** file first copies the corresponding **.syspar** file over to **Gudrun.syspar**, then runs the GUI. When the GUI is closed, the **Gudrun.syspar** file is copied back to its original file, in case any changes have been made. However this does not ensure the values in these files are correct, since the pathnames on the current system may be different from those assumed in the **.syspar** file.

If this happens, the only thing to be done is to edit the appropriate **.syspar** file and correct the path names and commands as necessary.

Finally, having got the GUI started with the correct **.syspar** file, it is possible the specified startup file is corrupt and will need to be edited. This is easier, since if the GUI is operating correctly it can be used to edit or create a new startup file with the current settings, then save to the folder specified in the **.syspar** file. Normally the startup file will have the four tabs INSTRUMENT, BEAM, NORMALISATION and SAMPLE BACKGROUND defined, but of course it can contain any number of SAMPLES and CONTAINERS as well.

Unfortunately, if Java hits an error it prints a long series of error messages, only the first few of which give useful information. These can be found in the command prompt which opens when **GudrunGUI.bat** or **GudrunX.bat** are started. However that information is quite important since it tells you exactly at which line in the program the error occurred. Based on what the error message says, it is often easy to diagnose what has gone wrong, but for this you might need help from one of us at ISIS.

Chapter 5

Outputs

The purpose of this chapter is to help you understand the large number of files that are produced when GudrunN and GudrunX run. The majority of the output files take their name from the first data file in the SAMPLE tab, or, in the case of diagnostic files, from the corresponding data file. In GudrunX if this name has spaces in it, the spaces are replaced by underscores, _.

5.1 Output files produced by GudrunN

Table 5.1: Output files produced by GudrunN. A * signifies the first part of the file name can vary from run to run.

File name	Description
***.dcs01**	Gives the extracted differential scattering cross section for each detector group as a function of Q. These data have had no post processing done on them.
***.dcsd01**	Same as for **.dcs01** but when the units are d-spacing.
***.dcse01**	Same as for **.dcs01** but when the units are energy (meV).
***.dcst01**	Same as for **.dcs01** but when the units are time-of-flight.
***.dcsw01**	Same as for **.dcs01** but when the units are wavelength.
***.int01**	Gives the extracted differential scattering cross section for each detector group as a function of Q IF the *Subtract single atom scattering* box is checked in the INSTRUMENT tab. They will have had the estimated single atom scattering subtracted.

***.mdcs01**	Gives the merged differential scattering cross section AFTER removing any backgrounds, such as those generated by the Top Hat function.
***.mdcsd01**	Same as for **.mdcs01** but when the units are d-spacing.
***.mdcse01**	Same as for **.mdcs01** but when the units are energy.
***.mdcst01**	Same as for **.mdcs01** but when the units are time-of-flight.
***.mdcsw01**	Same as for **.mdcs01** but when the units are wavelength.
***.mint01**	Gives the merge differential scattering cross section AFTER post processing using the Top Hat function and deconvoluting the function in real space, removing any scattering which gives rise to spurious structure below $r = r_{min}$ (see SAMPLE tab). This only applies when the output units are Q.
***.mgor01**	Gives the Fourier transform of **.mint01**, using the real space broadening parameters specified in the SAMPLE tab.
***.mdor01**	Gives the function $4\pi\rho r h(r)$.

5.2 Diagnostic files produced by GudrunN

Table 5.2: Diagnostic files produced by Gudrun. Where a * is shown the first part of the file name can vary from run to run. This list shows the main files - there are a few others not listed, but these are mostly not informative on the operation of the program.

File name	Description
deadtime.cor	Lists the deadtime constants for each module as well as the overall detector deadtime constant.
gudrun_run_par.dat	Lists various parameters picked up from the ISIS **.raw** file. In particular it shows how the detector numbers map onto spectrum numbers, how the spectrum numbers related to detector numbers and how the detectors are divided into modules, based on their crate numbers in the Data Acquisition Electronics (DAE).

gudrun_grp.dat	Lists the group scattering angles, flight paths and azimuthal angles, as well as the group number for each spectrum.
gudrun_calib.dat	Lists the flight path, scattering angle and azimuthal angle of each detector
gudrun_van_tcb.dat	Lists the time channel boundaries and widths for the vanadium and vanadium background data files. Note that these can be different from those for the sample, sample background, and container data files.
gudrun_sam_tcb.dat	Lists the time channel boundaries and widths for the sample, sample background and container data files. It is assumed all these files have the same time channel boundaries.
vanadium.soq	Shows the model vanadium differential cross section as derived from the **.bragg** or **.mdcs** file in the NORMALISATION tab, expressed on a Q scale.
***.abs01**	The calculated absorption corrections as a function of wavelength, scattering angle, and where appropriate azimuthal angle. The wavelengths, then the scattering angles are listed down the page, while the azimuthanl angles are listed across the page. If there is no container, only the $A_{s,s}$ is listed. If there is one container, then $A_{s,sc}$, $A_{c,sc}$, and $A_{c,c}$ are listed. If there are two containers then $A_{s,scf}$, $A_{c,scf}$, $A_{f,scf}$, and $A_{f,f}$ are listed. This repeats itself if the sample has three containers.
***.abscor**	This shows the result of the final absorption correction after dividing by the number of atoms in the sample as a function of wavelength. This file only appears if a diagnostic spectrum has been specified (INSTRUMENT tab).
***.bad**	Lists the bad detectors from this run - same as **spec.bad**
***.bak**	Shows the result of Fourier transform the **.gr2** data back to Q space.
***.cnt**	The neutron counts per unit time as read from the RAW file. This file only appears if a diagnostic spectrum has been specified (INSTRUMENT tab).
***.gr1**	Shows the result of Fourier transforming the data prior to deconvoluting the top hat function in r space.
***.gr2**	Shows the result of deconvoluting the top hat function in r space.

***.grp**	Shows the groups of good detectors for this run.
***.gud**	Gives a summary of the results from this run, giving estimations of the scattering level of each group.
***.merge**	Shows the same data as **.premerge** after rebinning onto the final Q scale, for the specified diagnostic spectrum.
***.module**	Lists the detector module deadtime corrections for the corresponding data file.
***.mul01**	The calculated multiple scattering corrections. For each specified scattering angle the file shows the neutron wavelength, the calculated single scattering and the calculated multiple scattering over the specified wavelength range as defined in the NORMALISATION tab.
***.mulcor**	Shows the result of subtracting the multiple scattering for the specified diagnostic spectrum.
***.mut01**	Calculated or measured transmission total cross section (barns per atom) as a function of neutron wavelength.
***.normmon**	The scattering data normalised to the monitor for the specified diagnostic spectrum.
***.normvan**	For the specified diagnostic spectrum shows the result of dividing by the smoothed vanadium as a function of wavelength.
***.pla01**	The calculated Placzek correction for the specified sample as a function of wavelength for each specified scattering angle.
***.premerge**	Shows the result of converting the data from **.abscor** onto a Q scale.
***.rat**	Lists the ratio of counts in this spectrum to counts in the corresponding vanadium spectrum. Used in **purge_det**.
***.rawmon**	The monitor counts per unit wavelength as a function of wavelength.
***.rawtrans**	The transmission monitor counts per unit wavelength as a function of wavelength.
***.smo**	Shows the result of Top Hat smoothing if this has been invoked from the SAMPLE tab, as a function of Q. This will be shown for the last group.
***.smomon**	Shows the smoothed monitor spectrum. This should overlap the corresponding **.rawmon** data.

***.smovan**	Shows the smoothed vanadium for the specified diagnostic spectrum.
***.subbak**	Shows the result of subtracting the background for the specified diagnostic spectrum as a function of wavelength.
***.sub**	Shows the result of subtracting the exponential background as specified in the SAMPLE tab as a function of Q. This will be shown for the last group.
***.trans01**	Shows the transmission for this sample as estimated from the transmission monitor as a function of wavelength.
***.vanbin**	Shows the merge weighting for the specified diagnostic spectrum.
***.vancor**	The vanadium data after correction for the total scattering differential cross section for the specified diagnostic spectrum. These are the data that are put through the vanadium smoothing.
***.vdcsbin**	Shows the model vanadium differential cross section for the specified diagnostic spectrum, as derived from the **.vdcscor** file, binned onto the same wavelength scale as the data.
***.vdcscor**	Shows the model vanadium differential cross section for the specified diagnostic spectrum, as derived from the **vanadium.soq** file, expressed on a wavelength scale.

5.3 Output files produced by GudrunX

Compared to Gudrun, GudrunX produces relatively few output files, and the extensions are not always the same as Gudrun. For most files the first part of the name is adopted from the corresponding data file, with any spaces replaced by underscores.

Table 5.3: Output files produced by GudrunX. A * signifies the first part of the file name can vary from run to run.

File name	Description
***.gofr**	Gives the Fourier transform of **.int01**, using the real space broadening parameters specified in the SAMPLE tab.

***.int01**	Gives the differential scattering cross section AFTER post processing using the Top Hat function and deconvoluting the function in real space, removing any scattering which gives rise to spurious structure below $r = r_{min}$ (see SAMPLE tab).
***.soq**	Gives the interference differential scattering cross section AFTER removing the single atom scattering, but BEFORE any post processing such as subtracting any backgrounds generated by the Top Hat function, as a function of Q.

5.4 Diagnostic files produced by GudrunX

There is no *Spectrum for diagnostic files* to be specified for GudrunX, so the diagnostic files are simply those produced whenever the program runs.

Table 5.4: Diagnostic files produced by GudrunX. A * signifies the first part of the file name can vary from run to run and is normally the first part of the first data file name for each sample.

File name	Description
BeamParameters.txt	This lists the information in the BEAM tab, to be read by the attenuation and multiple scattering corrections program.
***.abs**	The calculated absorption corrections as a function of scattering angle for the specified x-ray wavelength, as for the **.abs01** files in Gudrun.
***.abscor**	The scattering data corrected for attenuation and container scatter as a function of scattering angle for the specified x-ray wavelength.
***.brem**	Shows the bremsstrahlung spectrum either as input from the specified file or using the parameters given in the BEAM and SAMPLE tabs
***.fluor**	Shows the calculated fluorescence spectrum calculated as a function of scattering from the supplied data in the SAMPLE tab.
***.gr1**	Shows the result of Fourier transforming the data prior to deconvoluting the top hat function in r space in *tophatsub*.

***.gr2**	Shows the result of deconvoluting the top hat function in r space in *tophatsub*.
***.mul**	The calculated multiple scattering corrections as a function of scattering angle for the specified x-ray wavelength. If the sample has containers, the multiple scattering is listed for these containers beside the sample multiple scattering for each scattering angle. As for the **.mul01** files in Gudrun, both the estimated single and multiple scattering are shown.
***.mulcor**	The sample and container (when present) data after correction for multiple scattering.
***.qbak**	Shows the result of Fourier transform the **.gr2** data back to Q space in *tophatsub*.
***.qbin**	Rebin of the input data, **.soq**, onto the output Q scale in *tophatsub*.
***.qsmooth**	Shows the result of Top Hat smoothing if this has been invoked from the SAMPLE tab, as a function of Q in *tophatsub*.
***.qsub**	Shows the effect of subtracting the **.qsmooth** data from the input data in *tophatsub*.
***.subbak**	Shows the result of subtracting the background for the sample and any containers as a function of scattering angle. There is a pair of columns for each sample and container.

***.subcan**	This is the main diagnostic file from GudrunX. It has 6 groups of data arranged in standard column format. Leftmost column is the scattering angle, Group 1 (columns 2 and 3) is the estimated differential cross section prior to normalisation or subtraction of the single atom scattering but after subtracting the bremsstrahlung contribution, Group 2 (columns 4 and 5) is the calculated single atom scattering, Group 3 (columns 6 and 7) shows the single atom scattering again, UNLESS the data is not being normalised (NORMALISATION tab) when it shows just the Compton scattering to be subtracted from the data, Group 4 (columns 8 and 9) shows the normalisation to be applied to the data (if no normalisation is being done this is simply a factor of 1.0), Group 5 (columns 10 and 11) shows the data after subtracting Group 3 (either the single atom scattering or the Compton scattering) and dividing by Group 4 normalising factor, Group 6 shows the estimated bremsstrahlung contribution to the total scattering - this has already been subtracted from Group 1.
***.submul**	Shows the result of subtracting the multiple scattering for the sample as a function of scattering angle.
***.temp**	Temporary file produced by *tophatsub* showing the input **.soq** data BEFORE rebinning onto the output Q scale.

Appendix A

List of neutron resonances

A.1 Neutron resonances in eV

Z	Element	Resonance energies (eV)			
17	^{35}Cl	400			
23	V	170			
25	Mn	350			
27	Co	140			
29	^{63}Cu	600			
	^{65}Cu	240			
30	^{65}Zn	220	450		
	^{68}Zn	510			
31	^{69}Ga	110	350		
	^{71}Ga	95	300		
32	Ge	100	110	200	
33	As	46	95	250	
34	Se	2.6	210	270	
35	Br	35	55		
36	Kr	28	41	110	
38	Sr	3.5	600		
40	Zr	300	700		
41	Nb	35	42	95	
42	Mo	12	45	70	
43	Tc	5.6	20	40	
44	Ru	10	15	25	
45	Rh	1.2	34	46	
46	Pd	3	13	25	
47	^{107}Ag	16	40		
	^{109}Ag	5	30	40	
48	Cd	0.18	19	29	
49	In	1.5	4	9	12
50	Sn	40	45	65	
51	Sb	6	15	21	
52	Te	2.3	8.5	25	
53	I	20	31		
54	Xe	5	9.4	14	

Z	Element	Resonance energies (eV)				
55	Cs	6	22	50		
56	Ba	25	80			
57	La	7				
59	Pr	85	210			
60	Nd	4.3	45	55		
61	Pm	5.4	6.9	7.0	16	
62	^{147}Sm	3.4	18			
	^{149}Sm	0.1	0.9	5	9	15
	^{152}Sm	8				
63	Eu	0.5	1	2.5	3.4	
64	Gd	2.1	2.6	2.9	6.3	7
65	Tb	3.3	11			
66	Dy	1.7	2.7	3.7		
67	Ho	3.9	12.8			
68	Er	0.45	0.58	4.4	6	9
69	Tm	3.9	14	17.5		
70	Yb	0.6	7.9	13		
71	Lu	0.14	2.6	5.2		
72	Hf	1.1	2.4			
73	Ta	4.3	10.3	14		
74	W	4.2	7.6	18.8		
75	Re	2.16	4.4			
76	Os	6.7	9.0	10.3		
77	Ir	0.66	1.3	5.4		
78	Pt	12	20			
79	Au	4.9	60	80		
80	Hg	23	32			
81	Tl	240				
88	Ra	0.5				
90	Th	22	23	60		
91	Pa	0.4	5			
92	^{233}U	1.8	2.3	6.8		
	^{234}U	5.2				
	^{235}U	8.8	11.7	12.4	19.3	
	^{236}U	5.4				
	^{238}U	6.67	20.9			
93	Np	0.5	1.5			
94	^{238}Pu	2.9	10	18		
	^{239}Pu	0.3	7.8	11		
	^{240}Pu	1.06	20.5			
	^{241}Pu	0.3	4.3			
	^{242}Pu	2.7				
95	Am	0.3	0.6	1.3		

A.2 Neutron resonances in Å

Z	Element	Resonance wavelength (Å)			
17	^{35}Cl	0.014			
23	V	0.022			
25	Mn	0.015			
27	Co	0.024			
29	^{63}Cu	0.012			
	^{65}Cu	0.018			
30	^{65}Zn	0.019	0.013		
	^{68}Zn	0.013			
31	^{69}Ga	0.027	0.015		
	^{71}Ga	0.029	0.017		
32	Ge	0.029	0.027	0.020	
33	As	0.042	0.029	0.018	
34	Se	0.177	0.020	0.017	
35	Br	0.048	0.039		
36	Kr	0.054	0.045	0.027	
38	Sr	0.153	0.012		
40	Zr	0.017	0.011		
41	Nb	0.048	0.044	0.029	
42	Mo	0.083	0.043	0.034	
43	Tc	0.121	0.064	0.045	
44	Ru	0.090	0.074	0.057	
45	Rh	0.261	0.049	0.042	
46	Pd	0.165	0.079	0.057	
47	^{107}Ag	0.072	0.045		
	^{109}Ag	0.128	0.052	0.045	
48	Cd	0.674	0.066	0.053	
49	In	0.234	0.143	0.095	0.083
50	Sn	0.045	0.043	0.035	
51	Sb	0.117	0.074	0.062	
52	Te	0.189	0.098	0.057	
53	I	0.064	0.051		
54	Xe	0.128	0.093	0.076	

Z	Element	Resonance wavelength (Å)				
55	Cs	0.117	0.061	0.040		
56	Ba	0.057	0.032			
57	La	0.108				
59	Pr	0.031	0.020			
60	Nd	0.138	0.043	0.039		
61	Pm	0.123	0.109	0.108	0.072	
62	^{147}Sm	0.155	0.067			
	^{149}Sm	0.904	0.301	0.128	0.095	0.074
	^{152}Sm	0.101				
63	Eu	0.404	0.286	0.181	0.155	
64	Gd	0.197	0.177	0.168	0.114	0.108
65	Tb	0.157	0.086			
66	Dy	0.219	0.174	0.149		
67	Ho	0.145	0.080			
68	Er	0.426	0.376	0.136	0.117	0.095
69	Tm	0.145	0.076	0.068		
70	Yb	0.369	0.102	0.079		
71	Lu	0.764	0.177	0.125		
72	Hf	0.273	0.185			
73	Ta	0.138	0.089	0.076		
74	W	0.140	0.104	0.066		
75	Re	0.195	0.136			
76	Os	0.111	0.095	0.089		
77	Ir	0.352	0.251	0.123		
78	Pt	0.083	0.064			
79	Au	0.129	0.037	0.032		
80	Hg	0.060	0.051			
81	Tl	0.018				
88	Ra	0.404				
90	Th	0.061	0.060	0.037		
91	Pa	0.452	0.128			
92	^{233}U	0.213	0.189	0.110		
	^{234}U	0.125				
	^{235}U	0.096	0.084	0.081	0.065	
	^{236}U	0.123				
	^{238}U	0.111	0.063			
93	Np	0.404	0.234			
94	^{238}Pu	0.168	0.090	0.067		
	^{239}Pu	0.522	0.102	0.086		
	^{240}Pu	0.278	0.063			
	^{241}Pu	0.522	0.138			
	^{242}Pu	0.174				
95	Am	0.522	0.369	0.251		

References

A K Soper and E R Barney. Extracting the pair distribution function from white-beam x-ray total scattering data. *J. Appl. Cryst.*, 44:714 – 726, 2011.

G. Caglioti, A. Paoletti, and F.P. Ricci. Choice of collimators for a crystal spectrometer for neutron diffraction. *Nucl. Inst.*, 3(4):223 – 228, 1958.

J. P. Hansen and I. R. MacDonald. *Theory of Simple Liquids*. Academic Press, London, 1986.

N. E. Cusack. *The Physics of Structurally Disordered Matter*. Adam Hilger, 1987. ISBN 0852745915.

T Schenk, D Holland-Moritz, V Simonet, R Bellissent, and DM Herlach. Icosahedral short-range order in deeply undercooled metallic melts. *Phys. Rev. Lett.*, 89:075507, 2002.

G W Lee, A K Gangopadhyay, K F Kelton, R W Hyers, T J Rathz, J R Rogers, and D S Robinson. Difference in icosahedral short-range order in early and late transition metal liquids. *Phys. Rev. Lett.*, 93:037802, 2004.

T. E. Faber and J. M. Ziman. A theory of electrical properties of liquid metals 3. resistivity of binary alloys. *Phil. Mag.*, 11(109):153–&, 1965.

A Ben-Naim. *Moleulcar Theory of Solutions*. Oxford University Press, London, 2006.

D Gazzillo. Stability of fluids with more than two components i. general thermodynamic theory and concentration-concentration structure factor. *Mol. Phys.*, 83:1171–1190, 1994.

C. G. Gray and K. E. Gubbins. *Theory of Molecular Fluids. Volume 1: Fundamentals*. Oxford University Press, 1984.

O Glatter and O Kratky, editors. *Small-angle X-ray Scattering*. Academic Press, London, 1982.

V F Sears. Theory of cold neutron scattering by homonuclear diatomic liquids .i. free rotation. *CANADIAN JOURNAL OF PHYSICS*, 44:1279, 1966.

A H Compton. A quantum theory of the scattering of x-rays by light elements. *Phys. Rev.*, 21:483–502, 1923.

G Placzek. The scattering of neutrons by systems of heavy nuclei. *Phys. Rev.*, 86:377 – 388, 1952.

J G Powles. Slow-neutron scattering by molecules 5. recoil corrections for any molecule. *Mol. Phys.*, 37:623 – 641, 1979.

P A Egelstaff. Methods of experimental physics, vol 23: Neutron scattering. chapter 14, pages 405 – 470. London and New York: Academic, 1987. Part B, Editors D. L. Price and K. Sk'old.

P A Egelstaff and A K Soper. The scattering of slow-neutrons by diatomic molecular fluids 1. models. *Mol. Phys.*, 40:553 – 567, 1980.

M A Howe, R L Mcgreevy, and W S Howells. The analysis of liquid structure data from time-of-flight neutron diffractometry. *J. Phys. Condens. Matter*, 1:3433 – 3451, 1989.

J. E. Enderby, D. M. North, and P. A. Egelstaff. Partial structure factors of liquid cu-sn. *Phil. Mag.*, 14(131):961–&, 1966.

F. G. Edwards, J. E. Enderby, R. A. Howe, and D. I. Page. Structure of molten sodium-chloride. *J. Phys. C - Sol. Stat. Phys.*, 8(21):3483–3490, 1975.

S. Biggin and J. E. Enderby. The structure of molten zinc-chloride. *J. Phys. C - Sol. Stat. Phys.*, 14(22):3129–3136, 1981.

A K Soper. Partial structure factors from disordered materials diffraction data: An approach using empirical potential structure refinement. *Phys. Rev. B*, 72:104204, 2005.

A K Soper. On the uniqueness of structure extracted from diffraction experiments on liquids and glasses. *J. Phys. Condens. Matter*, 19:415108, 2007.

G. Palinkas, E. Kalman, and P. Kovacs. Liquid water 2. experimental atom pair-correlation functions of liquid d2o. *Mol. Phys.*, 34:525–537, 1977.

J J Rehr and R C Albers. Theoretical approaches to x-ray absorption fine structure. *Rev. Mod. Phys.*, 72:621–654, 2000.

A Filipponi, A DiCicco, and CR Natoli. X-ray-absorption spectroscopy and n-body distribution functions in condensed matter .1. theory. *PHYs. Rev. B*, 52:15122–15134, 1995.

A Filipponi and A DiCicco. X-ray-absorption spectroscopy and n-body distribution functions in condensed matter .2. data analysis and applications. *Phys. Rev. B*, 52:15135–15149, 1995.

DL Price and ML Saboungi. Anomalous x-ray scattering from disordered materials. In SJL Billinge and MF Thorpe, editors, *Local Structure from Diffraction*, pages 23 – 34. Klewer Academic Publishers, 2002.

S Ramos, GW Neilson, AC Barnes, and P Buchanan. An anomalous x-ray diffraction study of the hydration structures of cs+ and i- in concentrated solutions. *J. Chem. Phys.*, 123, 2005.

A. K. Soper. Inelasticity corrections for time-of-flight and fixed wavelength neutron diffraction experiments. *Mol. Phys.*, 107:1667–1684, 2009.

L Van Hove. Correlations in space and time and born approximation scattering in systems of interacting particles. *Phys. Rev.*, 95(1):249–262, Jul 1954. doi: 10.1103/PhysRev.95.249.

H E Fischer, A C Barnes, and P S Salmon. Neutron and x-ray diffraction studies of liquids and glasses. *Rep. Prog. Phys.*, 69:233 – 299, 2006.

G. Breit. A correspondence principle in the compton effect. *Phys. Rev.*, 27:362–372, 1926.

P.A.M. Dirac. Relativity quantum mechanics with an application to compton scattering. *Proc. Roy. Soc. Lon. Series A*, 111:405–423, 1926.

O Klein and Y Nishina. *Z. Phys.*, 52:853, 1929.

J H Hubbell, W J Veigele, E A Briggs, R T Brown, D T Cromer, and R J Howerton. Atomic form factors, incoherent scattering functions, and photon scattering cross sections. *J. Phys. Chem. Ref. Data*, 4:471–538, 1975.

J. Read and C. C. Lauritsen. An investigation of the klein-nishina formula for x-ray scattering, in the wavelength region 50 to 20 x-units. *Phys. Rev.*, 45(7):433 – 436, 1934.

R Ribberfors. X-ray incoherent scattering total cross sections and energy-absorption cross sections by means of simple calculation routines. *Phys. Rev. A*, 27:3061–3070, 1983.

H H M Balyuzi. Analytic approximations to incoherently scattered x-ray intensities. *Acta. Cryst. Sect. A*, 31:600–602, 1975.

D. Waasmaier and A. Kirfel. New analytical scattering factor functions for freem atoms and ions. *Acta. Cryst.*, A51:416–431, 1995.

H H Paalman and C J Pings. Numerical evaluation of x-ray absorption factors for cylindrical samples and annular sample cells. *J. Appl. Phys.*, 33:2635, 1962.

V. F. Sears. Neutron scattering lengths and cross sections. *Neutron News*, 3:26–37, 1992.

A K Soper and P A Egelstaff. Multiple-scattering and attenuation of neutrons in concentric cylinders .1. isotropic first scattering. *Nucl. Inst. Meth.*, 178:415 – 425, 1980.

A K Soper. Multiple-scattering from an infinite-plane slab. *Nucl. Inst. Meth. in Phys. Res.*, 212:337 – 347, 1983.

A. P. Kendig and C. J. Pings. X-ray absorption factors for cylindrical samples in annular sample cells exposed to incident beams of limited width. *J. of Appl. Phys.*, 36(5):1692–1698, 1965.

I A Blech and B L Averbach. Multiple scattering of neutrons in vanadium and copper. *Phys. Rev.*, 137:1113, 1965.

G. H. Vineyard. Multiple scattering of neutrons. *Phys. Rev.*, 96(1):93–98, Oct 1954. doi: 10.1103/PhysRev.96.93.

J Krogh-Moe. A method for converting experimental x-ray intensities to an absolute scale. *Acta Cryst.*, 9:951–953, 1956.

N Norman. The fourier transform method of normalizing intensities. *Acta Cryst.*, 10: 370–373, 1957.

R Kahn, R Fourme, A Gadet, J Janin, C Dumas, and D Andre. Macromolecular crystallography with synchrotron radiation: Photographic data collection and polarization correction. *J. Appl. Cryst.*, 15:330–337, 1982.

G H McCall. Calculation of x-ray bremsstrahlung and characteristic line emission produced by a maxwellian electron distribution. *J. Phys. D Appl. Phys.*, 15:823–831, 1982.

E Lorch. Neutron diffraction by germania silica and radiation-damaged silica glasses. *J. Phys. C Sol. Stat. Phys.*, 2:229, 1969.
using multind.sty